

การศึกษาเชิงทฤษฎีการเปลี่ยนแอลกอฮอล์เป็นอีเทอร์และเอทีลีน โดยแอช-แซดเอสเอ็ม-5

ด้วยวิธีอนเนียม



นายเชษฐพิชาญ แสนหาญ

สถาบันวิทยบริการ

วิทยานิพนธ์นี้เป็นส่วนหนึ่งของการศึกษาตามหลักสูตรปริญญาวิทยาศาสตรมหาบัณฑิต

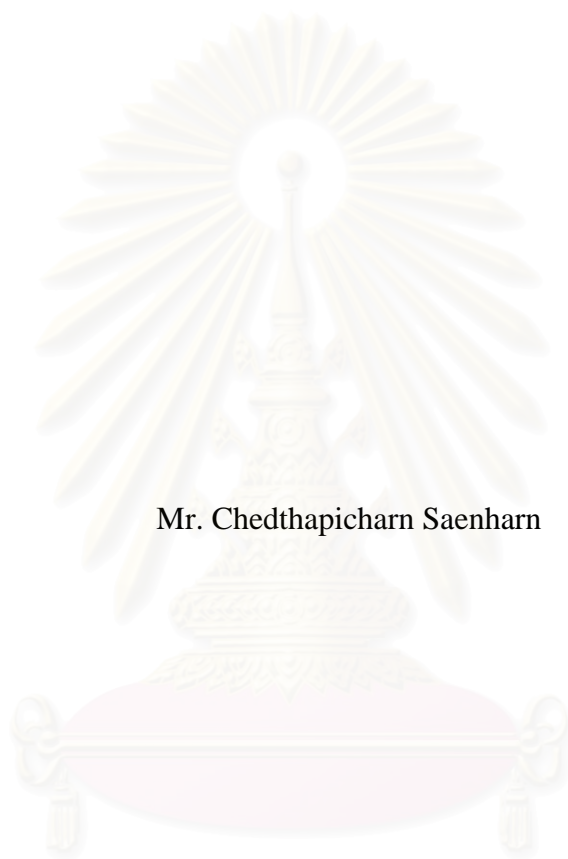
สาขาวิชาปิโตรเคมีและวิทยาศาสตร์พอลิเมอร์

คณะวิทยาศาสตร์ จุฬาลงกรณ์มหาวิทยาลัย

ปีการศึกษา 2550

ลิขสิทธิ์ของจุฬาลงกรณ์มหาวิทยาลัย

THEORETICAL STUDY OF ALCOHOLS CONVERSION TO ETHERS
AND ETHYLENE BY H-ZSM-5 USING ONIOM METHOD



Mr. Chedthapicharn Saenharn

สถาบันวิทยบริการ
จุฬาลงกรณ์มหาวิทยาลัย

A Thesis Submitted in Partial Fulfillment of the Requirements
for the Degree of Master of Science Program in Petrochemistry and Polymer Science

Faculty of Science

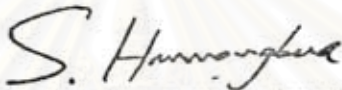
Chulalongkorn University

Academic Year 2007

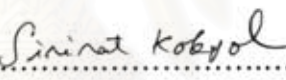
Copyright of Chulalongkorn University


Thesis Title THEORETICAL STUDY OF ALCOHOLS CONVERSION TO
ETHERS AND ETHYLENE BY H-ZSM-5 USING ONIOM
METHOD
By Mr. Chedthapicharn Saenharn
Field of study Petrochemistry and Polymer Science
Thesis Advisor Associate Professor Vithaya Ruangpornvisuti, Dr.rer.nat.

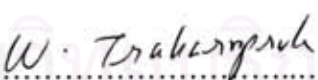
Accepted by the Faculty of Science, Chulalongkorn University in Partial
Fulfillment of the Requirements for the Master's Degree



.....Dean of the Faculty of Science
(Professor Supot Hannongbua, Ph.D.)

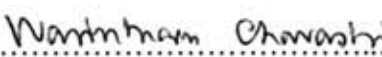
THESIS COMMITTEE


.....Chairman
(Associate Professor Sirirat Kokpol, Ph.D.)


.....Thesis Advisor
(Associate Professor Vithaya Ruangpornvisuti, Dr.rer.nat.)


.....Member
(Associate Professor Wimonrat Trakarnpruk, Ph.D.)



.....Member
(Associate Professor Buncha Pulpoka, Ph.D.)


.....Member
(Assistant Professor Warinthorn Chavasiri, Ph.D.)

เชษฐพิชาญ แสนหาญ: การศึกษาเชิงทฤษฎีการเปลี่ยนแอลกอฮอล์เป็นอีเทอร์และเอทิลีน โดยแอซ-แซคเอสเอ็ม-5 ด้วยวิธีออนเนียม (THEORETICAL STUDY OF ALCOHOLS CONVERSION TO ETHERS AND ETHYLENE BY H-ZSM-5 USING ONIOM METHOD) อ.ที่ปรึกษา: รศ.ดร.วิทยา เรืองพรวิสุทธิ, 107 หน้า.

ศึกษากลไกการเกิดปฏิกิริยาการเปลี่ยนแอลกอฮอล์ไปเป็นไดเมทิลอีเทอร์ ไดเอทิลอีเทอร์ และเอทิลีน บนตัวเร่งปฏิกิริยาซีโอไลต์ชนิดเอซ-แซคเอสเอ็ม-5 ขนาดคัลสเตอร์ 56/5T ด้วยวิธี ONIOM(B3LYP/6-31G(d):AM1) พบว่ากลไกการเกิดปฏิกิริยามีทั้งแบบที่เป็นขั้นตอนเดียวและหลายขั้นตอน โดยได้ทำการเปรียบเทียบกัน พบว่าในปฏิกิริยาการเปลี่ยนเมทานอลไปเป็นไดเมทิลอีเทอร์ และเอทานอลไปเป็นไดเอทิลอีเทอร์นั้น กลไกการเกิดปฏิกิริยาในแบบขั้นตอนเดียวสามารถเกิดได้ดีกว่าในแบบหลายขั้นตอนด้วยค่าพลังงานกระตุ้นที่ต่ำกว่าเท่ากับ 11.37 และ 20.15 กิโลแคลอรีต่อโมล ตามลำดับ ในปฏิกิริยาการเปลี่ยนเอทานอลไปเป็นเอทิลีนนั้น พบว่ากลไกการเกิดปฏิกิริยาในแบบหลายขั้นตอนเกิดได้ดีกว่าในแบบขั้นตอนเดียวด้วยค่าพลังงานกระตุ้นที่ต่ำกว่าเท่ากับ 9.11 กิโลแคลอรีต่อโมล ในปฏิกิริยาการเปลี่ยนเอทานอลไปเป็นไดเอทิลอีเทอร์ในแบบขั้นตอนเดียวนั้น พบว่าเกิดได้ดีกว่าในปฏิกิริยาการเปลี่ยนเอทานอลไปเป็นเอทิลีนในแบบขั้นตอนเดียวด้วยค่าพลังงานกระตุ้นที่ต่ำกว่าเท่ากับ 29.26 กิโลแคลอรีต่อโมล ส่วนในปฏิกิริยาการเปลี่ยนเอทานอลไปเป็นเอทิลีนในแบบหลายขั้นตอนนั้น พบว่าเกิดได้ดีกว่าในปฏิกิริยาการเปลี่ยนเอทานอลไปเป็นไดเอทิลอีเทอร์ในแบบหลายขั้นตอนด้วยค่าพลังงานกระตุ้นที่ต่ำกว่าเท่ากับ 28.07 กิโลแคลอรีต่อโมล โดยกลไกของปฏิกิริยาเหล่านี้ในระบบที่ใช้กรดเป็นตัวเร่งได้มีการศึกษาและเปรียบเทียบกับปฏิกิริยาที่สอดคล้องกับปฏิกิริยาข้างต้น โดยได้แสดงค่าพลังงานและสมบัติทางเทอร์โมไดนามิกของปฏิกิริยาทั้งหมดในขั้นตอนต่างๆ

สาขา...ปิโตรเคมีและวิทยาศาสตร์พอลิเมอร์...ลายมือชื่อนิสิต... เชษฐพิชาญ แสนหาญ...

ปีการศึกษา... 2550 ...ลายมือชื่ออาจารย์ที่ปรึกษา... 

4872311923: PETROCHEMISTRY AND POLYMER SCIENCE PROGRAM

KEY WORD: METHANOL; ETHANOL; DIMETHYL ETHER; DIETHYL ETHER;
ETHYLENE; ACID-CATALYZED; H-ZSM-5; ONIOM

CHEDTHAPICHARN SAENHARN: THEORETICAL STUDY
OF ALCOHOLS CONVERSION TO ETHERS AND ETHYLENE
BY H-ZSM-5 USING ONIOM METHOD. THESIS ADVISOR: ASSOC.
PROF. VITHAYA RUANGPORNVISUTI, Dr.rer.nat., 107 pp.

Reaction mechanisms of methanol and ethanol conversion to dimethyl ether, diethyl ether and ethylene on the H-ZSM-5 were investigated using a 56/5T cluster model of H-ZSM-5 in corporation with the two-layered ONIOM(B3LYP/6-31G(d):AM1) approach. The concerted and stepwise mechanisms of methanol and ethanol conversion to dimethyl ether, diethyl ether and ethylene were comparatively studied. The concerted process occurring over Brønsted acid site of H-ZSM-5 zeolite is more favorable by 11.37 kcal/mol than the stepwise process in methanol conversion to dimethyl ether and 20.15 kcal/mol than the stepwise reaction in ethanol conversion to diethyl ether. In the stepwise reaction of ethanol conversion to ethylene occurring over Brønsted acid site of H-ZSM-5 zeolite is more favorable by 9.11 kcal/mol than the concerted reaction. In the concerted reaction of ethanol conversion to diethyl ether occurring over Brønsted acid site of H-ZSM-5 zeolite is more favorable by 29.26 kcal/mol than the concerted process in ethanol conversion to ethylene. In the stepwise reaction of ethanol conversion to ethylene occurring over Brønsted acid site of H-ZSM-5 zeolite is more favorable by 28.07 kcal/mol than the stepwise process in ethanol conversion to diethyl ether. These reaction mechanisms in acid-catalyzed system were also investigated and compared to their corresponding reactions. The reaction energies and thermodynamic properties of all reaction mechanisms are reported.

Field of Study Petrochemistry and Polymer Science Student's signature พรวิภาดา วัฒนกุล,

Academic year 2007 Advisor's signature O. Sornthanasathien

ACKNOWLEDGEMENTS

First, I would like to express my sincere gratitude to my advisor Associate Professor Dr. Vithaya Ruangpornvisuti for his continuous attention and guidance thought the years of my study. I deeply appreciate the support, encouragement and valuable advice of my committee members, Associate Professor Sirirat Kokpol, Ph.D., Associate Professor Dr. Wimonrat Trakarnpruk, Associate Professor Dr. Buncha Pulpoka and Assistant Professor Dr. Warinthon Chavasiri, Ph.D.. I also acknowledge Mr. Banchob Wannoo who always assists in intensive quantum and computational chemistry details.

Special appreciation is extended to my colleagues at Supramolecular Chemistry Research Unit (SCRU), Department of Chemistry, Faculty of Science, Chulalongkorn University, Bangkok, Thailand for their kind, friendship, support and encouragement throughout my study.

I gratefully acknowledge the financial assistance from research grant from the Graduate School, Chulalongkorn University for giving an encouragement of present work. The generous supply of computing time by, personal computers at Supramolecular Chemistry Research Unit, Chulalongkorn University is also gratefully acknowledged for research support.

Finally, I would like to dedicate this thesis to my parent, Pramote and Bunplook Saenharn, and my lovely younger sister, Passaraporn Saenharn. Their love and support for me is priceless. I hope my family is proud of my success.

สถาบันวิทยบริการ
จุฬาลงกรณ์มหาวิทยาลัย

CONTENTS

	Page
ABSTRACT (THAI)	iv
ABSTRACT (ENGLISH)	v
ACKNOWLEDGEMENTS	vi
CONTENTS	vii
LIST OF FIGURES	x
LIST OF TABLES	xiii
LIST OF ABBREVIATIONS	xv
CHAPTER I INTRODUCTION	1
1.1 Background.....	1
1.2 Zeolite.....	2
1.2.1 Structure of zeolites.....	3
1.2.2 Properties of zeolites.....	5
1.2.2.1 Shape and size selectivity.....	5
1.2.2.3 Acid sites (acidity).....	6
1.2.3 ZSM-5 (Zeolite Socony Mobil-5).....	8
1.3 The methanol-to-gassoline (MTG).....	9
1.4 The bioethanol-to-gassoline (BTG).....	9
1.5 Literature reviews.....	10
1.4.1 Experimental studies.....	10
1.4.2 Computational studies.....	14
1.6 Objectives.....	17
CHAPTER II THEORY	18
2.1 Quantum mechanics(QM).....	18
2.2 Solution of the Schrödinger Equation of Molecular Systems.....	19
2.2.1 The Schrödinger Equation.....	19
2.2.2 Born-Oppenheimer Approximation.....	21

	Page
2.3 The Hartree-Fock Method.....	22
2.4 Basis Sets.....	24
2.4.1 Minimal Basis Sets.....	26
2.4.2 Scaled Orbital by Splitting the Minimum Basis Sets.....	27
2.4.3 Polarized Basis Sets.....	28
2.4.4 Diffuse Function Basis Sets.....	29
2.5 Density Functional Theory (DFT).....	29
2.6 ONIOM method.....	30
2.6.1 ONIOM energy definition.....	30
2.6.2 Treatment of link atoms.....	32
2.7 Transition State Theory and Statistical Mechanics.....	34
2.8 Rate constant.....	36
2.9 Arrhenius equation.....	39
2.9.1 Arrhenius plot.....	40
CHAPTER III DETAILS OF THE CALCULATIONS.....	42
3.1 Computational method in acid-catalyzed system.....	42
3.2 Computational method in H-ZSM-5-catalyzed system.....	42
3.3 The transition state, equilibrium constant and rate constant calculations...	42
CHAPTER IV RESULTS AND DISCUSSION.....	45
4.1 Synthesis reaction for dimethyl ether.....	45
4.1.1 Acid-catalyzed system.....	45
4.1.2 H-ZSM-5-catalyzed system.....	49
4.1.2.1 Stepwise reaction mechanism.....	49
4.1.2.2 Concerted reaction mechanism.....	53
4.2 Synthesis reaction for diethyl ether.....	57
4.2.1 Acid-catalyzed system.....	57

	Page
4.2.2 H-ZSM-5-catalyzed system.....	60
4.2.2.1 Stepwise reaction mechanism.....	60
4.2.2.2 Concerted reaction mechanism.....	64
4.3 Synthesis reaction for ethylene.....	68
4.3.1 Acid-catalyzed system.....	68
4.3.2 H-ZSM-5-catalyzed system.....	71
4.3.2.1 Stepwise reaction mechanism.....	71
4.3.2.2 Concerted reaction mechanism.....	75
4.4 Arrhenius plot for diethyl ether and ethylene formation.....	79
4.5 Discussion.....	81
CHAPTER V CONCLUSIONS AND SUGGESTIONS.....	86
5.1 Acid-catalyzed system.....	86
5.2 H-ZSM-5-catalyzed system.....	87
5.3 Suggestions for further work.....	89
REFERENCES.....	90
APPENDIX.....	97
CURRICURUM VITAE.....	107

สถาบันวิทยบริการ
จุฬาลงกรณ์มหาวิทยาลัย

LIST OF FIGURES

Figure	Page
1.1 ZSM-5 zeolite pores and channels.....	4
1.2 Active sites of zeolite structure.....	4
1.3 Diagram depicting the three types of selectivity: (a) reactant, (b) product and (c) transition state shape selectivity.....	6
1.4 Diagram of the “surface” of a zeolite framework.....	7
1.5 The structure of ZSM-5 showing two different channel structures: (a) framework (b) channel system (the straight channel and the zigzag channels).....	8
2.1 The ONIOM extrapolation scheme for a molecular system partitioned into (left) and three (right) layers.....	31
2.2 Definition of different atom sets within the ONIOM scheme.....	33
2.3 Schematic illustration of reaction path.....	35
2.4 The difference between rate constant(k) and equilibrium constant (K).....	36
2.5 Energy profile E: Potential energy reaction coordinate: parameter hanging during the course of the reaction (as bond length or bond angle) Transition state: Maximum of energy in the path way.....	37
3.1 Atomic numbering for (a) methanol, (b) ethanol and (c) 56/5T cluster of H-ZSM-5 for two-layered(lines were atoms of low layered, balls were atoms of high layered).....	44
4.1 Reaction cycle of MeOH conversion to DME in acid-catalyzed system.....	47
4.2 Relative energy profile for MeOH conversion to DME in acid-catalyzed system.....	47
4.3 Stepwise mechanism of MeOH conversion to DME on 56/5T cluster model of H-ZSM-5.....	50
4.4 Relative energy profile for MeOH conversion to DME on H-ZSM-5 (modeled as 56/5T cluster) via stepwise mechanism.....	51

Figure	Page
4.5 Concerted mechanism of MeOH conversion to DME on 56/5T cluster model of H-ZSM-5.....	54
4.6 Relative energy profile for MeOH conversion to DME on H-ZSM-5 (modeled as 56/5T cluster) via concerted mechanism.....	55
4.7 Reaction cycle of EtOH conversion to DEE in acid-catalyzed system.....	58
4.8 Relative energy profile for EtOH conversion to DEE in acid-catalyzed system.....	58
4.9 Stepwise mechanism of EtOH conversion to DEE on 56/5T cluster model of H-ZSM-5.....	61
4.10 Relative energy profile for EtOH conversion to DEE on H-ZSM-5 (modeled as 56/5T cluster) via stepwise mechanism.....	62
4.11 Concerted mechanism of EtOH conversion to DEE on 56/5T cluster model of H-ZSM-5.....	65
4.12 Relative energy profile for EtOH conversion to DEE on H-ZSM-5 (modeled as 56/5T cluster) via concerted mechanism.....	66
4.13 Reaction cycle of EtOH conversion to ETL in acid-catalyzed system.....	69
4.14 Relative energy profile for EtOH conversion to ETL in acid-catalyzed system.....	69
4.15 Stepwise mechanism of EtOH conversion to ETL on 56/5T cluster model of H-ZSM-5.....	72
4.16 Relative energy profile for EtOH conversion to ETL on H-ZSM-5 (modeled as 56/5T cluster) via stepwise mechanism.....	73
4.17 Concerted mechanism of EtOH conversion to ETL on 56/5T cluster model of H-ZSM-5.....	76
4.18 Relative energy profile for EtOH conversion to ETL on H-ZSM-5 (modeled as 56/5T cluster) via concerted mechanism.....	77

Figure	Page
4.19 Arrhenius plot: temperature (T) dependence of the natural logarithm of the rate constants, $\ln k$, in the conversion of EtOH to DEE and ETL via concerted mechanism using H-ZSM-5 catalyst.....	80
4.20 In situ ^{13}C MAS NMR spectra of zeolite H-Y recorded during the formation of methoxy groups (56.2 ppm), methanol (50.2) and dimethyl ether (63.5) at different temperatures.....	84
4.21 The reaction of ^{13}C -enriched surface methoxy groups with $^{12}\text{CH}_3\text{OH}$ leading to $^{13}\text{CH}_3\text{O}^{12}\text{CH}_3$	84
4.22 Effect of reaction temperature on conversion of ethanol and selectivity of each product over H-ZSM-5 zeolite catalyst.....	85

LIST OF TABLES

Table	Page
4.1 Geometrical data based on the B3LYP/6-31G(d) calculations of intermediate and transition state in MeOH conversion to DME in acid-catalyzed system.....	48
4.2 Energies and thermodynamic quantities of MeOH conversion to dimethyl ether in acid-catalyzed system.....	48
4.3 Geometrical data based on the ONIOM(B3LYP/6-31G(d):AM1) calculations of intermediate and transition state in MeOH conversion to DME via stepwise mechanism in gas phase.....	51
4.4 Energies and thermodynamic quantities of the stepwise mechanism of the MeOH conversion to DME on the H-ZSM-5 catalyst.....	52
4.5 Geometrical data based on the ONIOM(B3LYP/6-31G(d):AM1) calculations of intermediate and transition state in MeOH conversion to DME via concerted mechanism in gas phase.....	55
4.6 Energies and thermodynamic quantities of the concerted mechanism of MeOH conversion to DME on the H-ZSM-5 catalyst.....	56
4.7 Geometrical data based on the B3LYP/6-31G(d) calculations of intermediate and transition state in EtOH conversion to DEE in acid-catalyzed system.....	59
4.8 Energies and thermodynamic quantities of EtOH conversion to diethyl ether in acid-catalyzed system.....	59
4.9 Geometrical data based on the ONIOM(B3LYP/6-31G(d):AM1) calculations of intermediate and transition state in EtOH conversion to diethyl ether via stepwise mechanism in gas phase.....	62
4.10 Energies and thermodynamic quantities of the stepwise mechanism of the EtOH conversion to DEE on the H-ZSM-5 catalyst.....	63
4.11 Geometrical data based on the ONIOM(B3LYP/6-31G(d):AM1) calculations of intermediate and transition state in EtOH conversion to diethyl ether via concerted mechanism in gas phase.....	66

Table	Page
4.12 Energies and thermodynamic quantities of the concerted mechanism of EtOH conversion to DEE on the H-ZSM-5 catalyst.....	67
4.13 Geometrical data based on the B3LYP/6-31G(d) calculations of intermediate and transition state in EtOH conversion to ETL in acid-catalyzed system.....	70
4.14 Energies and thermodynamic quantities of EtOH conversion to ETL in acid-catalyzed system.....	70
4.15 Geometrical data based on the ONIOM(B3LYP/6-31G(d):AM1) calculations of intermediate and transition state in EtOH conversion to ETL via stepwise mechanism in gas phase.....	73
4.16 Energies and thermodynamic quantities of the stepwise mechanism of the EtOH conversion to ETL on the H-ZSM-5 catalyst.....	74
4.17 Geometrical data based on the ONIOM(B3LYP/6-31G(d):AM1) calculations of intermediate and transition state in EtOH conversion to ETL via concerted mechanism in gas phase.....	77
4.18 Energies and thermodynamic quantities of the concerted mechanism of EtOH conversion to ETL on the H-ZSM-5 catalyst.....	78
4.19 Rate constants between intermediate(INT1) and the transition state(TS) for different temperature in DEE and ETL formation via concerted mechanism.....	79
4.20 Rate constants k (s^{-1}), equilibrium constants K and activation energies ΔE^\ddagger (kcal/mol) of the synthesis reactions for DME, DEE and ETL using hydronium ion catalyst and H-ZSM-5 zeolite catalyst.....	81

LIST OF ABBREVIATIONS

au	=	Atomic units
AM1	=	Austin model 1
B3LYP	=	Becke's three parameter hybrid functional using the LYP correlation function
BLYP	=	Beck-Lee-Yang-Parr function
BSSE	=	Basis set superposition error
CBS	=	Complete basis set
CP	=	Counterpoise method
DFT	=	Density functional theory
ECP	=	Effective core potential
E-ONIOM	=	Embedded ONIOM
FQEC	=	Full quantum embedded cluster
FT-IR	=	Fourier transform infrared
GGA	=	Generalized gradient approximation
HF	=	Hartree-Fock
IMOMO	=	Integrated molecular orbital-molecular orbital
IR	=	Infrared spectroscopy
IRC	=	Intrinsic reaction coordinate
kcal/mol	=	Kilocalorie per mole
KS	=	Kohn-Sham
LCAO	=	Linear combination of atomic orbitals
LDA	=	Local density approximation
LSD	=	Local spin density approximation
LYP	=	Lee-Yang-Parr functional
MAS NMR	=	Magic angle spinning nuclear magnetic resonance
MFI	=	Mobil-five
MM	=	Molecular mechanics
MNDO	=	Modified neglect of differential overlap
MO	=	Molecular orbital

MP2	=	The second-order Møller-Plesset perturbation theory
NMR	=	Nuclear magnetic resonance
ONIOM	=	Our own N-layered integrated molecular orbital and molecular mechanics
ppm	=	Parts per million
QM	=	Quantum mechanics
QM/MM	=	Quantum mechanical/molecular mechanical
QM-Pot	=	Combined quantum mechanics - interatomic potential functions
SBU	=	Secondary building unit
SCF	=	Self-consistent field
STO	=	Slater type orbital
STO-3G	=	Slater type orbital approximated by 3 gaussian type orbitals
STQN	=	Synchronous transit-guided quasi-newton
TPD	=	Temperature programmed desorption
UFF	=	Universal force field
UV	=	Ultraviolet
VWN	=	Vosko-Wilk-Nusair functional
XRD	=	X-ray diffraction
ZPE	=	Zero-point energy
ZSM-5	=	Zeolite Socony Mobil-5
MTG	=	Methanol to gasoline
BTG	=	Bioethanol to gasoline
DME	=	Dimethyl ether
DEE	=	Diethyl ether
ETL	=	Ethylene

CHAPTER I

INTRODUCTION

1.1 Background

Various reactions can be catalyzed by acid and base catalysts such as H_2SO_4 , H_3PO_4 , NaOH etc. However, these corrosive catalysts cause a number of problems concerning handling, safety, corrosion and waste disposal. Therefore, the conventional liquid-acid catalysts are progressively being replaced by heterogeneous catalysts. Many types of catalysts have been used for many reactions such as various metal oxides and various zeolites. In recent years, there have been considerable academic and industrial research efforts carried out in the field of zeolite catalysis.

The few last decade up to present, zeolites have played very important role in the petroleum and petrochemical industries. They have been known as the one of the most important heterogeneous catalysts. [1-4] Therefore, zeolites were widely studied for their acidic properties of Brønsted acid sites [5-6] using several techniques. [7-21] ZSM-5 (Zeolite Socony Mobil-5) is one of the most useful catalysts that have been widely used in the petroleum and petrochemical industries. ZSM-5 is a representative member of a new class of high-silica zeolites having considerable significance as catalyst materials. Examples of their uses include the conversion of methanol to gasoline (MTG), dewaxing of distillates, and the interconversion of aromatic compounds. Proton-exchanged zeolites present high acidity, and so, they are commonly used in acid-catalyzed reactions such as double bond migration, skeletal reorganization, or aldol condensation. [1, 2]

To elucidate the information of the zeolite structure and the chemistry of the active site of zeolitic catalysts, the wide range of experimental techniques have been used such as UV, IR, NMR, XRD and TPD techniques. As an alternative, theoretical methods and computational technologies have been developed as a practical tool to retrieve information of the system at the molecular level. Theoretical interest in zeolites originates from the need to understand their function as catalysts, adsorbents, and ion-exchangers, and from a vision of making improved materials by design. This is not

possible without knowledge of the relationship between structure, properties, and reactivity. Although numerous experiments have been made many questions still remain unsolved. The crystal structure of certain complex solids can be solved only with the aid of modeling techniques. Numerous theoretical models, including the periodic calculations, have been proposed to study the crystalline zeolite. Such a large deviation indicates an important effect of the extended framework in stabilizing the adsorption complex. To accurately include the effects of the extended zeolite framework on the catalytic properties, one can employ the periodic electronic structure methods such as the periodic density functional theory (DFT) methodology. However, due to the large unit cells of typical zeolites, such calculations are often computationally unfeasible. On the other hand, the hybrid methods, such as the embedded cluster or combined quantum mechanics/molecular mechanics (QM/MM) methods, as well as the more general ONIOM (Our-own-N-layer Integrated molecular Orbital + molecular Mechanics) [22] provide a cost effective computational strategy for including the effects of the zeolite framework.

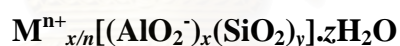
1.2 Zeolite

Zeolite was discovered in 1756 by the Swedish mineralogist, Boron Axel F. Cronstrdt, as the natural minerals. The word “zeolite” is Greek in origin, derived from the words “zein” and “lithos” meaning “to boil” and “rock”. Many new types of natural minerals have been discovered and a large number of synthetic zeolites have been developed for specifically commercial proposes. The synthetic zeolite was interested in the application of shape selective zeolite catalyst in the petrochemical companies such as Union Carbide and Mobil. In the 1950s and early 1960s, Union Carbide Company made several discoveries which proved to be of great economic significance and propelled them to the forefront of zeolite science. Milton and Breck of the Linde division of the Union Carbide company, over a period of 5 years, developed and characterized three novel zeolites classified as types A, X and Y, which have become 3 of the most profitable synthetic zeolites. In 1962 Mobil Oil introduced the use of synthetic of zeolite X as a cracking catalyst. In 1969 Grace described the first modification chemistry based on steaming zeolite Y to form an “ultrastable” Y. In 1967-1969 Mobil Oil reported the synthesis of the high silica zeolites beta and ZSM-5. In 1974 Henkel introduced zeolite A in detergents as a

replacement for the environmentally suspect phosphates. By 1977 industry-wide 22,000 tons of zeolite Y was in use in catalytic cracking. In 1977 Union Carbide introduced zeolite for ion-exchange separations.

1.2.1 Structure of zeolites

Zeolites are three-dimensional, microporous, crystalline aluminosilicate materials constructed from tetrahedral units, TO_4 , such as $[\text{SiO}_4]^{4-}$ and $[\text{AlO}_4]^{5-}$. Each of tetrahedral centers is connected via oxygen atom formed Si-O-Si and Si-O-Al bridges. These tetrahedra are linked together by corner sharing of Si or Al atoms in various ways, forming a secondary building unit. Most zeolite frameworks can be generated from several different SBU. A secondary building unit consists of selected geometric groupings of those tetrahedra, which can be used to describe all of known zeolite structures. The various types of zeolites are built up from different composition and framework to generate different pores and channels which demonstrate the ability to prevent or allow the program of a reaction (Fig. 1.1). A representative unit cell formula for the composition of a zeolite is:



where M is the exchangeable cation of valence n; y/x is the Si/Al molar ratio, and is equal to or greater than 1 because Al^{3+} does not occupy adjacent tetrahedral sites, otherwise the negatively charged units next to each other will be obtained; and z is the number of water molecules located in the channels and cavities inside a zeolite.

Exceptions of type of zeolites, the active site region also shows the dramatic effect in the properties of zeolites. The difference of oxidation state of Si^{4+} and Al^{3+} in zeolites is the crucial reason for the active site occurring. The charges imbalance occurs when the Si^{3+} substituted by Al^{4+} , and to maintain the system natural, each $[\text{AlO}_4]^{5-}$ tetrahedral center needs a balancing positive charge such as proton or monovalence cation (Fig. 1.2). These compensation species present the specific active sites of zeolite in various applications. If the charge compensating cation is H^+ , a bridged hydroxyl group, (Si-O(H)-Al), is formed, which functions as a strong Brønsted acid site. Due to these acid sites, zeolites are solid acids and are used as catalysts. The catalytic activity of zeolites is often related to strength of the acid sites, which

depends on chemical composition and topology of zeolite frameworks. There are numerous naturally occurring and synthetic zeolites. However, most zeolites used commercially are produced synthetically, each with a unique structure. Zeolites have void and space (cavities or channels) that can host cations, water or other molecules.

Zeolites are widely used industrially as a catalyst for a variety of reactions and separation processes. The active site of zeolite also plays a crucial role in catalyzing the reactions.

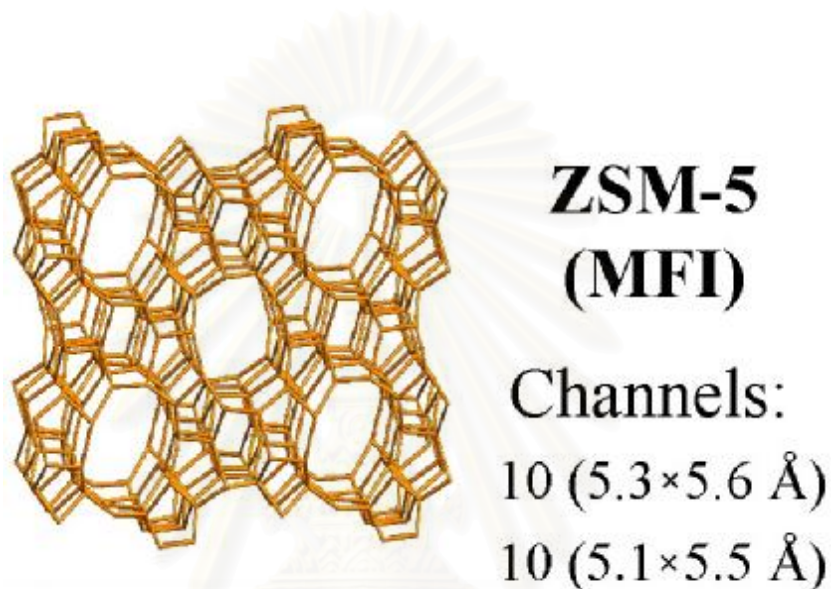


Figure 1.1 ZSM-5 zeolite pores and channels.



Figure 1.2 Active sites of zeolite structure.

1.2.2 Properties of zeolites [23]

1.2.2.1 Shape and size selectivity

Shape and size selectivity plays a very important role in catalysis. Highly crystalline and regular channel structures are among the principal features that molecular sieves used as catalysts offer over other materials.

There are three types of shape selectivity: reactant shape selectivity, product shape selectivity, and transition-state shape selectivity. These types of selectivity are depicted in Fig. 1.3. Reactant shape selectivity results from the limited diffusion of some of the reactants, which cannot effectively enter and diffuse inside the crystal. Product shape selectivity occurs when slowly diffusing product molecules cannot rapidly escape from the crystal, and undergo secondary reactions. Restricted transition-state shape selectivity is a kinetic effect arising from the local environment around the active site, i.e. the rate constant for a certain reaction mechanism is reduced if the necessary transition state is too bulky to form readily.

The critical diameter (as opposed to the length) of the molecules is important in predicting shape selectivity. However, molecules are deformable and can pass through smaller opening than their critical diameter. Hence not only size but also the dynamics and structure of the molecules must be taken into account.

An equivalent to activation energy exists for the diffusion of molecules inside the molecular sieve because the temperature-dependent translational energy of molecule (as move through the force fields in the pores) must increase significantly as the dimensions of the molecular configuration approach the void dimensions of the crystal. It should be noted that the effective diffusivity varies with molecular type; adsorption affinity affects diffusivity, and rapidly reacting molecules (such as olefins) show diffusion mass transfer limitations inside the structure due to their extreme reactivity.

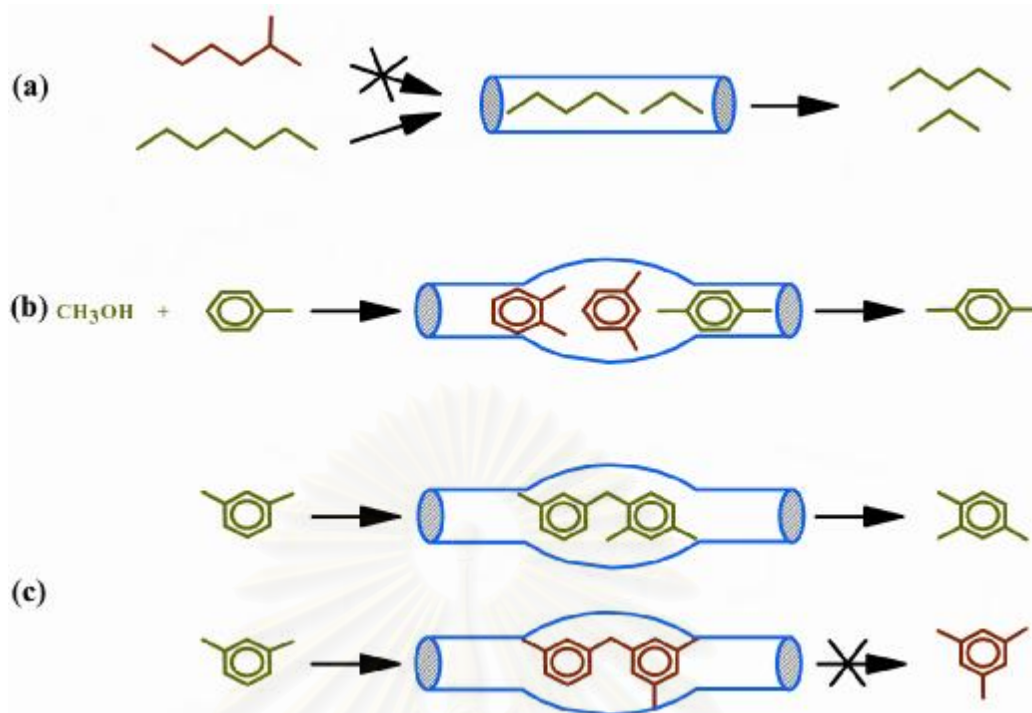


Figure 1.3 Diagram depicting the three types of selectivity: (a) reactant, (b) product and (c) transition state shape selectivity.

The effective size and relative accessibility of the pore and cavities can be altered by partially blocking the pore and/or by changing the molecular sieve crystal size. The effect of shape selective are especially induced by the above two methods when the diffusivities of these species differ significantly.

1.2.2.2 Acid sites (acidity)

All of the variation pretreatment conditions as well as synthesis and post-treatments (hydrothermal, thermal and chemical), affect the ultimate acidity an activity observed in the zeolite molecular sieves. Both Brønsted and Lewis acid sites are exhibited in these materials, with assertions by various investigations that:

1. Brønsted acid sites are the active center.
2. Lewis acid sites are the active center.
3. Brønsted and Lewis acid sites together act as the active centers.
4. Cations or the other types of sites in small concentrations act in the conjunction with the Brønsted/Lewis acid sites to function as the active center.

Strong electric fields in the zeolites arise from the various charge species. This is Brønsted/Lewis acidity model usually employed to describe the active sites of molecular sieves. Fig. 1.4 depicts a zeolite structure with Brønsted and Lewis acid sites.

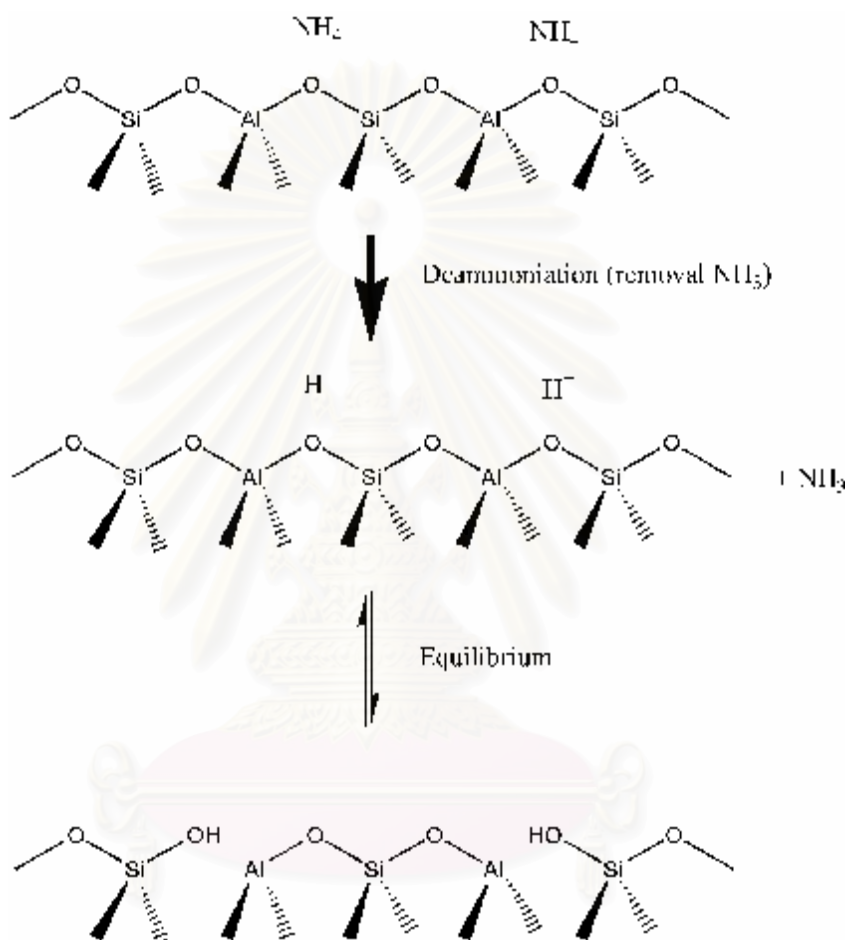


Figure 1.4 Diagram of the “surface” of a zeolite framework.

The ammonium-form zeolite was converted to the hydrogen-form one by calcinations at elevated temperature. The thermal treatment causes removal of NH_3 from the cation sites and leaves protons as the balancing cations. The aluminum sites with its associated bridged Si-O-H are a classical Brønsted acid. The Brønsted acid site has been proposed to exist in equilibrium with the so call Lewis acid site, the trigonally coordinated aluminum.

1.2.3 ZSM-5 (Zeolite Socony Mobil-5)

ZSM-5 (Zeolite Socony Mobil-5 is discovered by Mobil Oil Company) is a commercial name of MFI zeolite with high silica to alumina ratio, and H-ZSM-5 is ZSM-5, which is compensated negative charge by H^+ . The dimensions of the pores and channels are of the order of a nanometer ($1 \text{ nm} = 10 \text{ \AA}$). In some cases, the channels of the internal surface form intersections that are considerably larger than their channels. For example, the diameter of the roughly cylindrical pores and channels of zeolites having the MFI topology as ZSM-5 are about 5 \AA (Fig. 1.5), but the diameter of the roughly spherical intersection is about 9 \AA which act as nanoscopic catalytic reactors. ZSM-5 has two types of channel, both formed by 10-membered oxygen rings. The first of these channel is straight channel and elliptical in cross section ($5.1 \times 5.5 \text{ \AA}$), the second pores is zigzag or sinusoidal channels and are circular ($5.4 \times 5.6 \text{ \AA}$) in cross section. The intersection of both channels is called intersection channel.

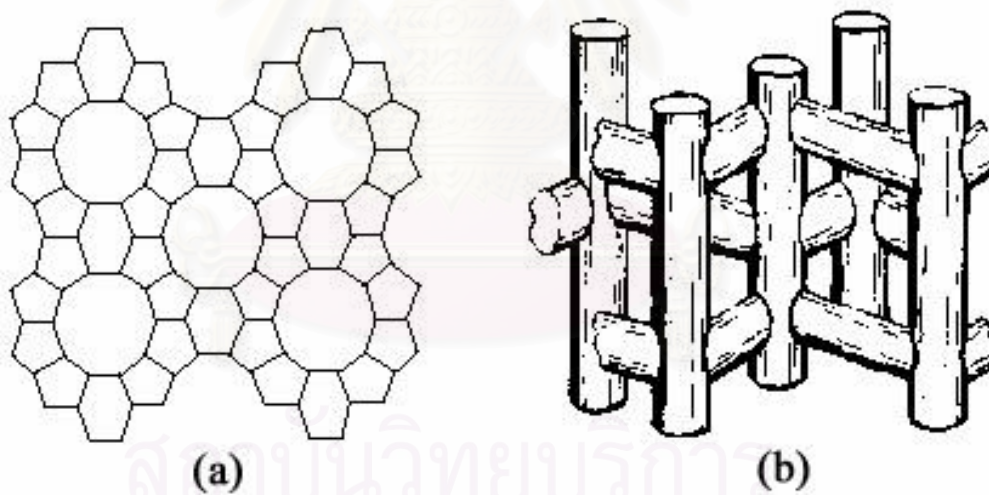


Figure 1.5 The structure of ZSM-5 showing two different channel structures: (a) framework (b) channel system (the straight channel and the zigzag channels).

1.3 The methanol-to-gassoline (MTG)

The methanol-to-gasoline, MTG, process is one of the most successful routes for the acid zeolite catalyzed conversion of methanol to synthetic fuels, say hydrocarbons, in the gasoline boiling range (30-200 °C). A large variety of different experiments that methanol is first dehydrated to dimethyl ether and that an equilibrium mixture of methanol and dimethyl ether is then converted to olefins, aliphatics, and aromatics up to C₁₀. The mechanism of methanol dehydration and, especially, the formation of the first C-C bond and the nature of the intermediates involved are still not fully understood.

1.4 The bioethanol-to-gassoline (BTG)

Conversion of methanol and ethanol to gasoline and other hydrocarbons has received wide attention due to the global energy crisis and the heavy demand for hydrocarbons. The ethanol obtained by fermentation of vegetable biomass and agricultural residues (a renewable and relatively abundant raw material) is an interesting alternative in developing countries wishing to reduce their dependency on petroleum as well as revitalize both agricultural activity and the local fermentation industry. Fermentation of biomass to ethanol results in mixtures containing about 95% water and 5% ethanol. Methods for separating water including distillation or extraction with liquid solvents or with CO₂, azeotropic distillation to obtain absolute ethanol are energy-consuming and expensive. Catalytic transformation of alcohol into hydrocarbons is useful for petrochemical raw materials or as a motor fuel. The process is called BTG (bioethanol-to-gasoline), one major product is ethylene. Several catalysts were developed including zeolites.

1.5 Literature reviews

1.5.1 Experimental study

In 2007, Varislia *et al.* [24] studied dehydration reaction of ethanol in a temperature range of 140–250 °C with three different heteropoly acid catalysts (HPA), namely tungstophosphoric acid (TPA), silicotungstic acid (STA) and molybdophosphoric acid (MPA). Very high ethylene yields over 0.75% wt/wt obtained at 250 °C with TPA was highly promising. At temperatures lower than 180 °C the main product was diethyl ether (DEE). Presence of water vapor was shown to cause some decrease of catalyst activity. Results showing that product selectivities did not change much with the space time in the reactor indicated two parallel routes for the production of ethylene and diethyl ether. Among the three HPA catalysts, the activity trend was obtained as STA>TPA>MPA.

In 2007, Bjørgen *et al.* [25] studied the reaction mechanism with respect to both catalyst deactivation and product formation in the conversion of methanol to hydrocarbons over zeolite H-ZSM-5. The reactivity of the organics residing in the zeolite voids during the reaction was assessed by transient ¹²C/¹³C methanol-switching experiments. In contrast to previously investigated catalysts (H-SAPO-34 and H-beta), hexamethylbenzene is virtually unreactive in H-ZSM-5 and is thus not a relevant reaction intermediate for alkene formation. However, the lower methylbenzenes are reaction intermediates in a hydrocarbon pool-type mechanistic cycle and are responsible for the formation of ethene and propene. An additional reaction cycle not applicable for ethene also must be taken into account. The C₃+ alkenes are to formed through rapid alkene methylation and cracking steps to a considerable extent; thus, methanol is converted to hydrocarbons according to two catalytic cycles over H-ZSM-5. Moreover, in contrast to what occurs for large-pore zeolites/zeotypes, molecules larger than hexamethylbenzenes are not built up inside the H-ZSM-5 channels during deactivation. Thus, deactivation is explained by coke formation on the external surface of the zeolite crystallites only. This is a plausible rationale for the superior lifetime properties of H-ZSM-5 in the methanol-to-hydrocarbon reaction.

In 2007, Timur et al. [26] studied the dehydration of ethanol and methanol to diethyl ether and dimethyl ether, respectively, using acidic catalysts, such as nafion, Al_2O_3 , and heteropolyacids, may be used for. It was also reported that H-ZSM-5 showed good activity for vapor phase dehydration of methanol to dimethyl ether in the presence of water vapor. The activities of Cs salt, and titania-supported molybdophosphoric and molybdovanadophosphoric acid catalysts in the dehydration of alcohols were also illustrated in the literature. Generally speaking, acid catalysts show high activity in the dehydration of ethanol to diethyl ether and ethylene, while basic catalysts act to dehydrogenate ethanol to produce acetaldehyde. In the dehydration reaction, alcohols are thought to adsorb on an acid site, forming ethoxy or methoxy species in diethyl ether or dimethyl ether synthesis, respectively. The work by Damyanova et al. indicated that the incorporation of Ni into the heteropolyacid structure improved the dehydrogenation selectivity by decreasing the dehydration selectivity of methanol.

In 2006, Arenamnarta and Trakarnpruk et al. [27] studied the aqueous ethanol conversion on dealuminated mordenite (DM) and a series of DM/metal catalysts prepared by impregnation (IMP) and solid-state ion exchange (SSIE). The catalysts were characterized by X-ray fluorescence (XRF), X-ray diffraction (XRD), Fourier transform infrared spectroscopy (FT-IR), nitrogen adsorption method (BET). The conversion of aqueous ethanol (10.0%) on mordenite/metal catalysts was compared at temperature of 350°C . reaction time of 1 h, WHSV (weight hourly space velocity) of 1 h^{-1} and catalyst weight of 1 g. The product is mainly ethylene with small quantity of other light olefins. At higher temperature (550°C) methane was formed as a result of decomposition reaction. Among several metals (Zn, Mn, Co, Rh, Ni, Fe and Ag) which were incorporated onto the mordenite to prepare DM/single and mixed metal catalysts tested in this work, it was found that DM/Zn and DM/Zn-Ag catalysts prepared by impregnation method gave the highest selectivity to ethylene. For DM/Ni catalyst, it showed high selectivity to ethane due to its hydrogenation ability.

In 2006, Wang *et al.* [28] studied mechanistic investigations of the methanol-to-olefin (MTO) process by in situ solid-state NMR spectroscopy, mainly performed under continuous-flow and stopped-flow conditions. During methanol conversion on the silicoaluminophosphate H-SAPO-34 under continuous-flow conditions, a hydrocarbon-pool consisting of a mixture of C₆–C₁₂ olefins and aromatics was found. The hydrocarbon-pool mechanism was verified as the dominating route in the MTO process under steady-state conditions. By in situ MAS NMR experiments under continuous-flow conditions it could be demonstrated that methanol molecules are added to the hydrocarbon-pool and light olefins are split off as reaction products. The reactivity of surface methoxy groups in the MTO process were evidenced by the reaction with different probe molecules. By the new developed in situ MAS NMR-UV/vis technique, the initial formation of the hydrocarbon-pool during the induction period was investigated.

In 2005, Inaba *et al.* [29] studied the bio-ethanol conversion to hydrocarbons over zeolite catalysts was investigated. Among the zeolites with no metal loaded, H-ZSM-5 (Si/Al₂ = 29) zeolite had especially high activity for the formation of BTX compounds (benzene, toluene, xylenes), while other zeolites exclusively formed ethylene. The addition of Ga and Pd on H-ZSM-5 support resulted in the increased formation of BTX. The addition of Fe and Ni as well as Cr and some noble metals raised the formation of C₃₊ olefins in some degree. Carbon deposition on catalyst occurred during the reaction. In general, the catalysts yielding BTX in high selectivity deposit large amount of carbon, except for the cases of zeolites other than H-ZSM-5. Among the metal catalysts supported on H-ZSM-5 zeolite, Cr, Fe and Au catalysts can inhibit carbon deposition in some degrees and the catalytic activity for the formation of BTX was kept constant.

In 2004, Jiang *et al.* [30] studied methanol dehydration to dimethyl ether over ZSM-5 zeolites and compared with that of γ -Al₂O₃. Although the catalytic activity was decreased with an increase in silica/alumina ratio, the dimethyl ether selectivity increased. H-ZSM-5 and NaH-ZSM-5 zeolites were more active for conversion of methanol to dimethyl ether than γ -Al₂O₃. Na⁺ ion-exchanged H-ZSM-5 (NaH-ZSM-5) shows higher dimethyl ether selectivity than H-ZSM-5 due to the selective removal of strong acid sites.

In 2004, Fua *et al.* [31] studied the nature, strength and number of surface acid sites of H-ZSM-5, steam de-aluminated H-Y zeolite (SDY), Al_2O_3 and $\text{Ti}(\text{SO}_4)_2/\text{Al}_2\text{O}_3$ catalysts for the dehydration of methanol to dimethyl ether using microcalorimetry and infrared spectroscopy for ammonia adsorption. The conversion of isopropanol was also performed as a probe reaction to characterize the acid strength. The H-ZSM-5 and SDY possessed strong Brønsted acidity and exhibited high activity for the conversion of methanol to dimethyl ether at relatively low temperatures, but they did not seem to be suitable as the dehydration component of the hybrid catalyst for the direct synthesis of dimethyl ether from syngas since the two zeolite catalysts produced hydrocarbons and coke from methanol at temperatures higher than 513 K. The coke was serious over the two zeolite catalysts at 553 K. The dehydration of methanol to dimethyl ether on Al_2O_3 was found to be low at the temperatures below 573K though the dimethyl ether selectivity is high. The modification of the Al_2O_3 by $\text{Ti}(\text{SO}_4)_2$ greatly enhanced the surface Brønsted acidity and also the reaction activity for the dehydration of methanol to dimethyl ether. In addition, no detectable hydrocarbon by-products and coke were formed on the $\text{Ti}(\text{SO}_4)_2/\text{Al}_2\text{O}_3$ catalyst in the temperature range of 513–593 K. Thus, the Brønsted acid sites with suitable strength may be responsible for the effective conversion of methanol to dimethyl ether with high stability.

In 2000, Wetwatana [32] studied dehydration of ethanol to ethylene on modified ZSM-5 zeolites. Containing a iron metal was investigated in this research. The catalyst were prepared by ion exchange method and rapid crystallization method. It has been found that the appropriate reaction temperature, the percentage of Fe loading and GHSV over Fe-ZSM-5 catalyst were 600 °C, 5% by weight and 2000 h^{-1} , respectively. The main hydrocarbon products from this reaction were ethylene and diethyl ether. The selectivity to ethylene was 83% at 95% ethanol conversion. It was suggested that the formation of ethylene possible proceeded via diethyl ether intermediate. With the effect of space velocity of ethanol was decreased from 6000 h^{-1} to 2000 h^{-1} , resulted increase selectivity to ethylene. Comparison between 5% Fe-ZSM-5 prepared by ion-exchange method and rapid crystallization method. It has been found that 5% Fe-ZSM-5 prepared by ionexchange method resulted in the higher selective than 5% Fe-ZSM-5 prepared by rapid crystallization method.

In 2000, Phillips and Datta [33] studied the dramatic rise in the use of ethers as fuel oxygenates, an alternative process for the production of ethyl *tert*-butyl ether (ETBE) based solely on biomass-derived ethanol feedstock is proposed. The first step in this process is ethanol dehydration on H-ZSM-5 to produce ethylene. Hydrous ethanol is a particularly attractive feedstock for this step since the production of anhydrous ethanol is very energy/cost intensive. In fact, the presence of water in the ethanol feed enhances the steady-state activity and selectivity of H-ZSM-5 catalysts. Reaction kinetic data were collected in a microreactor at temperatures between 413 and 493 K, at ethanol partial pressures of less than 0.7 atm, and at water feed molar ratios of less than 0.25. A sharp initial decline in catalyst activity observed within a few minutes on stream was attributed to the formation of “low-temperature coke” from ethylene oligomerization. Deactivation occurred at a much slower rate after 100 min on stream, allowing near-steady-state data to be collected. Water in the ethanol feed enhanced the steady-state catalytic activity and ethylene selectivity by moderating the acidity of the catalytic sites, resulting in less extensive deactivation due to coking.

In 1999, Carlson *et al.* [34] studied the conversion of methanol to gasoline (MTG) range hydrocarbons on zeolite catalyst HZSM-5 extensively using solid-state NMR. We have studied the reaction under batch and flow conditions using an isolated flow variable-temperature (VT) MAS NMR probe. This probe was developed to study heterogeneous catalysis reactions in situ at temperatures greater than 300°C with reactant flow. In the batch studies, when ¹³C-labeled methanol was adsorbed on zeolite HZSM-5, sealed, and heated to 250°C, dimethyl ether was formed. Two-dimensional exchange NMR shows that dimethyl ether was in equilibrium with methanol at 250°C. When ¹³C-methanol was flowed over H-ZSM-5 at temperatures 200°C, only dimethyl ether was observed. Between 160°C and 200°C, both methanol and dimethyl ether were observed. The flow results are significant in that they suggest that there is no equilibrium between methanol and dimethyl ether in the catalyst at high temperatures, and that surface methoxy groups do not exist on the catalyst at high temperatures.

1.5.2 Computational studies

In 2006, Dulya and Ruangpornvisuti [35] studied the geometry optimizations of all involved species in conversion of aldehydes to α -hydroxy phosphonate derivatives using the B3LYP/6-31G(d) and B3LYP/6-311+G(d,p) methods. Mechanisms of these conversion reactions in acid-catalyzed solutions in term of energetic and thermodynamic properties were reported. Rate constants at 298.15 K, determining-step, in gaseous and aqueous phase for both acetaldehyde and *i*-propyl aldehyde conversions were obtained.

In 2005, Rattanasumrit and Ruangpornvisuti [36] studied the conversions of acetaldehyde to hydroxyethylene, acetone to 2-hydroxypropylene, butanone to 2-hydroxybutene and 2-pentanone to 2-hydroxypentene catalyzed by H-ZSM-5 using quantum chemical methods. Geometry optimizations of the local structures of species reacting with H-ZSM-5 zeolite using 3T-DFT and 5T-DFT cluster models computed at B3LYP/6-31G(d) level and 50/3T-ONIOM2 cluster model computed at ONIOM(B3LYP/6-31G(d):AM1) level have been carried out. Three steps of the reaction mechanism were found and thermodynamic properties of each reaction steps and equilibrium constants of overall reaction have been obtained. The overall reaction of the conversion for all systems is endothermic reaction. The activation energies of all conversion reactions derived at three different methods are reported.

In 2004, Zheng and Blowers [37] studied the transition state structures and activation energies of ethane cracking, hydrogen exchange, and dehydrogenation reactions catalyzed by a zeolite model cluster using ab initio methods. The reactant and transition state structures are optimized by HF and MP2 methods and the final energies are calculated using a complete basis set composite energy method. The computed activation barriers are 71.39 kcal/mol for cracking, 31.39 kcal/mol for hydrogen exchange and 75.95 kcal/mol for dehydrogenation using geometries optimized with the MP2 method. The effects of cluster size and acidity on the reaction barriers were also investigated. The relationships between activation barriers and zeolite deprotonation energies for each reaction are proposed so that accurate activation energies can be obtained when using different zeolites as catalysts.

In 2002, Govind *et al.* [38] studied mechanisms in the methanol to gasoline (MTG) process in a zeolite catalyst using density functional theory (DFT) calculations. Various reaction paths and energy barriers involving C-O bond cleavage and the first C-C bond formation are investigated in detail using all-electron periodic supercell calculations and recently developed geometry optimization and transition state search algorithms. The formation of ethanol and have identified a different mechanism than previously reported, a reaction where water does not play any visible role. Contrary to recent cluster calculations were not able to find a stable surface yield structure. However, a stable yield structure built into the zeolite framework was found to be possible, albeit a very high reaction barrier.

In 2000, Vollmer and Truong [39] studied the mechanism of hydrogen exchange of methane with H-Zeolite Y using ab initio embedded cluster. They found that inclusion of the Madelung field stabilizes the formation of a carbonium-like transition state, and consequently reduces the reaction barrier by 17-23 kJ/mol, relative to the corresponding bare cluster predictions. Using the CCSD(T)/6-31G(d,p) level of theory, including zero-point energy (-10 kJ/mol) and tunneling (1.6 kJ/mol) corrections, the activation energy is predicted to be 124 and 137 kJ/mol for hydrogen exchange from two different binding sites. These predictions agree well with the experimental estimate of 122-130 kJ/mol. It is necessary to include the Madelung potential to find preferential proton siting at site O1 versus site O4, in agreement with experimental observation.

In 1997, Gale and Payne [40] studied the stability of various possible reactive intermediates resulting from the initial adsorption of methanol in the zeolite chabazite using nonlocal periodic density functional calculations. The formation of dimethyl ether has been examined both for pathways via framework coordinated methyl groups and by direct condensation with the framework acting as a solvent. Both are found to offer a reasonable energetic route to dimethyl ether, which is only hydrogen bonded in its bound state, proton transfer being disfavored. No evidence is found for the existence of carbenes or ylide species as local minima within the microporous environment, though trimethyl oxonium is stable with respect dimethyl ether and a framework methoxy group.

1.6 Objectives

In this work, conversion reactions of methanol to dimethyl ether, ethanol to diethyl ether and ethanol to ethylene in gas phase catalyzed by acid catalyst and H-ZSM-5 zeolite catalyst have been theoretically studied employing the calculations of using B3LYP/6-31G(d) method for acid-catalyzed system and ONIOM(B3LYP/6-31G(d):AM1) method for H-ZSM-5-catalyzed system (H-ZSM-5 zeolite 56/5T cluster models catalyst) in gas phase and temperature 298.15 K. The energetic and thermodynamic quantities of catalytic reactions for each models have been determined via their transition structures.

The goals of this study are, firstly, to analyze the catalytic effect of hydronium and H-ZSM-5 on conversion of alcohols to ethers and ethylene and compare its pathway of the conversion, to discuss the behavior of rate-constant and equilibrium-constant of the reactions and the activation energies.

This work has used density functional theory to obtain reactants, adsorption complexes, transition states, and products involved in all paths of dimethyl ether formation, diethyl ether formation and ethylene formation. Different conformations have been used to represent the acidic zeolite. Adsorption energies and activation barriers give the possibility for a comparison between the different studied paths. Additional calculation of thermodynamics properties allows an analysis of the equilibrium constants and the rate constants. Lastly, the temperature change effects over the rate constant between the conversion of ethanol to diethyl ether and ethylene via the concerted mechanisms in H-ZSM-5 zeolites are presented.

สถาบันวิทยบริการ
จุฬาลงกรณ์มหาวิทยาลัย

CHAPTER II

THEORY OF CALCULATION

There are three broad areas within computational chemistry devoted to the structure of molecules and their reactivity: molecular mechanics, electronic structure methods (also referred to as quantum mechanics), and density functional methods. The basic types of calculation includes computing the energy or properties related to energy of a particular molecular structure; performing geometry optimizations; and, computing the vibrational frequencies of molecules resulting from interatomic motion within the molecule. This chapter will explore these methods and their limitations to highlight the choices made for the methods employed in this research.

2.1 Quantum mechanics (QM)

The word *quantum* comes from Latin (*quantus*, “how much?”, plural *quanta*) and was first used in our sense by Max Planck in 1900, as an adjective and noun, to denote the constrained *quantities* or amounts in which energy can be emitted or absorbed. Although the term *quantum* mechanics was apparently first used by Born (of the Born-Oppenheimer approximation) in 1924, in contrast to classical mechanics, the matrix algebra and differential equation techniques that we now associate with the term were presented in 1925 and 1926.

“Mechanics” as used in physics is traditionally the study of the behavior of bodies under the action of forces like, e.g. gravity (celestial mechanics). Molecules are made of nuclei and electrons, and quantum chemistry deals, fundamentally, with the motion of electrons under the influence of the electromagnetic force exerted by nuclear charges.

Quantum mechanics (QM) is the correct mathematical description of the behavior of electrons and thus of chemistry. In theory, QM can predict any property of an individual atom or molecule exactly. In practice, the QM equations have only been solved exactly for one electron systems. A myriad collection of methods has been developed for approximating the solution for multiple electron systems. These approximations can be

very useful, but this requires an amount of sophistication on the part of the researcher to know when each approximation is valid and how accurate the results are likely to be.

The QM was formulated independently by Erwin Schrödinger and Werner Heisenberg in 1925. Schrödinger's method is formulated in terms of the partial differential equations used to describe waves (hence its name of wave mechanics). Heisenberg's method used matrices and at first glance appears very different from Schrödinger's. It was shown, however, that the two ways are mathematically equivalent. Chemistry customarily uses the wave mechanics method to develop its treatment of quantum mechanics. I will start our formulation of quantum mechanics with an introduction to wave mechanics.

The solutions to the Schrödinger equation are called wave functions and these wave functions give a complete description of any system. The Schrödinger equation can not be derived, instead it is postulated, that is, assumed to be true for the purposes of our reasoning. It is in fact the fundamental postulate of quantum mechanics.

2.2 Solution of the Schrödinger Equation of Molecular Systems

2.2.1 The Schrödinger Equation

The ultimate goal of most quantum chemical approaches is the approximate solution of the time-independent, non-relativistic Schrödinger equation:

$$\hat{H}\psi_i(\vec{x}_1, \vec{x}_2, \dots, \vec{x}_N, \vec{R}_1, \vec{R}_2, \dots, \vec{R}_M) = \epsilon_i \psi_i(\vec{x}_1, \vec{x}_2, \dots, \vec{x}_N, \vec{R}_1, \vec{R}_2, \dots, \vec{R}_M) \quad (1)$$

where \hat{H} is the Hamilton operator for a molecular system consisting of M nuclei and N electrons in the absence of magnetic or electric fields. \hat{H} is a differential operator representing the total energy:

$$\hat{H} = -\frac{1}{2} \sum_{i=1}^N \nabla_i^2 - \frac{1}{2} \sum_{A=1}^M \frac{1}{M_A} \nabla_A^2 - \sum_{i=1}^N \sum_{A=1}^M \frac{Z_A}{r_{iA}} + \sum_{i=1}^N \sum_{j>i}^N \frac{1}{r_{ij}} + \sum_{A=1}^M \sum_{B>A}^M \frac{Z_A Z_B}{R_{AB}} \quad (2)$$

Here, A and B run over the M nuclei while i and j denote the N electrons in the system. The first two terms describe the kinetic energy of the electrons and nuclei

respectively, where the Laplacian operator ∇_q^2 is defined as a sum of differential operators (in cartesian coordinates):

$$\nabla_q^2 = \frac{\partial^2}{\partial x_q^2} + \frac{\partial^2}{\partial y_q^2} + \frac{\partial^2}{\partial z_q^2} \quad (3)$$

M_A is the mass of nucleus A in multiples of the mass of an electron. The remaining three terms define the potential parts of the Hamiltonian and represent the attractive electrostatic interaction between the nuclei and the electrons and the repulsive potential due to electron-electron and nucleus-nucleus interactions, respectively. R_{pq} (and similarly R_{qp}) is the distance between the particles p and q, i.e., $r_{pq} = |\vec{r}_p - \vec{r}_q|$. $\psi_j(\vec{x}_1, \vec{x}_2, \dots, \vec{x}_N, \vec{R}_1, \vec{R}_2, \dots, \vec{R}_M)$ stands for the wave function of the i 'th state of the system, which depends on the $3N$ spatial coordinates $\{\vec{r}_j\}$, and the N spin coordinates $\{S_j\}$ of the electrons, which are collectively termed $\{\vec{\lambda}_j\}$, and the $3M$ spatial coordinates of the nuclei, $\{\vec{R}_j\}$. The wave function ψ_j contains all information that can possibly be known about the quantum system at hand. Finally, E_j is the numerical value of the energy of the state described by ψ_j .

All equations given in this text appear in a very compact form, without any fundamental physical constants. We achieve this by employing the so-called system of atomic units, which is particularly adapted for working with the atoms and molecules. In this system, physical quantities are expressed as multiples of fundamental constants and, if necessary, as combinations of such constants. The mass of an electron, m_e , the modulus of its charge, $|e|$, Planck's constant h divided by 2π , \hbar , and $4\pi\epsilon_0$, the permittivity of the vacuum, are all set to unity. Mass, charge, action etc. are then expressed as multiples of these constants, which can therefore be dropped from all equations [41].

2.2.2 Born-Oppenheimer Approximation

The Schrödinger equation can be further simplified if we take advantage of the significant differences between the masses of nuclei and electrons. Even the lightest of all nuclei, the proton (${}^1\text{H}$), weighs roughly 1800 times more than an electron. Thus, the nuclei move much slower than the electrons. The practical consequence is that we can at least to a good approximation take the extreme point of view and consider the electrons as moving in the field of fixed nuclei. This is the famous *Born-Oppenheimer* or clamped-nuclei approximation. If the nuclei are fixed in space and do not move, their kinetic energy is zero and the potential energy due to nucleus-nucleus repulsion is merely a constant. Thus, the complete Hamiltonian given in equation (4) reduces to the so-called electronic Hamiltonian:

$$\hat{H}_{elec} = \frac{1}{2} \sum_{i=1}^n \nabla_i^2 - \sum_{i=1}^n \sum_{A=1}^K \frac{Z_A}{r_{iA}} + \sum_{i=1}^n \sum_{j>1}^n \frac{1}{r_{ij}} \quad (4)$$

The solution of the Schrödinger equation with \hat{H}_{elec} is the electronic wave function Ψ_{elec} and the electronic energy E_{elec} . Ψ_{elec} depends on the electron coordinates, while the nuclear coordinates enter only parametrically and do not explicitly appear in Ψ_{elec} . The total energy E_{tot} is then the sum of E_{elec} and the constant nuclear repulsion term [42]:

$$E_{nuc} = \sum_{A=1}^K \sum_{B>A}^M \frac{Z_A Z_B}{r_{AB}} \quad (5)$$

$$\hat{H}_{elec} \Psi_{elec} = E_{elec} \Psi_{elec} \quad (6)$$

and

$$E_{tot} = E_{elec} + E_{nuc} \quad (7)$$

The attractive potential exerted on the electrons due to the nuclei – the expectation value of the second operator \hat{V}_{Ne} in equation (4) is often termed the external potential, V_{ext} , in density functional theory, even though the external potential is not necessarily limited to the nuclear field but may include external magnetic or electric fields etc. From now on we will only consider the electronic problem of equations (4)- (6) and the subscript “elec” will be dropped.

2.3 The Hartree-Fock Method

The Hartree-Fock method seeks to approximately solve the electronic Schrödinger equation, and it assumes that the wave function can be approximated by a single Slater determinant made up of one spin orbital per electron. Since the energy expression is symmetric, the variation theorem holds, and so we know that the Slater determinant with the lowest energy is as close as we can get to the true wave function for the assumed functional form of a single Slater determinant. The Hartree-Fock method determines the set of spin orbitals which minimize the energy and give us this best single determinant. So, we need to minimize the Hartree-Fock energy expression with respect to changes in the orbitals:

$$c_i \rightarrow c_i + \delta c_i \quad (8)$$

We have also been assuming that the orbitals are orthonormal, and we want to ensure that our variational procedure leaves them orthonormal. The Hartree-Fock equations can be solved numerically (exact Hartree-Fock), or they can be solved in the space spanned by a set of basis functions (Hartree-Fock-Roothan equations). In either case, note that the solutions depend on the orbitals. Hence, we need to guess some initial orbitals and then refine our guesses iteratively. For this reason, Hartree-Fock is called a *self-consistent-field* (SCF) approach.

The first term above in square brackets:

$$\sum_{j \neq i} \left[\int dx_2 |c_j(x_2)|^{2r-1} \right] c_i(x_1), \quad (9)$$

gives the Coulomb interaction of an electron in spin orbital c_i with the average charge distribution of the other electrons. Here we see in what sense Hartree-Fock is a mean field theory. This is called the *Coulomb term*, and it is convenient to define a Coulomb operator as:

$$J_j(x_1) = \int dx_2 |c_j(x_2)|^2 r_{12}^{-1}, \quad (10)$$

which gives the average local potential at point x_1 due to the charge distribution from the electron in orbital c_j .

We can define an exchange operator in terms of its action on an arbitrary spin orbital c_i :

$$K_j(x_1)c_i(x_1) = \left[\int dx_2 c_j^*(x_2) r_{12}^{-1} c_i(x_2) \right] c_j(x_1). \quad (11)$$

Introducing a basis set transforms the Hartree-Fock equations into the Roothaan equations. Denoting the atomic orbital basis functions as \bar{c} , we have the expansion:

$$c_i = \sum_{m=1}^K C_{mi} \bar{c}_m \quad (12)$$

for each spin orbital i . This leads to:

$$f(x_1) \sum_v C_{vi} \tilde{c}_v(\mathbf{X}_1) = \epsilon_i \sum_v C_{vi} \tilde{c}_v(\mathbf{X}_1). \quad (13)$$

This can be simplified by introducing the matrix element notation:

$$S_{mv} = \int dx_1 \bar{c}_m^*(x_1) \bar{c}_v(x_1), \quad (14)$$

$$F_{mv} = \int dx_1 \bar{c}_m^*(x_1) \bar{c}_v(x_1). \quad (15)$$

Now the Hartree-Fock-Roothaan equations can be written in matrix form as:

$$\sum_v F_{mv} C_{vi} = \epsilon_i \sum_v S_{mv} C_{vi} \quad (16)$$

or even more simply as matrices:

$$\mathbf{FC} = \mathbf{\epsilon SC} \quad (17)$$

where $\mathbf{\epsilon}$ is a diagonal matrix of the orbital energies ϵ_i . This is like an eigenvalue equation except for the overlap matrix S . One performs a transformation of basis to go to an orthogonal basis to make S vanish. Then it's just a matter of solving an eigenvalue equation. Well, not quite. Since F depends on its own solution (through the orbitals), the process must be done iteratively. This is why the solution of the Hartree-Fock-Roothaan equations are often called the self-consistent-field procedure [42].

2.4 Basis Sets

The approximate treatment of electron-electron distribution and motion assigns individual electrons to one-electron function, termed *spin orbital*. These consist of a product of spatial functions, termed *molecular orbitals (MO)*, $y_1(x, y, z)$, $y_2(x, y, z)$, $y_3(x, y, z)$, ..., and either *a* or *b* spin components. The spin orbitals are allowed complete freedom to spread throughout the molecule. Their exact forms are determined to minimize the total energy. In the simplest level of theory, a single assignment of electron to orbital is made by using y as atomic orbital wavefunction based on the Schrödinger equation for the hydrogen atom. This is not a suitable approach for molecular calculation. This problem can be solved by representing MO as linear combination of basis functions.

In practical calculation, the molecular orbitals y_1, y_2, \dots , are further restricted to be linear combinations of a set of N known one-electron function $f_1(x, y, z), f_2(x, y, z), \dots, f_N(x, y, z)$:

$$y_i = \sum_{m=1}^N c_{mi} f_m \quad (18)$$

The functions f_1, f_2, \dots, f_N , which are defined in the specification of the model, are known as one-electron basis function called basis function. The set of basis functions is called basis set. If the basis functions are the atomic orbitals for the atoms making up the molecule, function in equation (18) is often described as the *linear combination of atomic orbitals* (LCAO). There are two types of basis function which commonly used in the electronic structure calculations, *Slater type orbitals* (STO) and *Gaussian type orbitals* (GTO).

The Slater orbitals are primarily used for atomic and diatomic systems where high accuracy is required and semiempirical calculations where all three- and four-center integrals are neglected. The Slater type orbitals have the function form:

$$b = A e^{-Zr} r^{n^*-1} Y_{lm}(q, f) \quad (19)$$

where parameter n^* and x are chosen to make the larger part of the orbitals look like atomic Hartree-Fock orbitals. There are a lot like hydrogen orbitals, but without the complicated nodal structure.

The Gaussian type orbitals can be written in terms of polar or cartesian coordinates:

$$g = x^a y^b z^c e^{-ar^2} Y_{lm}(q, f) \quad (20)$$

in which a, b , and c are integers and a is a parameter that is usually fixed. Primitive Gaussian function is shown in equation (20). Normally, several of these Gaussian functions are summed to define more realistic atomic orbitals basis functions, as shown below:

$$b_m = \sum_p k_{mp} g_p \quad (21)$$

The coefficients k_{mp} in this expansion are chosen to make the basis functions look as much like Slater orbitals as possible. Slater functions are good approximation to atomic wavefunctions but required excessive computer time more than Gaussian functions, while single-Gaussian functions are a poor approximation to the nearly ideal description of an atomic wavefunction that Slater function provides. The solution to the problem of this poor functional behavior is to use several Gaussians to approximate a Slater function. In the simplest version of this basis, n Gaussian functions are superimposed with fixed coefficients to form one-Slater type orbital. Such a basis is denoted STO- n G, and $n = 3, 4$.

The limit of quantum mechanics involves an infinite set of basis function. This is clearly impractical since the computational expanse of molecular orbital calculations is proportional to the power of the total number of basis functions. Therefore, ultimate choice of basis set size demands on a compromise between accuracy and efficiency. The classification of basis sets is given below.

2.4.1 Minimal Basis Sets

The minimum basis set is a selected basis function for every atomic orbital that is required to describe the free atom. For hydrogen atom, the minimum basis set is just one $1s$ orbital. But for carbon atom, the minimum basis set consisted of a $1s$ orbital, a $2s$ orbital and the full set of three $2p$ orbitals. For example, the minimum basis set for the methane molecule consists of 4 $1s$ orbitals, one per hydrogen atom, and the set of $1s$, $2s$ and $2p$ orbitals described above for carbon. Thus, total basis set comprises of 9 basis functions.

Several minimum basis sets are used as common basis sets especially the STO- n G basis sets because they are available for almost all elements in the periodic table. The most common of minimum basis sets is STO-3G, where a linear combination of three Gaussian type orbitals (GTOs) is fitted to a Slater-type orbital (STO). The individual GTOs are called primitive orbitals, while the combined functions are called contracted functions. For example, the STO-3G basis set for methane consists of a total of 9 contracted functions built from 27 primitive functions. Other commonly uses of STO- n G basis sets are STO-4G and STO-6G where each STO is fitted to 4 and 6 GTOs, respectively.

2.4.2 Scaled Orbital by Splitting the Minimum Basis Sets

In the early calculation on the hydrogen molecule, it is discovered that the STO $1s$ orbitals do not give the best result in the molecular environment when the Schrödinger equation is solved, because electron is attracted to both nuclei rather than just one nucleus. In each molecular orbital, both large and small sets of orbital appear and they are mixed in the ratio that gives the lowest energy. The combination of a large orbital and a small orbital is essentially equivalent to an orbital of intermediate size. The result orbital is a size that best fit for the molecular environment since it is obtained from minimizing the energy. The advantage of this procedure is that the mixing coefficients in the molecular orbitals appear in a linear function. This simple dodge is equivalent to scaling the single minimal basis set orbitals. The minimum basis set can scaled not only the valence orbitals of the minimal basis set (split valence basis set), but also all the orbitals of the minimal basis set (double zeta basis sets).

a) Split the Valence Orbitals (Split Valence Basis Sets)

The split valence basis sets mean that each valence orbital is spited into two parts, an inner shell and an outer shell. For example, the 3-21G basis set is referred to basis function of the inner shell represented by two Gaussian functions and that of the outer shell represented by one Gaussian function The core orbitals are represented by one basis function and each function composes of three Gaussian functions. The purpose of splitting the valence shell is to give the SCF algorithm more flexibility in adjusting the contributions of the basis function to the molecular orbitals, achieving a more realistic simulated electron distribution.

b) Split all Orbitals (Double Zeta Basis Sets)

Double zeta basis set is a member of minimum basis set replaced by two functions. In this way both core and valence orbitals are scaled in size. For some heavier atoms, double zeta basis sets may have slightly less than double the number of minimum basis set orbitals. For example, some double zeta basis sets for the atoms Ga-Br have 7 rather than 8 s basis functions, and 5 rather than 6 p basis functions.

The term “*double zeta*” arises from the fact that the exponent in a STO is often referred by the Greek letter “*zeta*”. Since it takes two orbitals with different exponents, it is called “*double zeta*”. The minimum basis set is “*single zeta*”. The normal abbreviation for a double zeta basis set is DZ. It is also quite common to use split valence basis sets where the valence orbitals are spitted into three functions. Basis sets where this is done for all functions are called triple zeta functions and referred to as TZ, TZP, TZ2P etc.

2.4.3 Polarized Basis Sets

In the discussion on the scaling of the hydrogen orbitals in the H₂ molecule, it is argued that the orbital on one atom in the molecule becomes smaller because of the attraction of the other nucleus. However, it is also clear that the influence of the other nucleus may distort or polarize the electron density near the nucleus. This problem desires orbitals that have more flexible shapes in a molecule than the *s*, *p*, *d*, etc., shapes in the free atoms. This is best accomplished by add basis functions of higher angular momentum quantum number. Thus, the spherical *1s* orbital on hydrogen is distorted by mixing in an orbital with *p* symmetry. The positive lobe at one side increases the value of the orbital while the negative lobe at the other side decreases the orbital. The orbital has overall “moved” sideways. It has been polarized. Similarly, the *p* orbital can polarize if it mixes in an orbital of *d* symmetry. These additional basis functions are called polarization functions. The polarization functions are added to the 6-31G basis set as follows:

6-31G* added a set of *d* orbitals to the atoms in the first and second rows .

6-31G** added a set of *d* orbitals to the atoms in the first and second rows and a set of *p* functions to hydrogen.

The nomenclature above is slowly being replaced. The 6-31G* is called 6-31G(d), while the 6-31G** is called 6-31G(d,p). This new nomenclature allows the possibility of adding several polarization functions. Thus 6-31G (3df,pd) added 3 *d*-type GTOs and 1 *f*-type GTO and added 1 *p*-type and 1 *d*-type function to H.

2.4.4 Diffuse Function Basis Sets

In some cases the normal basis functions are not adequate. This is particular the case in excited states and in anions where the electronic density is spread out more over the molecule. This model has correctly by using some basis functions which themselves are more spread out. This means that small exponents are added to GTOs. These additional basis functions are called diffuse functions. The diffuse functions added to the 6-31G basis set as follows:

6-31+G added a set of diffuse s and p orbitals to the atoms in the first and second rows.

Diffuse functions can be added along with polarization functions also. Some examples of these functions are 6-31+G*, 6-31++G*, 6-31+G** and 6-31++G** basis sets.

2.5 Density Functional Theory (DFT)

The ab initio methods described The basis for Density Functional Theory (DFT) is the proof by Hohenberg and Kohn that the ground-state electronic energy is determined completely by the electron density ρ , see Appendix B for details. In other words, there exists a one-to-one correspondence between the electron density of a system and the energy. The significance of this is perhaps best illustrated by comparing to the wave function approach. A wave function for an N -electron system contains $3N$ coordinates, three for each electron (four if spin is included). The electron density is the square of the wave function, integrated over $N-1$ electron coordinates, this only depends on three coordinates, independently of the number of electrons. While the complexity of a wave function increases with the number of electrons, the electron density has the same number of variables, independently of the system size. The “only” problem is that although it has been proven that each different density yields a different ground-state energy, the functional connection these two quantities is not known. The goal of DFT methods is to design functionals connecting the electron density with the energy.

The foundation for the use of DFT methods in computational chemistry was the introduction of orbitals by Kohn and Sham. The basic idea in the Kohn and Sham

(KS) formalism is splitting the kinetic energy functional into two parts, one of which can be calculated exactly, and a small correction term.

The key to Kohn-Sham theory is thus the calculation of the kinetic energy under the assumption of non-interacting electrons. In reality the electrons are interacting. The remaining kinetic energy is absorbed into an exchange – correlation term, and a general DFT energy expression can be written as

$$E_{DFT}[p] = T_S[p] + E_{ne}[p] + J[p] + E_{xc}[p] \quad (22)$$

By equating E_{DFT} to the exact energy E_{xc} , it is the part which remains after subtraction of the non-interacting kinetic energy, and the E_{ne} and J potential energy terms:

$$E_{xc}[p] = (T[p] - T_S[p]) + (E_{ee}[p] - J[p]) \quad (23)$$

The first parenthesis may be considered the kinetic correlation energy, while the second contains both exchange and potential correlation energy [43].

2.6 ONIOM method

ONIOM (**O**ur **N**-layer **I**ntegrated molecular **O**rbital + molecular **M**echanics) is the hybrid method of Morokuma and co-workers that enables different levels of theory to be applied to different parts of a molecule/system and combined to produce a consistent energy expression. The objective is to perform a high-level calculation on just a small part of the system and to include the effects of the remainder at lower levels of theory, with the end result being of similar accuracy to a high-level calculation on the full system.

2.6.1 ONIOM energy definition

The basic idea behind the ONIOM approach can be explained most easily when it is considered as an extrapolation scheme in a two-dimensional space, spanned by the size of the system on one axis and the level of theory on the other axis. Fig. 2.1 shows

the extrapolation procedure schematically. The goal is to describe the real system at the highest level of theory, i.e. the approximation of the target E_4 (point 4) in a system partitioned into the two-layer ONIOM or E_9 (point 9) in the system consisting of three layers. In the case of two layers, the extrapolated energy E_{ONIOM2} is then defined as:

$$E_{\text{ONIOM2}} = E_3 - E_1 + E_2$$

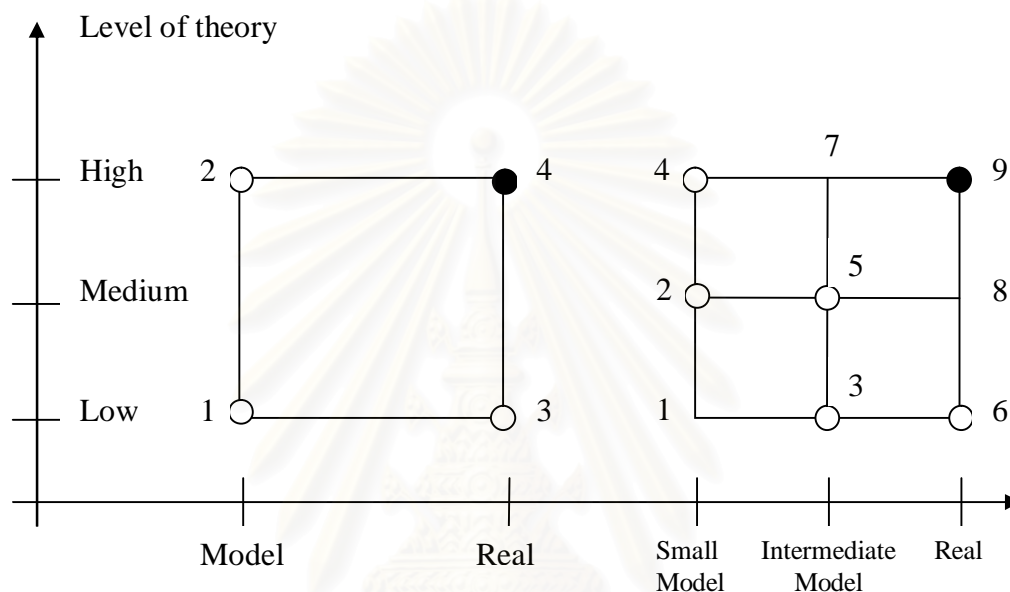


Figure 2.1 The ONIOM extrapolation scheme for a molecular system partitioned into two (left) and three (right) layers.

Where E_3 is the energy of the entire (real) system calculated at the low level method and E_1 and E_2 are the energies of the model system determined at the low and high level of theory, respectively. E_{ONIOM2} is an approximation to the true energy of the real system E_4 :

$$E_4 = E_{\text{ONIOM2}} + D \quad (24)$$

Thus, if the error D of the extrapolation procedure is constant for two different structure (e.g., between reactant and transition state) their relative energy ΔE_4 will be evaluated correctly by using the ONIOM energy ΔE_{ONIOM2} .

For a system partitioned into three different layers, the expression for the total energy E_{ONIOM3} as an approximation for E_9 read:

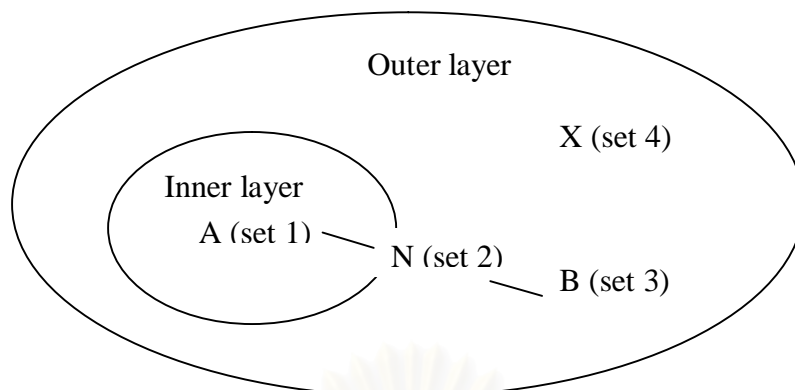
$$E_{\text{ONIOM3}} = E_6 - E_3 + E_5 - E_2 + E_4 \quad (25)$$

Since the evaluation of E_1 (the smallest model system at the lowest level of theory) does not require much computational effort, its value can be used to determine the effect of the three-layer approach as compared to a two-layer partitioning with points 1, 4, and 6. If the energy different between the two- and three-layer extrapolation is constant, a two layer partitioning with the intermediate layer omitted would give comparable accurate results.

2.10.2 Treatment of link atoms.

As mentioned before, an important and critical feature of all combination scheme is the treatment of the link atoms. For the following discussion, We first introduce some useful definition adopting a two layer ONIOM scheme as an example, as illustrated in Fig. 2.2. The methodology in the case of a three-layer ONIOM is exactly the same and will not be discuss explicitly.

The atoms present both in the model system and the real system are called set 1 atoms and their coordinates are donated by R_1 . The set 2 atoms are the artificially introduced link atoms. They only occur in the model system and their coordinate are described by R_2 . In the real system they are replaced by the atom describes by R_3 . Atoms belong to the outer layer and are not substituted.



Model System = inner layer + link atoms

Real System = inner layer + outer layer

Figure 2.2 Definition of different atom sets within the ONIOM scheme.

by link atoms are called set 4 atoms with coordinate R_4 . The geometry of the real system is thus described by R_1 , R_3 and R_4 and they are the independent coordinates for the ONIOM energy

$$E_{\text{ONIOM}} = E_{\text{ONIOM}}(R_1, R_3, R_4) \quad (26)$$

In order to generate the model system, described by R_1 and the link atom R_2 , we define R_2 as a function of R_1 and R_3 :

$$R_2 = f(R_1, R_3) \quad (27)$$

The explicit functional of the R_2 dependency can be chosen arbitrarily. However, considering the fact that link atoms are introduced to mimic the corresponding covalent bonds of the real system, they should follow the movement of the atom they replace. Therefore we adopt the following coupling scheme. If atoms A belong to set 1 and atoms B belong to set 3, the set 2 link atom is placed onto the bond axis A-B. In terms of internal coordinates we choose the same bond angles and dihedral angles for set 2 atoms as for set 3. Therefore, in the model calculations the link atoms are always aligned along the bond vectors of the real system. For the exact

position r_2 of the single H atom an A-B bond (r_3-r_1), we introduce a fixed scale factor (or distance parameter) g . Hence,

$$r_2 = r_1 + g(r_3-r_1) \quad (28)$$

In this work used B3LYP functional for high-layer, using Becke's exchange functional with part of the Hartree-Fock exchange mixed in and a scaling factor on the correlation part but using the LYP correlation function. The exchange-correlation energy has the form of

$$AE_X^{Slater} + (1-A)E_X^{HF} + B\Delta E_X^{Beck} + (1-C)E_C^{VWN} + CE_C^{LYP} \quad (29)$$

where the exchange includes the Slater exchange E_X^{Slater} , or local spin density exchange, along with corrections involving the gradient of the density and the correlation is provided by the LYP and VWN correlations. The constants A , B , and C are those determined by fitting to the G1 molecule set. The values of the three parameters are determined by fitting to the 56 atomization energies, 42 ionization potentials, 8 proton affinities, and 10 first-row atomic energies in the G1 molecule set, computing values of $A=0.80$, $B=0.72$, and $C=0.81$.

For low-layer, AM1(Austin method 1), developed at the University of Texas at Austin was introduced by Dewar, Zoebisch, Healy and Stewart in 1985 was used. AM1 use parameters derived from experimental data to simplify the computation to solve an approximate form of The Schrödinger Equation that depends on having appropriate parameters available for the type of chemical system under investigation.

2.7 Transition State Theory and Statistical Mechanics

Transition state theory (TST) assumes that a reaction proceeded from one energy minimum to another *via* an intermediate maximum. The *transition state* is the configuration which divides the reactant and product parts of surface. For example, a molecule which has reached the transition state is continuing to product. The geometrical configuration of the energy maximum is called the *transition structure*. Within standard TST, the transition state and transition structure are identical, but this

is not necessarily for more refined models. The direction of reaction coordinate is started from the reactant to product along a path where the energies are as low as possible and the TS is the point where the energy has a maximum. In the multidimensional case, TS is a first-order point on the potential energy surface as a maximum in the reaction coordinate direction and a minimum along all other coordinates, shown in Fig. 2.3.

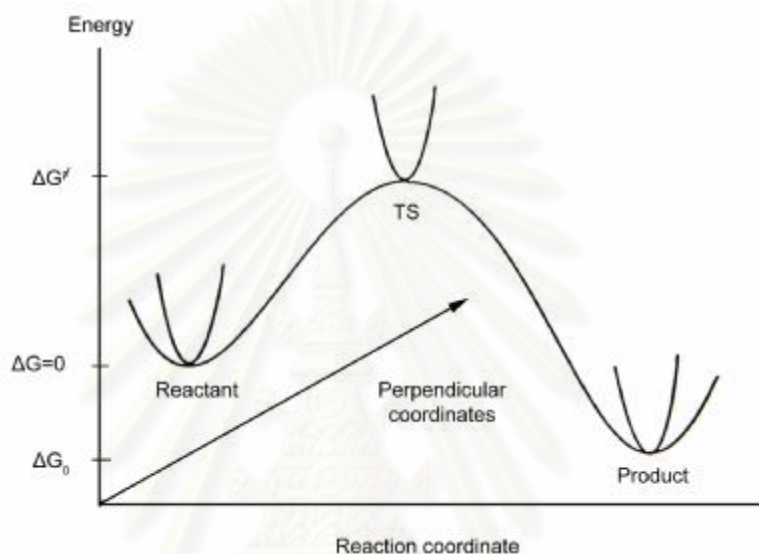


Figure 2.3 Schematic illustration of reaction path [42].

Transition state theory assumes equilibrium energy distribution among all possible quantum states at all points along the reaction coordinates. The probability of finding a molecular in a given quantum state is proportional to $e^{-\Delta E^\ddagger / k_B T}$, which is Boltzman distribution. Assuming that the molecule at the TS is in equilibrium with the reactant, the macroscopic rate constant can be expressed as:

$$k = \frac{k_B T}{h} \cdot e^{-\Delta G^\ddagger / RT} \quad (30)$$

in which ΔG^\ddagger is the Gibbs free energy difference between the TS and reactant, T is absolute temperature and k_B is Boltzmann's constant. It is clear that if the free energy of the reactant and TS can be calculated, the reactant rate follows trivially. The

equilibrium constant for a reaction can be calculated from the free energy difference between the reactant and product.

$$K = e^{-\Delta G_0 / RT} \quad (31)$$

The Gibbs free energy is given in terms of the enthalpy and entropy, $G = H - TS$. The enthalpy and entropy for a macroscopic ensemble of particles maybe calculated from properties of the individual molecules by means of statistical mechanics.

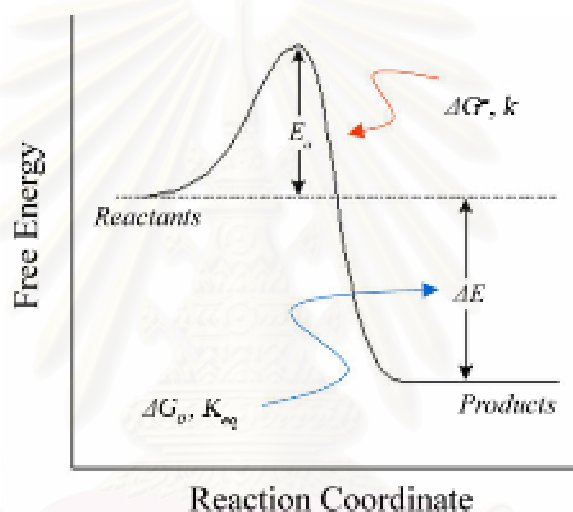
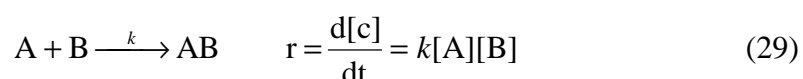


Figure 2.4 The difference between rate constant(k) and equilibrium constant (K) [42].

2.8 Rate constant

The most successful and widely employed theoretical approach for studying reaction rates involving species that are undergoing reaction at or near thermal equilibrium conditions is the transition state theory (TST) of Eyring.

The bimolecular reaction



According to the transition state model, the reactants are getting over into an unsteady intermediate state on the reaction pathway.

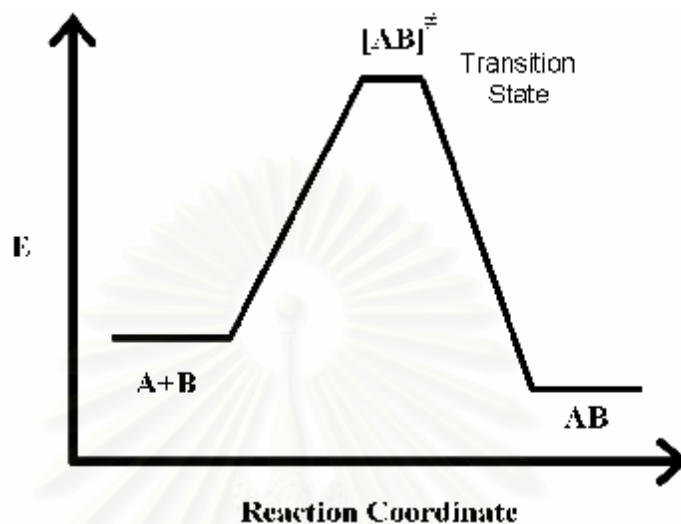


Figure 2.5 Energy profile E: Potential energy reaction coordinate: parameter hanging during the course of the reaction (as bond length or bond angle) Transition state: Maximum of energy in the path way.

There is an energy barrier on the pathway between the reactants (A, B) and the product (C). The barrier determines a threshold energy or minimum of energy necessary to permit the reaction to occur. It is called activation enthalpy activation energy).

An activated complex AB^\ddagger or transition state is formed at the potential energy maximum. The high-energy complex represents an unstable molecular arrangement, in which bonds break and form to generate the product C or to degenerate back to the reactants A and B. Once the energy barrier is surmounted, the reaction proceeds downhill to the product.

The change in the concentration of the complex AB^\ddagger over time can be described by the following equation:

$$\frac{d[AB^\ddagger]}{dt} = k_1[A][B] - k_{-1}[AB^\ddagger] - k_2[AB^\ddagger] \quad (31)$$

Due to the equilibrium between the activated complex AB^\ddagger and the reactants A and B, the components $k_1[A][B]$ and $k_{-1}[AB^\ddagger]$ cancel out. Thus the rate of the direct reaction is proportional to the concentration of AB^\ddagger

$$\frac{d[C]}{dt} = -\frac{d[AB^\ddagger]}{dt} = k_2[AB^\ddagger] \quad (32)$$

k_2 is given by statistical mechanics: $k_2 = \frac{k_B T}{h}$

k_B = Boltzmann's constant [$1.381 \times 10^{-23} \text{ J K}^{-1}$]

T = absolute temperature in degrees Kelvin (K)

h = Plank constant [$6.626 \times 10^{-34} \text{ Js}$]

k_2 is called universal constant for a transition state ($\sim 6 \times 10^{12} \text{ s}^{-1}$ at room temperature).

Additionally, $[AB^\ddagger]$ can be derived from the quasi stationary equilibrium between AB^\ddagger and A, B by applying the mass action law:

$$[AB^\ddagger] = K^\ddagger [A][B] \quad (33)$$

K^\ddagger = thermodynamic equilibrium constant

Due to the equilibrium that will be reached rapidly, the reactants and the activated complex decrease at the same rate. Therefore, considering both equation (32) and (33), equation (31) becomes

$$-\frac{d[AB^\ddagger]}{dt} = \frac{k_B T}{h} K^\ddagger [A][B] \quad (34)$$

Comparing the derived rate law (29) and the expression (34) yields for the rate constant of the overall reaction

$$k = \frac{k_B T}{h} K^\ddagger \quad (35)$$

Additionally, thermodynamics gives a further description of the equilibrium constant:

$$\Delta G = -RT \ln K^\ddagger \quad (36)$$

Furthermore ΔG^\ddagger is given by

$$\Delta G^\ddagger = \Delta H^\ddagger - T\Delta S^\ddagger \quad (36)$$

Combining equation (35) and the equation (36) and solving for $\ln k$ yields

$$\ln K^\ddagger = \frac{-\Delta H^\ddagger}{RT} + \frac{-\Delta S^\ddagger}{R} \quad (37)$$

The *Eyring equation*: is found by substituting equation (37) into equation (34)

$$k = \frac{k_B T}{h} e^{-\frac{\Delta H^\ddagger}{RT}} e^{-\frac{\Delta S^\ddagger}{R}} \quad \text{or} \quad k = \frac{k_B T}{h} e^{-\frac{\Delta G^\ddagger}{RT}} \quad (38)$$

2.9 Arrhenius equation

The Arrhenius equation is a simple, but remarkably accurate, formula for the temperature dependence of the rate constant, and therefore rate, of a chemical reaction. The equation was first proposed by the Dutch chemist J. H. van't Hoff in 1884; five years later in 1889, the Swedish chemist Svante Arrhenius provided a physical justification and interpretation for it. Nowadays it is best seen as an empirical relationship. It can be used to model the temperature-variance of diffusion coefficients, population of crystal vacancies, creep rates, and many other thermally-induced processes/reactions. The general rule of thumb, without solving the equation, is that for every 10°C increase in temperature the rate of reaction doubles. As with any rule of thumb, it does not always work.

In short, the Arrhenius equation gives "the dependence of the rate constant k of chemical reactions on the temperature T (in Kelvin) and activation energy ΔE^\ddagger ", as shown below:

$$k = Ae^{(-\Delta E^\ddagger / RT)} \quad (39)$$

where A is the pre-exponential factor or simply the prefactor and R is the gas constant. The units of the pre-exponential factor are identical to those of the rate constant and will vary depending on the order of the reaction. If the reaction is first order it has the units s^{-1} , and for that reason it is often called the frequency factor or attempt frequency of the reaction. When the activation energy is given in molecular units, instead of molar units, e.g. joules per molecule instead of joules per mole, the Boltzmann constant is used instead of the gas constant. It can be seen that either increasing the temperature or decreasing the activation energy (for example through the use of catalysts) will result in an increase in rate of reaction.

Taking the natural logarithm of the Arrhenius equation yields:

$$\ln k = \frac{-\Delta E^\ddagger}{R} \frac{1}{T} + \ln(A) \quad (40)$$

So, when a reaction has a rate constant which obeys the Arrhenius equation, a plot of $\ln(k)$ versus T^{-1} gives a straight line, whose slope and intercept can be used to determine ΔE^\ddagger and A. This procedure has become so common in experimental chemical kinetics that practitioners have taken to using it to define the activation energy for a reaction. That is the activation energy is defined to be (-R) times the slope of a plot of $\ln(k)$ vs. $(1/T)$:

2.9.1 Arrhenius plot

An Arrhenius plot displays the logarithm of a rate ($\ln(k)$, ordinate axis) plotted against inverse temperature ($1 / T$, abscissa). Arrhenius plots are often used to analyze the effect of temperature on the rates of chemical reactions. For a single rate-limited thermally activated process, an Arrhenius plot gives a straight line, from which the activation energy and the pre-exponential factor can both be determined. From the eq. (24) can written equivalently as :

$$\ln(k) = \ln(A) - \frac{\Delta E^\ddagger}{R} \left(\frac{1}{T}\right) \quad (41)$$

When plotted in the manner described above, the value of the extrapolated "y-intercept" will correspond to $\ln(A)$, and the gradient of the line will be equal to $-\Delta E^\ddagger / RT$

The pre-exponential factor, A , is a constant of proportionality that takes into account a number of factors such as the frequency of collision between and the orientation of the reacting particles.

The expression $-\Delta E^\ddagger / RT$ represents the fraction of the molecules present in a gas which have energies equal to or in excess of activation energy at a particular temperature.



สถาบันวิทยบริการ
จุฬาลงกรณ์มหาวิทยาลัย

CHAPTER III

DETAILS OF THE CALCULATIONS

3.1 Computational method in acid-catalyzed system.

Geometry optimizations of methanol and ethanol reactants, intermediates, transition states and dimethyl ether, diethyl ether and ethylene products have been carried out using the B3LYP/6-31G(d) [44-45] methodology and employed with the zero-point vibrational energy (ZPVE) corrections. The real reacting compounds are shown in Fig. 3.1.

3.2 Computational method in H-ZSM-5-catalyzed system.

Geometry optimizations and the energies of methanol and ethanol reactants, intermediates, transition states and dimethyl ether, diethyl ether and ethylene products on the 56/5T cluster model of H-ZSM-5 have been carried out using the ONIOM(MO:MO) methodology. The real system (56T cluster) of two-layer ONIOM approach [46-47] subdivided as a high and low layer employing the B3LYP/6-31G(d) [44-45] and the semiempirical AM1 [48] levels of theory, respectively. The active site of H-ZSM-5 modeled as 5T cluster and adsorption-state compounds are described at the highest level of theory whereas the rest of the zeolite is computed at a lower level. The ONIOM(B3LYP/6-31G(d):AM1) [46-47, 49-52] have also been employed with the zero-point vibrational energy (ZPVE) corrections. The real reacting compounds are shown in Fig. 3.1.

3.3 The transition state, equilibrium constant and rate constant calculations.

The transition-state structures of the reaction with hydronium ion catalyst optimized at the B3LYP/6-31G(d) and the 56/5T cluster model of H-ZSM-5 catalyst optimized at ONIOM(B3LYP/6-31G(d):AM1) level of theory have been located

using the reaction coordinate method referred to the synchronous transit-guided quasi-newton (STQN) calculation. [53] All computations were performed using the GAUSSIAN 03 program package.[54] The MOLDEN 3.7 program [55] was utilized to observe molecular energies and geometries convergence via the Gaussian output files. The molecular graphics of all species were generated with the MOLEKEL program. [56]

The reaction energy ΔE° , standard enthalpy ΔH_{298}° and Gibbs free energy changes ΔG_{298}° of all reactions have been derived from the frequency calculations at the ONIOM(B3LYP/6-31G(d):AM1). The rate constant k derived from the transition state theory was computed from activation of free energy, $\Delta^\ddagger G_0^\circ$, by using

$$k = \frac{k_B T}{hc^\circ} \exp(-\Delta^\ddagger G_0^\circ / RT) \quad (1)$$

where the concentration factor, c_0 of unity is used, k_B is the Boltzmann's constant, h is Plank's constant, T is the absolute temperature, and R is the gas constant [57]. The above formula was employed to compute the reaction rate constants for corresponding activation free energies as introduced in the previous works [58-63]. The equilibrium constants (K_{298}) is computed from the thermodynamic equation (2).

$$K_{298} = \exp(-\Delta G_{298}^\circ / RT) \quad (2)$$

สถาบันวิทยบริการ
จุฬาลงกรณ์มหาวิทยาลัย

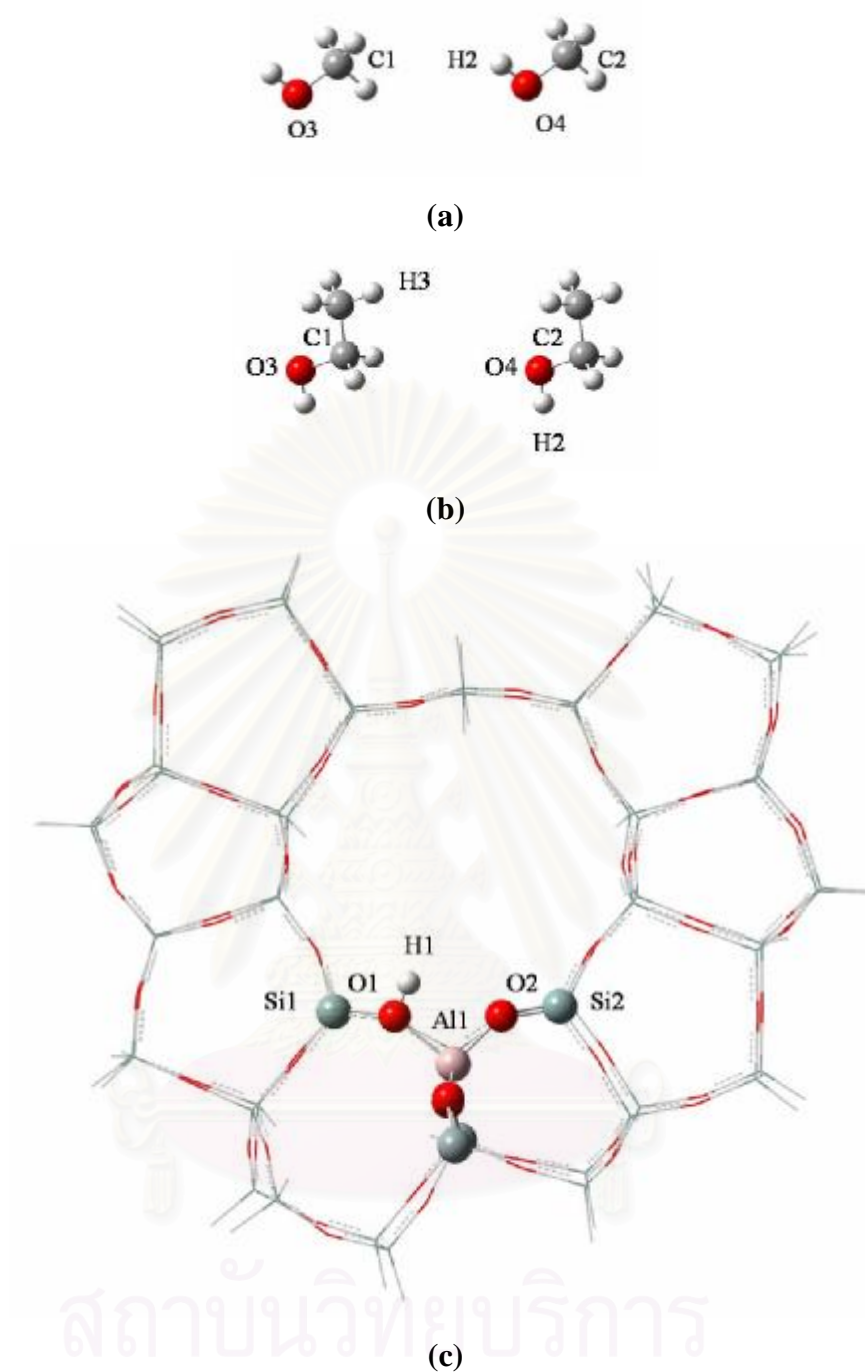


Figure 3.1 Atomic numbering for (a) methanol, (b) ethanol and (c) 56/5T cluster of H-ZSM-5 for two-layer (lines were atoms of low layer, balls were atoms of high layer).

CHAPTER IV

RESULTS AND DISCUSSION

As discussed, different paths for dimethyl ether, diethyl ether and ethylene formation are possible in hydronium ion and H-ZSM-5 catalyst. This work presents a detailed discussion of those paths. For instance geometry, activation energy and rate constants were obtained.

4.1 Synthesis reaction for dimethyl ether

The B3LYP/6-31G(d) optimized structures of methanol (MeOH), intermediates, transition states, dimethyl ether (DME) and all related species in MeOH conversion to DME in acid-catalyzed system were obtained. The ONIOM(B3LYP/6-31G(d):AM1) optimized structures of MeOH, intermediates, transition states, DME and all related species in MeOH conversion to DME in H-ZSM-5-catalyzed system were obtained.

4.1.1 Acid-catalyzed system

Reaction steps of MeOH conversion to DME in acid-catalyzed system are shown in Fig. 4.1. The B3LYP/6-31G(d) optimized structures of the reactants, intermediates INT1, INT2, transition states TS and products are also given in Fig. 4.1. Geometrical data based on the B3LYP/6-31G(d) calculations of intermediate and transition state in MeOH conversion to DME in acid-catalyzed system in gas phase are also given in Table 4.1.

The activation energy and free energy of activation, reaction thermodynamic quantities of MeOH conversion to DME in acid-catalyzed system are given in Table 4.2. It shows an activation of all five reaction steps. The first reaction step, the first MeOH molecule is protonated by hydronium ion to prepare the protonated methanol (MeOH_2^+) which reacts with the second MeOH molecule to produce INT1 of which binding energy -11.04 kcal/mol and free energy $\Delta G_{298}^{\circ} = -2.81$ kcal/mol.

Due to the transition states TS (the third step), the activation energies and their corresponding free energies of activations are 10.22 and 10.99 kcal/mol. Rate constant for the activation is $5.46 \times 10^4 \text{ s}^{-1}$, and its corresponding equilibrium constant is 1.13×10^7 . The fourth reaction step affords the protonated dimethyl ether (DME.H⁺). The last step is the releasing process for freeing a molecule of hydronium ion, see in Fig. 4.1. Relative energy profile of MeOH conversion to DME in acid-catalyzed systems is shown in Fig. 4.2.



สถาบันวิทยบริการ
จุฬาลงกรณ์มหาวิทยาลัย

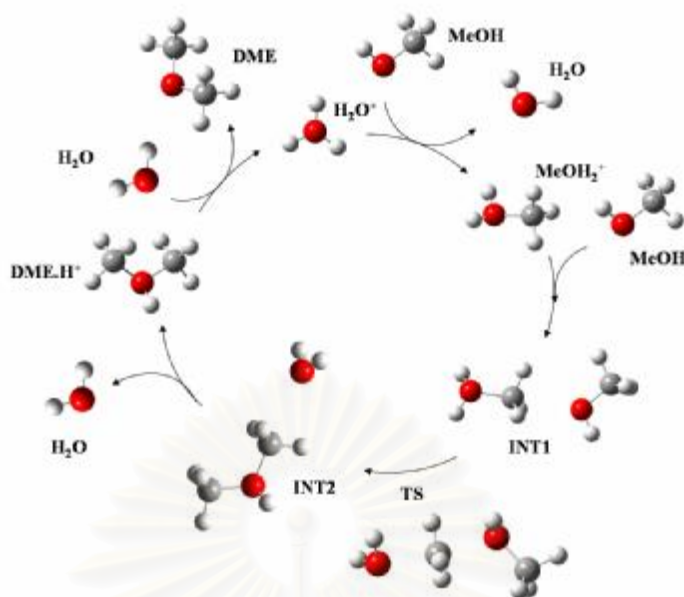


Figure 4.1 Reaction cycle of MeOH conversion to DME in acid-catalyzed system.

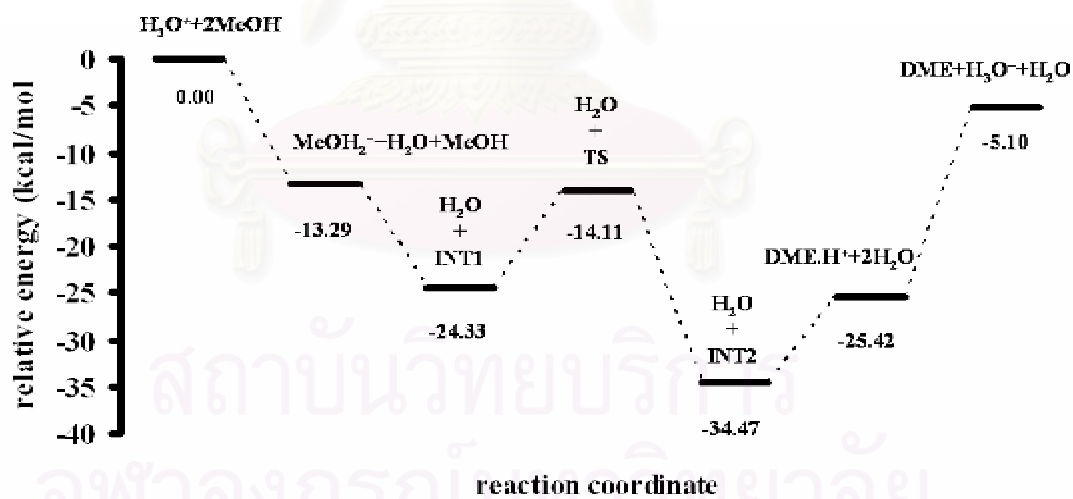


Figure 4.2 Relative energy profile for MeOH conversion to DME in acid-catalyzed system.

Table 4.1 Geometrical data based on the B3LYP/6-31G(d) calculations of intermediate and transitionstate in MeOH conversion to DME in acid-catalyzed system

Parameter/Conformer	INT1	TS	INT2
Bond distance (Å)			
O3-C1	1.559	1.964	2.678
O4-C1	2.573	1.939	1.516
O4-C2	1.435	1.442	1.488
O4-H2	0.969	0.988	0.978

Table 4.2 Energies and thermodynamic quantities of MeOH conversion to DME in acid-catalyzed system

Reaction ^a	$\Delta^{\ddagger}E$ ^{b,c}	$\Delta^{\ddagger}G$ ^{b,c}	k_{298} ^d	ΔE ^c	ΔG_{298}° ^c	ΔH_{298}° ^c	K_{298}
H ₃ O ⁺ +MeOH \rightleftharpoons MeOH ₂ ⁺ +H ₂ O	-	-	-	-13.29	-14.75	-14.11	6.52 x 10 ¹⁰
MeOH ₂ ⁺ +MeOH \rightleftharpoons INT1	-	-	-	-11.04	-2.81	-11.95	1.15 x 10 ²
INT1 \rightleftharpoons TS \rightleftharpoons INT2	10.22	10.99	5.46 x 10 ⁴	-10.15	-9.62	-9.69	1.13 x 10 ⁷
INT2 \rightleftharpoons DME ⁺ +H ₂ O	-	-	-	9.05	2.46	10.70	1.57 x 10 ⁻²
DME ⁺ +H ₂ O \rightleftharpoons DME+ H ₃ O ⁺	-	-	-	20.33	22.48	21.22	3.34 x 10 ⁻¹⁷

^a Based on acid-catalyzed system, computed at the B3LYP/6-31G(d) level.

^b Activation state.

^c In kcal/mol.

^d In s⁻¹.

สถาบันวิทยบริการ
จุฬาลงกรณ์มหาวิทยาลัย

4.1.2 H-ZSM-5-catalyzed system

Two possible mechanisms for the conversion of MeOH to DME as the concerted and stepwise processes were found. Relative energies and thermodynamic properties of two reaction mechanisms were derived from the frequency calculations at the ONIOM(B3LYP/6-31G(d):AM1) approach.

4.1.2.1 Stepwise reaction mechanism

Reaction steps of the stepwise mechanism of MeOH conversion on the 56/5T cluster model of H-ZSM-5 are shown in Fig. 4.3. The ONIOM(B3LYP/6-31G(d):AM1) optimized structures of the 56/5T-cluster-modeled H-ZSM-5 zeolite symbolized as HZ, MeOH, adsorbed-state intermediates INT1, INT2, INT3, INT4, methoxide species ZMe, transition states TS1 and TS2 (TS) are also given in Fig. 4.3.

The geometrical data based on the ONIOM(B3LYP/6-31G(d):AM1) calculations of intermediate and transition state in MeOH conversion to DME via stepwise mechanism in gas phase are also given in Table 4.3.

The activation energy and free energy of activation, reaction thermodynamic quantities of the stepwise mechanism of MeOH conversion to DME on H-ZSM-5 are given in Table 4.4. It shows two activations of all six reaction steps. The first step is an adsorption of a MeOH molecule on H-ZSM-5 of which binding energy -17.04 kcal/mol and free energy $\Delta G_{298}^{\circ} = -7.79$ kcal/mol. Due to the transition states TS1 (the second step) and TS2 (the fifth step), the activation energies and their corresponding free energies of activations are 74.76 and 79.65 kcal/mol, and 56.92 and 63.84 kcal/mol, respectively. Rate constant for the first and second activations are 2.54×10^{-46} and $9.89 \times 10^{-35} \text{ s}^{-1}$, respectively and their corresponding equilibrium constants are 6.21×10^{-10} and 1.47×10^8 , respectively. Therefore, we can conclude that the first step is the rate determining step of the stepwise process. The third step is a dehydration process of INT2 to afford MeZ species, see Fig. 4.3. The fourth step is an adsorption of MeOH on the methoxylated ZSM-5 as INT3 species. Reaction energies for these two reaction steps are not much different. The last reaction step is a desorption process of the product DME. Relative energy profile of stepwise

mechanism of MeOH conversion on 56/5T cluster model of H-ZSM-5 is shown in Fig. 4.4.

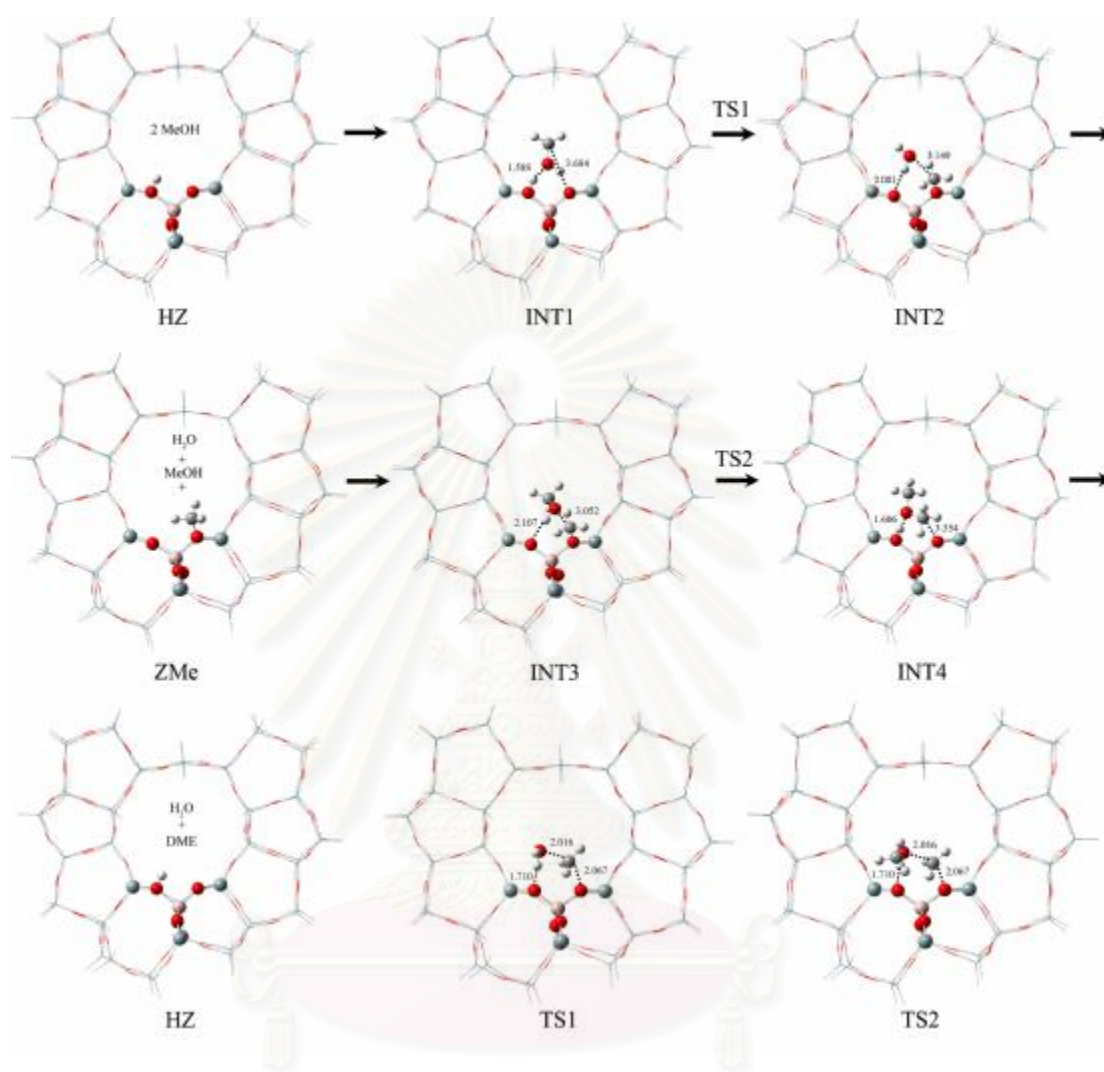


Figure 4.3 Stepwise mechanism of MeOH conversion to DME on 56/5T cluster model of H-ZSM-5.

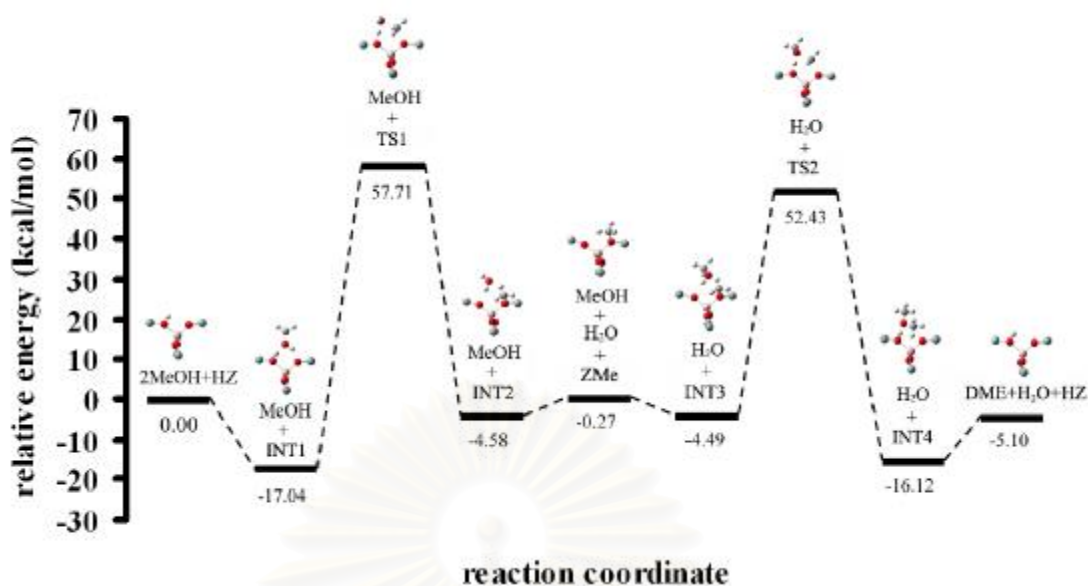


Figure 4.4 Relative energy profile for MeOH conversion to DME on H-ZSM-5 (modeled as 56/5T cluster) via stepwise mechanism.

Table 4.3 Geometrical data based on the ONIOM(B3LYP/6-31G(d):AM1) calculations of intermediate and transition state in MeOH conversion DME via stepwise mechanism in gas phase

Parameter/Conformer	INT1	TS1	INT2	INT3	TS2	INT4
Bond distance (Å)						
O1-H1	1.031	1.206	2.001	-	-	-
O2-C1	3.684	1.898	1.478	1.474	2.009	3.354
O3-H1	1.588	1.316	0.975	-	-	-
O3-C1	1.431	1.908	3.149	-	-	-
O1-H2	-	-	-	2.107	1.241	1.021
O4-H2	-	-	-	0.974	1.269	1.606
O4-C1	-	-	-	3.052	1.881	1.432
O4-C2	-	-	-	1.422	1.415	1.427
Bond Angle (Degree)						
Si1-O1-Al	138.86	131.13	154.27	153.16	131.78	138.06
Si2-O2-Al	140.47	137.56	126.85	127.24	136.94	145.17
O1-Al-O2	98.50	103.91	102.99	102.03	104.18	100.90

Table 4.4 Energies and thermodynamic quantities of the stepwise mechanism of the MeOH conversion to DME in H-ZSM-5-catalyzed system

Reaction ^a	$\Delta^\ddagger E$ ^{b,c}	$\Delta^\ddagger G$ ^{b,c}	k_{298} ^d	ΔE ^c	ΔG_{298}^o ^c	ΔH_{298}^o ^c	K_{298}
HZ + MeOH $\overset{\curvearrowright}{\rightleftharpoons}$ INT1	-	-	-	-17.04	-7.79	-18.81	5.18×10^5
INT1 $\overset{\curvearrowright}{\rightleftharpoons}$ TS1 $\overset{\curvearrowright}{\rightleftharpoons}$ INT2	74.76	79.65	2.54×10^{-46}	12.46	12.56	13.53	6.21×10^{-10}
INT2' $\overset{\curvearrowright}{\rightleftharpoons}$ ZMe + H ₂ O	-	-	-	4.31	-2.52	6.75	7.06×10^1
ZMe + MeOH $\overset{\curvearrowright}{\rightleftharpoons}$ INT3	-	-	-	-4.22	4.79	-5.21	3.07×10^{-4}
INT3 $\overset{\curvearrowright}{\rightleftharpoons}$ TS2 $\overset{\curvearrowright}{\rightleftharpoons}$ INT4	56.92	63.84	9.89×10^{-35}	-11.63	-11.14	-12.05	1.47×10^8
INT4 $\overset{\curvearrowright}{\rightleftharpoons}$ HZ + DME	-	-	-	11.03	1.86	11.96	4.32×10^{-2}

^a Based on the 56/5T cluster model of H-ZSM-5, computed at the ONIOM(B3LYP/6-31G(d):AM1) level.

^b Activation state.

^c In kcal/mol.

^d In s⁻¹.

สถาบันวิทยบริการ
จุฬาลงกรณ์มหาวิทยาลัย

4.1.2.2 Concerted reaction mechanism

Reaction steps of the concerted mechanism of methanol conversion on the 56/5T cluster model of H-ZSM-5 are shown in Fig. 4.5. The ONIOM(B3LYP/6-31G(d):AM1) optimized structures of the 56/5T-cluster-modeled H-ZSM-5 zeolite (symbolized as HZ and ZH for their acid protons positioned on oxygen atoms at the left and right of aluminum atom, respectively), free MeOH reactant, their adsorbed-state intermediate reactant (INT1), transition state (TS) and adsorbed-state intermediate product (INT2) are also given in Fig. 4.5.

The activation energy and free energy of activation, reaction thermodynamic quantities of the concerted mechanism of MeOH conversion to DME on H-ZSM-5 are given in Table 4.6. It shows that adsorption of two MeOH molecules on H-ZSM-5 is exothermic (-27.31 kcal/mol) and spontaneous ($\Delta G_{298}^{\circ} = -8.58$ kcal/mol) reactions. Due to the transition state of concerted mechanism, the activation energy and free energy of activation are somewhat high, 63.39 and 71.80 kcal/mol, respectively and this free energy of activation results very small rate constant, $k_{298} = 1.45 \times 10^{-40} \text{ s}^{-1}$. The equilibrium constant of conversion reaction over the activation step, computed using the thermodynamic equation $K_{298} = \exp(-\Delta G_{298}^{\circ}/RT)$ is 8.10×10^{-4} . The intermediate product, INT2 is the adsorption state of DME and a water molecule on Brønsted acid site of H-ZSM-5 zeolite in which the DME will be released during desorption process. Relative energy profile of concerted mechanism of MeOH conversion on 56/5T cluster model of H-ZSM-5 is shown in Fig. 4.6.

สถาบันวิทยบริการ
จุฬาลงกรณ์มหาวิทยาลัย

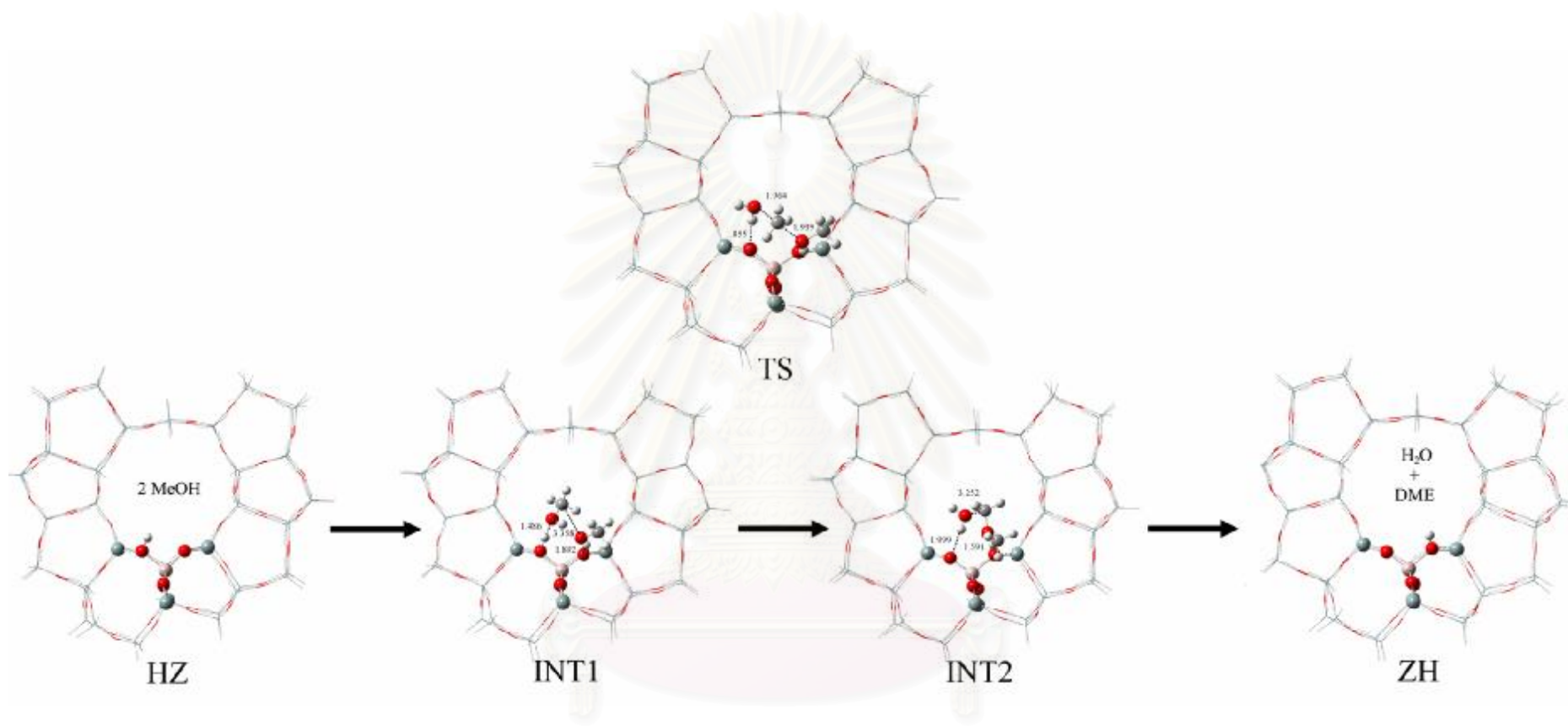


Figure 4.5 Concerted mechanism of MeOH conversion to DME on 56/5T cluster model of H-ZSM-5.

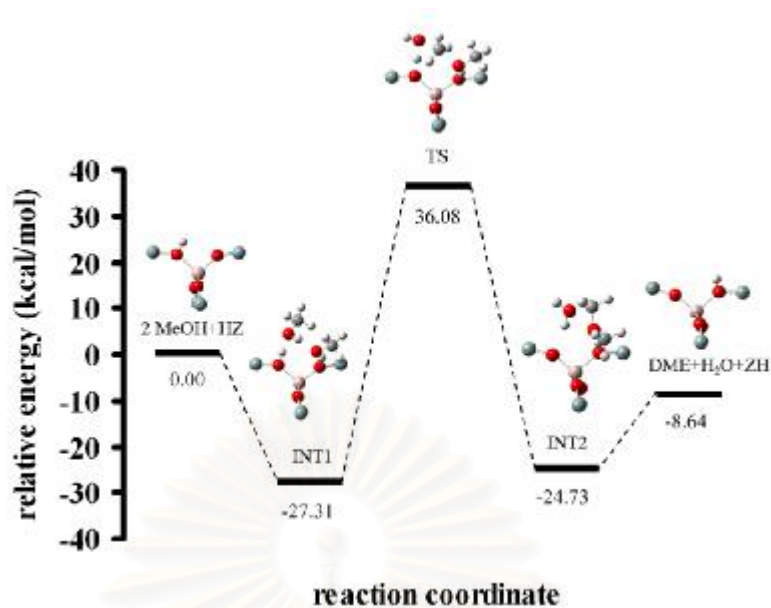


Figure 4.6 Relative energy profile for MeOH conversion to DME on H-ZSM-5 (modeled as 56/5T cluster) via concerted mechanism.

Table 4.5 Geometrical data based on the ONIOM(B3LYP/6-31G(d):AM1) calculations of intermediate and transition state in MeOH conversion to DME via concerted mechanism in gas phase

Parameter/Conformer	INT1	TS	INT2
Bond distance (Å)			
O1-H1	1.058	1.175	1.999
O2-H2	1.892	1.159	1.020
O3-H1	1.486	1.301	0.976
O3-C1	1.433	1.878	3.252
O4-H2	0.982	1.310	1.591
O4-C1	3.358	1.876	1.432
O4-C2	1.425	1.412	1.424
Bond Angle (Degree)			
*Si1-O1-Al	137.18	133.04	154.21
*Si2-O2-Al	141.16	136.42	132.19
*O1-Al-O2	101.27	106.33	103.88

Table 4.6 Energies and thermodynamic quantities of the concerted mechanism of MeOH conversion to DME in H-ZSM-5-catalyzed system

Reaction ^a	$\Delta^\ddagger E$ ^{b,c}	$\Delta^\ddagger G$ ^{b,c}	k_{298} ^d	ΔE ^c	ΔG_{298}^o ^c	ΔH_{298}^o ^c	K_{298}
HZ+2MeOH $\overset{\curvearrowright}{\text{S}}$ INT1	-	-	-	-27.31	-8.58	-30.43	1.95×10^6
INT1 $\overset{\curvearrowright}{\text{S}}$ TS $\overset{\curvearrowright}{\text{S}}$ INT2	63.39	71.80	1.45×10^{-40}	2.58	4.22	3.11	8.10×10^{-4}
INT2 $\overset{\curvearrowright}{\text{S}}$ DME + H ₂ O + ZH	-	-	-	16.09	-1.65	20.14	1.61×10^1

^a Based on the 56/5T cluster model of H-ZSM-5, computed at the ONIOM(B3LYP/6-31G(d):AM1) level.

^b Activation state.

^c In kcal/mol.

^d In s⁻¹.

สถาบันวิทยบริการ
จุฬาลงกรณ์มหาวิทยาลัย

4.2 Synthesis reaction for diethyl ether

The B3LYP/6-31G(d) optimized structures of ethanol (EtOH), intermediates, transition states, diethyl ether (DEE) and all related species in EtOH conversion to DEE in acid-catalyzed system were obtained. The ONIOM(B3LYP/6-31G(d):AM1) optimized structures of EtOH, intermediates, transition states, DEE product and all related species in EtOH conversion to DEE in H-ZSM-5-catalyzed system were obtained.

4.2.1 Acid-catalyzed system.

Reaction steps of EtOH conversion to DEE in acid-catalyzed system are shown in Fig. 4.7. The B3LYP/6-31G(d) optimized structures of the reactants, intermediates INT1, INT2, transition states TS and products are also given in Fig. 4.7.

Geometrical data based on the B3LYP/6-31G(d) calculations of intermediate and transition state in EtOH conversion to DEE on the hydronium ion catalyst in gas phase are also given in Table 4.7.

The activation energy and free energy of activation, reaction thermodynamic quantities of EtOH conversion to DEE in acid-catalyzed system are given in Table 4.8. It shows an activation of all five reaction steps. The first reaction step, the first EtOH molecule is protonated by hydronium ion to prepare the protonated ethanol (EtOH_2^+) which reacts with the second EtOH molecule to produce INT1 of which binding energy -10.91 kcal/mol and free energy $\Delta G_{298}^\circ = -1.99$ kcal/mol. Due to the transition states TS (the third step), the activation energies and their corresponding free energies of activations are 10.90 and 11.25 kcal/mol. Rate constant for the activation is $3.51 \times 10^4 \text{ s}^{-1}$, and its corresponding equilibrium constant is 1.28×10^9 . The fourth reaction step affords the protonated diethyl ether (DEE.H^+). The last step is the releasing process for freeing a molecule of hydronium ion, see Fig. 4.7. Relative energy profile of EtOH conversion to DEE in acid-catalyzed system is shown in Fig. 4.8.

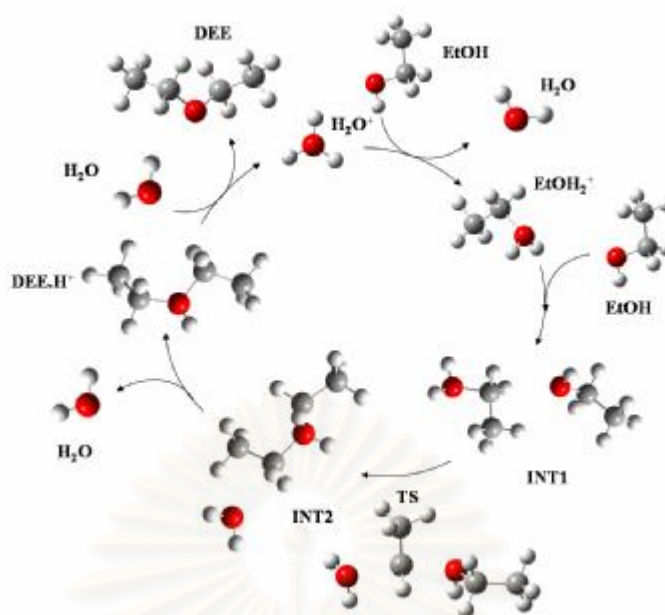


Figure 4.7 Reaction cycle of EtOH conversion to DEE in acid-catalyzed system.

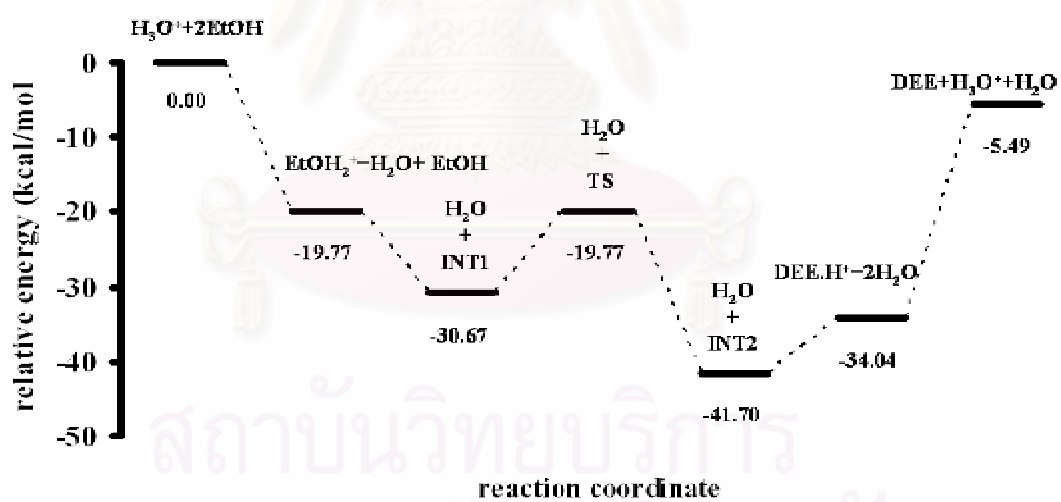


Figure 4.8 Relative energy profile for EtOH conversion to DEE in acid-catalyzed system.

Table 4.7 Geometrical data based on the B3LYP/6-31G(d) calculations of intermediate and transition state in EtOH conversion to DEE in acid-catalyzed system

Parameter/Conformer	INT1	TS	INT2
Bond distance (Å)			
O3-C1	1.592	2.015	2.988
O4-C1	2.800	2.008	1.539
O4-C2	1.443	1.446	1.512
O4-H2	0.970	0.999	0.978

Table 4.8 Energies and thermodynamic quantities of EtOH conversion to DEE in acid-catalyzed system

Reaction ^a	$\Delta^\ddagger E$ ^{b,c}	$\Delta^\ddagger G$ ^{b,c}	k_{298} ^d	ΔE ^c	ΔG_{298}° ^c	ΔH_{298}° ^c	K_{298}
H ₃ O ⁺ +MeOHŠ MeOH ₂ ⁺ +H ₂ O	-	-	-	-19.77	-20.89	-20.17	2.05 x 10 ¹⁵
MeOH ₂ ⁺ +MeOH Š INT1	-	-	-	-10.91	-1.99	-11.55	2.87 x 10 ¹
INT21Š TSŠ INT2	10.90	11.25	3.51 x 10 ⁴	-11.03	-12.43	-9.88	1.28 x 10 ⁹
INT2Š DME ⁺ +H ₂ O	-	-	-	7.66	2.81	8.82	8.65 x 10 ⁻³
DME ⁺ +H ₂ OŠ DME+ H ₃ O ⁺	-	-	-	28.55	30.53	29.21	4.16 x 10 ⁻²³

^a Based on acid-catalyzed system, computed at the B3LYP/6-31G(d) level.

^b Activation state.

^c In kcal/mol.

^d In s⁻¹.

สถาบันวิทยบริการ
จุฬาลงกรณ์มหาวิทยาลัย

4.2.2 H-ZSM-5-catalyzed system

Two possible mechanisms of the conversion reaction of EtOH reactant to DEE product as the concerted and stepwise processes were found. Relative energies and thermodynamic properties of two reaction mechanisms were derived from the frequency calculations at the ONIOM(B3LYP/6-31G(d):AM1) approach.

4.2.2.1 Stepwise reaction mechanism

Reaction steps of the stepwise mechanism of EtOH conversion on the 56/5T cluster model of H-ZSM-5 are shown in Fig. 4.9. The ONIOM(B3LYP/6-31G(d):AM1) optimized structures of the 56/5T-cluster-modeled H-ZSM-5 zeolite symbolized as HZ, EtOH, adsorbed-state intermediates INT1, INT2, INT3, INT4, ethoxide species ZEt, transition states TS1 and TS2 (TS) are also given in Fig. 4.9.

The activation energy and free energy of activation, reaction thermodynamic quantities of the stepwise mechanism of EtOH conversion to DEE on H-ZSM-5 are given in Table 4.10. It shows two activation of all six reaction steps. The first step is an adsorption of a EtOH molecule on H-ZSM-5 of which binding energy -16.93 kcal/mol and free energy $\Delta G_{298}^{\circ} = -7.32$ kcal/mol. Due to the transition states TS1 (the second step) and TS2 (the fifth step), the activation energies and their corresponding free energies of activations are 79.01 and 85.59 kcal/mol, and 57.07 and 65.41 kcal/mol, respectively. Rate constant for the first and second activations are 1.12×10^{-50} and $6.94 \times 10^{-36} \text{ s}^{-1}$, respectively and their corresponding equilibrium constants are 2.40×10^{-10} and 2.96×10^8 , respectively. Therefore, we can conclude that first step is the rate determining step of the stepwise process. The third step is a dehydration process of INT2 to afford ZEt species, see Fig. 4.9. The fourth step is an adsorption of a EtOH molecule on the methoxylated ZSM-5 as INT3 species. Reaction energies for these two reaction steps are not much different. The last reaction step is a desorption process of the product DEE. Relative energy profile of stepwise mechanism of EtOH conversion on 56/5T cluster model of H-ZSM-5 is shown in Fig. 4.10.

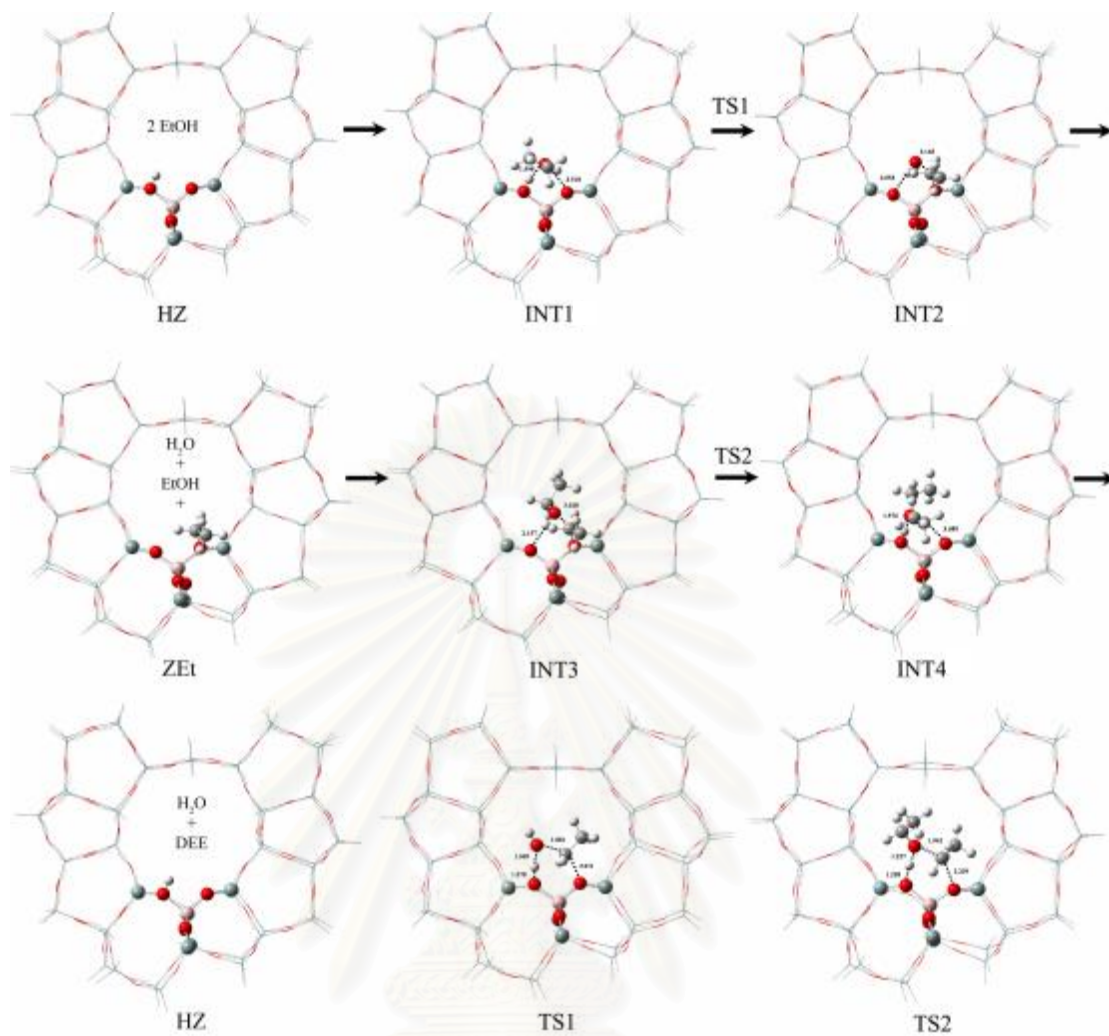


Figure 4.9 Stepwise mechanism of EtOH conversion to DEE on 56/5T cluster model of H-ZSM-5.

สถาบันวิทยบริการ
จุฬาลงกรณ์มหาวิทยาลัย

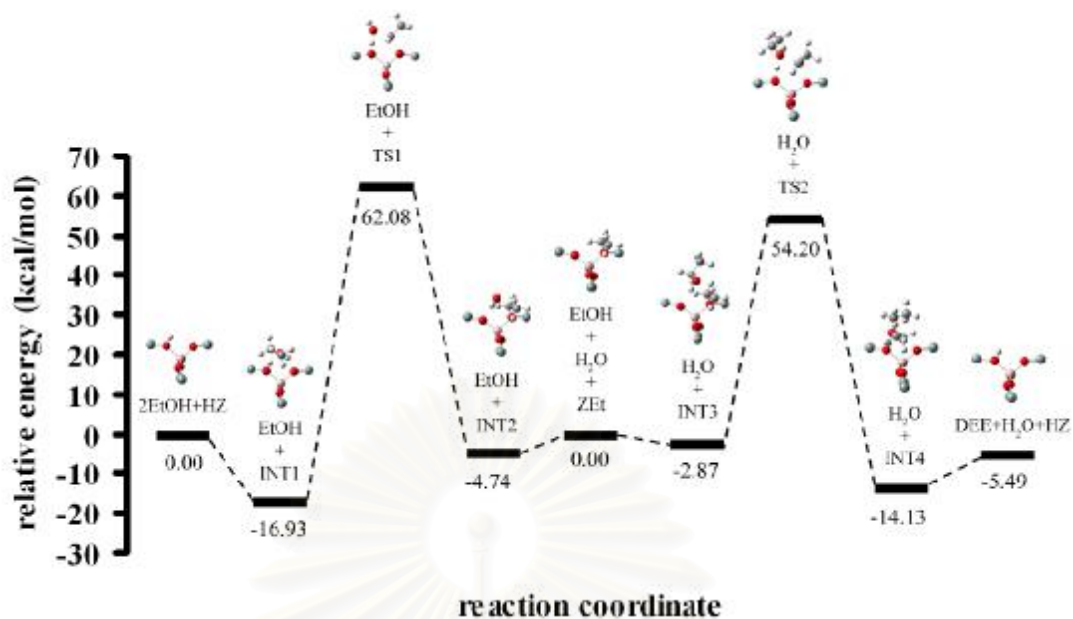


Figure 4.10 Relative energy profile for EtOH conversion to DEE on H-ZSM-5 (modeled as 56/5T cluster) via stepwise mechanism.

Table 4.9 Geometrical data based on the ONIOM(B3LYP/6-31G(d):AM1) calculations of intermediate and transition state in EtOH conversion to DEE via stepwise mechanism in gas phase

Parameter/Conformer	INT1	TS1	INT2	INT3	TS2	INT4
Bond distance (Å)						
O1-H1	1.030	1.078	2.053	-	-	-
O2-C1	3.518	2.011	1.492	1.493	2.239	3.689
O3-H1	2.157	1.369	0.974	-	-	-
O3-C1	1.443	1.881	3.165	-	-	-
O1-H2	-	-	-	2.157	1.258	1.026
O4-H2	-	-	-	0.973	1.227	1.576
O4-C1	-	-	-	3.028	1.942	1.444
Bond Angle (Degree)						
Si1-O1-Al	139.20	132.31	156.75	155.85	131.78	138.24
Si2-O2-Al	140.53	129.37	125.93	126.08	145.95	145.58
O1-Al-O2	99.07	100.30	101.38	101.67	107.97	101.85

Table 4.10 Energies and thermodynamic quantities of the stepwise mechanism of the EtOH conversion to DEE in H-ZSM-5-catalyzed system

Reaction ^a	$\Delta^\ddagger E$ ^{b,c}	$\Delta^\ddagger G$ ^{b,c}	k_{298} ^d	ΔE ^c	ΔG_{298}^o ^c	ΔH_{298}^o ^c	K_{298}
HZ + EtOH $\overset{\curvearrowright}{\rightleftharpoons}$ INT1	-	-	-	-16.93	-7.32	-18.60	2.33×10^5
INT1 $\overset{\curvearrowright}{\rightleftharpoons}$ TS1 $\overset{\curvearrowright}{\rightleftharpoons}$ INT2	79.01	85.59	1.12×10^{-50}	12.19	13.12	13.43	2.40×10^{-10}
INT2' $\overset{\curvearrowright}{\rightleftharpoons}$ ZEt + H ₂ O	-	-	-	4.74	-2.24	7.13	4.42×10^1
ZMe + EtOH $\overset{\curvearrowright}{\rightleftharpoons}$ INT3	-	-	-	-2.86	7.47	-3.50	3.32×10^{-6}
INT3 $\overset{\curvearrowright}{\rightleftharpoons}$ TS2 $\overset{\curvearrowright}{\rightleftharpoons}$ INT4	57.07	65.41	6.94×10^{-36}	-11.27	-11.56	-11.31	2.96×10^8
INT4 $\overset{\curvearrowright}{\rightleftharpoons}$ HZ + DEE	-	-	-	8.64	-1.43	9.29	1.12×10^1

^a Based on the 56/5T cluster model of H-ZSM-5, computed at the ONIOM(B3LYP/6-31G(d):AM1) level.

^b Activation state.

^c In kcal/mol.

^d In s⁻¹.

สถาบันวิทยบริการ
จุฬาลงกรณ์มหาวิทยาลัย

4.2.2.2 Concerted reaction mechanism

Reaction steps of the concerted mechanism of ethanol conversion on the 56/5T cluster model of H-ZSM-5 are shown in Fig. 4.11. The ONIOM(B3LYP/6-31G(d):AM1) optimized structures of the 56/5T-cluster-modeled H-ZSM-5 zeolite (symbolized as HZ and ZH for their acid protons positioned on oxygen atoms at the left and right of aluminum atom, respectively), free EtOH reactant, their adsorbed-state intermediate reactant (INT1), transition state (TS) and adsorbed-state intermediate product (INT2) are also given in Fig. 4.11.

The activation energy and free energy of activation, reaction thermodynamic quantities of the concerted mechanism of EtOH conversion to DEE on H-ZSM-5 are given in Table 4.12. It shows that adsorption of two EtOH molecules on H-ZSM-5 is exothermic (-27.11 kcal/mol) and spontaneous ($\Delta G_{298}^{\circ} = -6.77$ kcal/mol) reactions. Due to the transition state of concerted mechanism, the activation energy and free energy of activation are somewhat high, 58.86 and 67.31 kcal/mol, respectively and this free energy of activation results very small rate constant, $k_{298} = 2.83 \times 10^{-37} \text{ s}^{-1}$. The equilibrium constant of conversion reaction over the activation step, computed using the thermodynamic equation $K_{298} = \exp(-\Delta G_{298}^{\circ}/RT)$ is 3.22×10^{-3} . The intermediate product, INT2 is the adsorption state of DEE and a water molecule on Brønsted acid site of H-ZSM-5 zeolite in which the DEE will be released during desorption process. Relative energy profile of concerted mechanism of EtOH conversion on 56/5T cluster model of H-ZSM-5 is shown in Fig. 4.12.

สถาบันวิทยบริการ
จุฬาลงกรณ์มหาวิทยาลัย

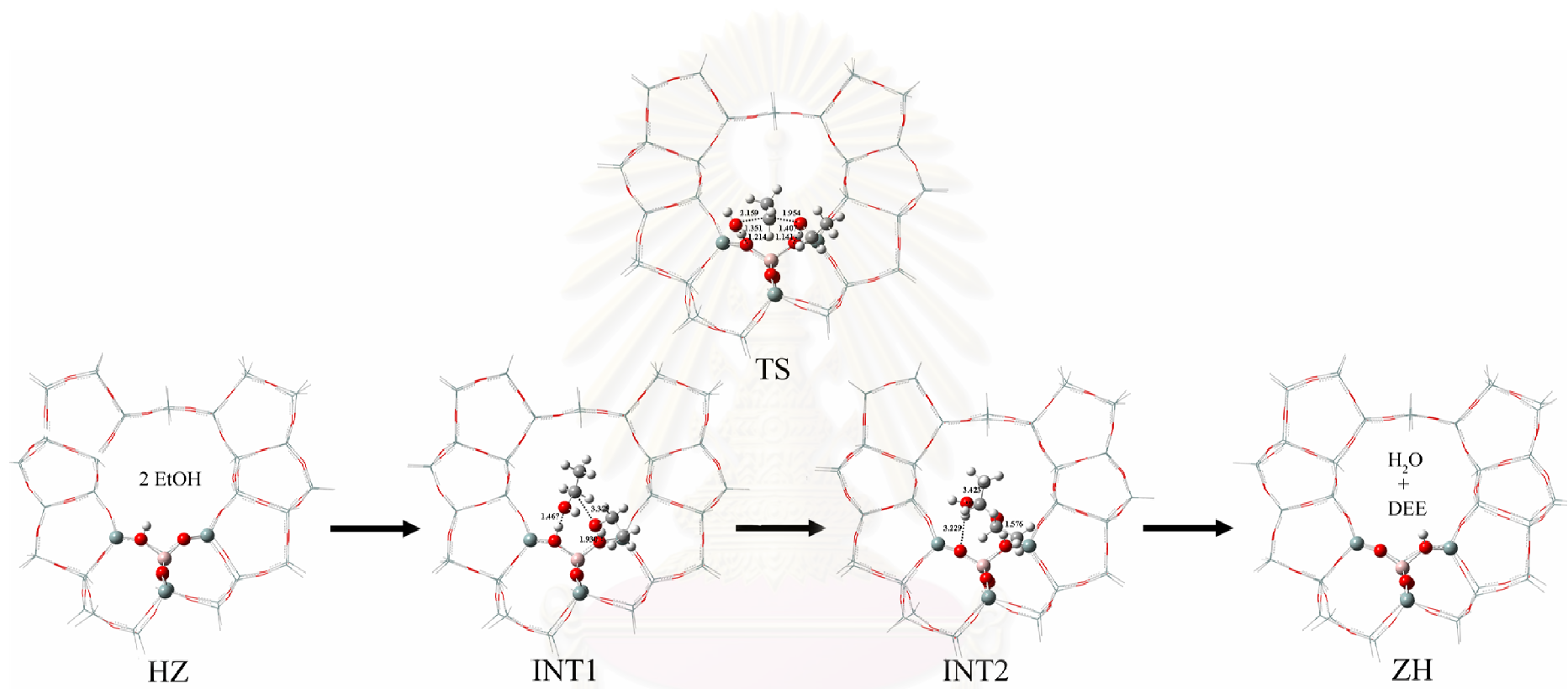


Figure 4.11 Concerted mechanism of EtOH conversion to DEE on 56/5T cluster model of H-ZSM-5.

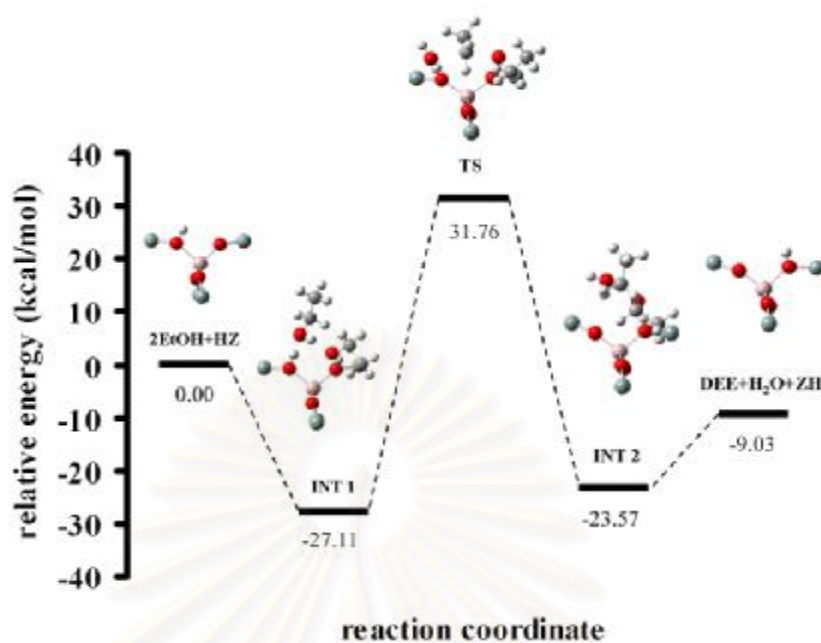


Figure 4.12 Relative energy profile for EtOH conversion to DEE on H-ZSM-5 (modeled as 56/5T cluster) via concerted mechanism.

Table 4.11 Geometrical data based on the ONIOM(B3LYP/6-31G(d):AM1) calculations of intermediate and transition state in EtOH conversion to DEE via concerted mechanism in gas phase

Parameter/Conformer	INT1	TS	INT2
Bond distance (Å)			
O1-H1	1.065	1.214	3.229
O2-H2	1.930	1.141	1.025
O3-H1	1.467	1.351	0.970
O3-C1	1.443	2.159	3.423
O4-H2	0.981	1.407	1.576
O4-C1	3.375	1.954	1.448
O4-C2	1.433	1.523	1.438
Bond Angle (Degree)			
*Si1-O1-Al	137.55	142.14	157.48
*Si2-O2-Al	141.44	132.91	132.18
*O1-Al-O2	101.51	108.78	105.00

Table 4.12 Energies and thermodynamic quantities of the concerted mechanism of EtOH conversion to DEE in H-ZSM-5-catalyzed system

Reaction ^a	$\Delta^\ddagger E$ ^{b,c}	$\Delta^\ddagger G$ ^{b,c}	k_{298} ^d	ΔE ^c	ΔG_{298}° ^c	ΔH_{298}° ^c	K_{298}
HZ+2EtOH $\overset{\curvearrowright}{\rightleftharpoons}$ INT1	-	-	-	-27.11	-6.77	-29.56	9.14×10^4
INT1 $\overset{\curvearrowright}{\rightleftharpoons}$ TS $\overset{\curvearrowright}{\rightleftharpoons}$ INT2	58.86	67.31	2.83×10^{-37}	3.54	3.40	5.71	3.22×10^{-3}
INT2 $\overset{\curvearrowright}{\rightleftharpoons}$ DEE + H ₂ O + ZH	-	-	-	14.54	-2.35	16.93	5.32×10^1

^a Based on the 56/5T cluster model of H-ZSM-5, computed at the ONIOM(B3LYP/6-31G(d):AM1) level.

^b Activation state.

^c In kcal/mol.

^d In s⁻¹.



สถาบันวิทยบริการ
จุฬาลงกรณ์มหาวิทยาลัย

4.3 Synthesis reaction for ethylene

The B3LYP/6-31G(d) optimized structures of EtOH, intermediates, transition states, ethylene (ETL) and all related species in EtOH conversion to ETL in acid-catalyzed system were obtained. The ONIOM(B3LYP/6-31G(d):AM1) optimized structures of EtOH, intermediates, transition states, DEE product and all related species in EtOH conversion to DEE in H-ZSM-5-catalyzed system were obtained.

4.3.1 Acid-catalyzed system

Reaction steps of EtOH conversion to ETL in acid-catalyzed system are shown in Fig. 4.13. The B3LYP/6-31G(d) optimized structures of the reactants, intermediates INT1, INT2, transition states TS and products are also given in Fig. 4.13.

Geometrical data based on the B3LYP/6-31G(d) calculations of intermediate and transition state in EtOH conversion to ETL in acid-catalyzed system in gas phase are also given in Table 4.13.

The activation energy and free energy of activation, reaction thermodynamic quantities of EtOH conversion to ETL in acid-catalyzed system are given in Table 4.14. It shows an activation of all four reaction steps. The first reaction step, the first EtOH molecule is protonated by hydronium ion to prepare the protonated ethanol (EtOH_2^+) which reacts with the second EtOH molecule to produce INT1 of which binding energy -10.91 kcal/mol and free energy $\Delta G_{298}^\circ = -1.99$ kcal/mol. Due to the transition states TS (the third step), the activation energies and their corresponding free energies of activations are 4.44 and 9.66 kcal/mol. Rate constant for the activation is $5.12 \times 10^5 \text{ s}^{-1}$, and its corresponding equilibrium constant is 8.52×10^{-2} . The last reaction step affords the protonated ethanol (EtOH_2^+) and ETL product, see Fig. 4.13. Relative energy profile of EtOH conversion to ETL in acid-catalyzed system is shown in Fig. 4.14.

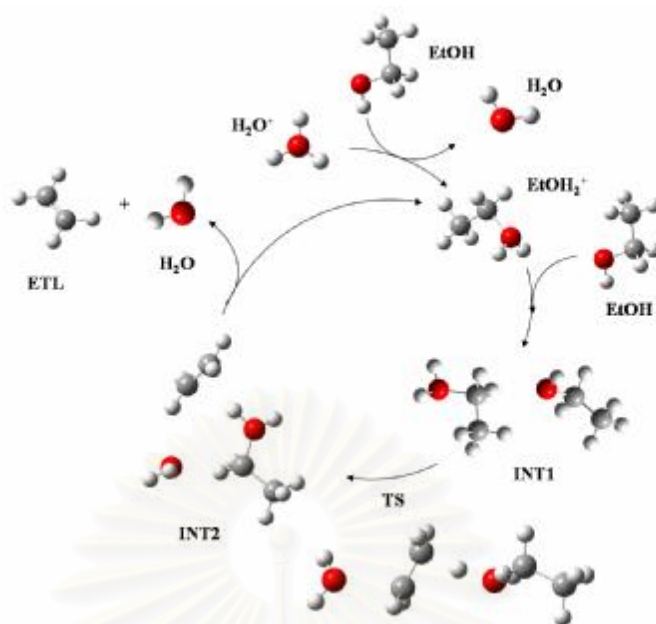


Figure 4.13 Reaction cycle of EtOH conversion to ETL in acid-catalyzed system.

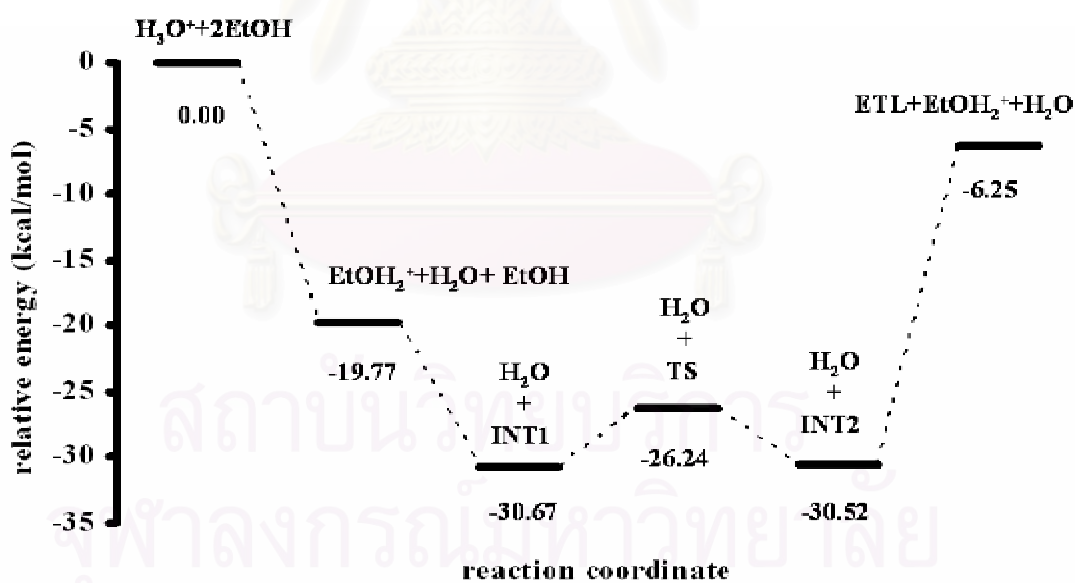


Figure 4.14 Relative energy profile for EtOH conversion to ETL in acid-catalyzed system.

Table 4.13 Geometrical data based on the B3LYP/6-31G(d) calculations of intermediate and transition state in EtOH conversion to ETL in acid-catalyzed system

Parameter/Conformer	INT1	TS1	INT2
Bond distance (Å)			
O3-C1	1.592	2.345	3.368
O4-H3	2.465	1.286	1.030
O4-C2	1.443	1.482	1.533
O4-H2	0.970	0.976	0.979

Table 4.14 Energies and thermodynamic quantities of EtOH conversion to ETL in acid-catalyzed system

Reaction ^a	$\Delta^\ddagger E$ ^{b,c}	$\Delta^\ddagger G$ ^{b,c}	k_{298} ^d	ΔE ^c	ΔG_{298}° ^c	ΔH_{298}° ^c	K_{298}
H ₃ O ⁺ +EtOH \rightleftharpoons EtOH ₂ ⁺ +H ₂ O	-	-	-	-19.77	20.89	-20.17	2.05 x 10 ¹⁵
EtOH ₂ ⁺ +EtOH \rightleftharpoons INT1	-	-	-	-10.91	-1.99	-11.55	2.87 x 10 ¹
INT1 \rightleftharpoons TS \rightleftharpoons INT2	4.44	9.66	5.12 x 10 ⁵	0.16	1.46	4.37	8.52 x 10 ⁻²
INT2 \rightleftharpoons ETL+EtOH ₂ ⁺ +H ₂ O	-	-	-	24.26	10.75	27.27	1.32 x 10 ⁸

^a Based on acid-catalyzed system, computed at the B3LYP/6-31G(d) level.

^b Activation state.

^c In kcal/mol.

^d In s⁻¹.

สถาบันวิทยบริการ
จุฬาลงกรณ์มหาวิทยาลัย

4.3.2 H-ZSM-5-catalyzed system

Two possible mechanisms of the conversion reaction of EtOH to ETL as the stepwise and concerted processes were found. Relative energies and thermodynamic properties of two reaction mechanisms were derived from the frequency calculations at the ONIOM(B3LYP/6-31G(d):AM1) approach.

4.3.2.1 Stepwise reaction mechanism

Reaction steps of the stepwise mechanism of EtOH conversion on the 56/5T cluster model of H-ZSM-5 are shown in Fig 4.13. The ONIOM(B3LYP/6-31G(d):AM1) optimized structures of the 56/5T-cluster-modeled H-ZSM-5 zeolite symbolized as HZ, EtOH, adsorbed-state intermediates INT1, INT2, INT3, INT4, ethoxide species ZEt, transition states TS1 and TS2 (TS) are also given in Fig. 4.13.

The activation energy and free energy of activation, reaction thermodynamic quantities of the stepwise mechanism of EtOH conversion to ETL on H-ZSM-5 are given in Table 4.14. It shows two activation of all six reaction steps. The first step is an adsorption of a EtOH molecule on H-ZSM-5 of which binding energy -16.93 kcal/mol and free energy $\Delta G_{298}^{\circ} = -7.32$ kcal/mol. Due to the transition states TS1 (the second step) and TS2 (the fifth step), the activation energies and their corresponding free energies of activations are 79.01 and 85.59 kcal/mol, and 29.00 and 33.99 kcal/mol, respectively. Rate constant for the first and second activations are 1.12×10^{-50} and $7.47 \times 10^{-13} \text{ s}^{-1}$, respectively and their corresponding equilibrium constants are 2.40×10^{-10} and 4.75×10^{-8} , respectively. Therefore, we can conclude that the first step is the rate determining step of the stepwise process. The third step is a dehydration process of INT2 to afford ZEt species, see Fig. 4.13. The fourth step, the ethoxylated ZSM-5 as INT3 species protonate its proton to prepare INT4. Reaction energies for these two reaction steps are not much different. The last reaction step is a desorption process of the product ETL. Relative energy profile of stepwise mechanism of EtOH conversion on 56/5T cluster model of H-ZSM-5 is shown in Fig. 4.14.

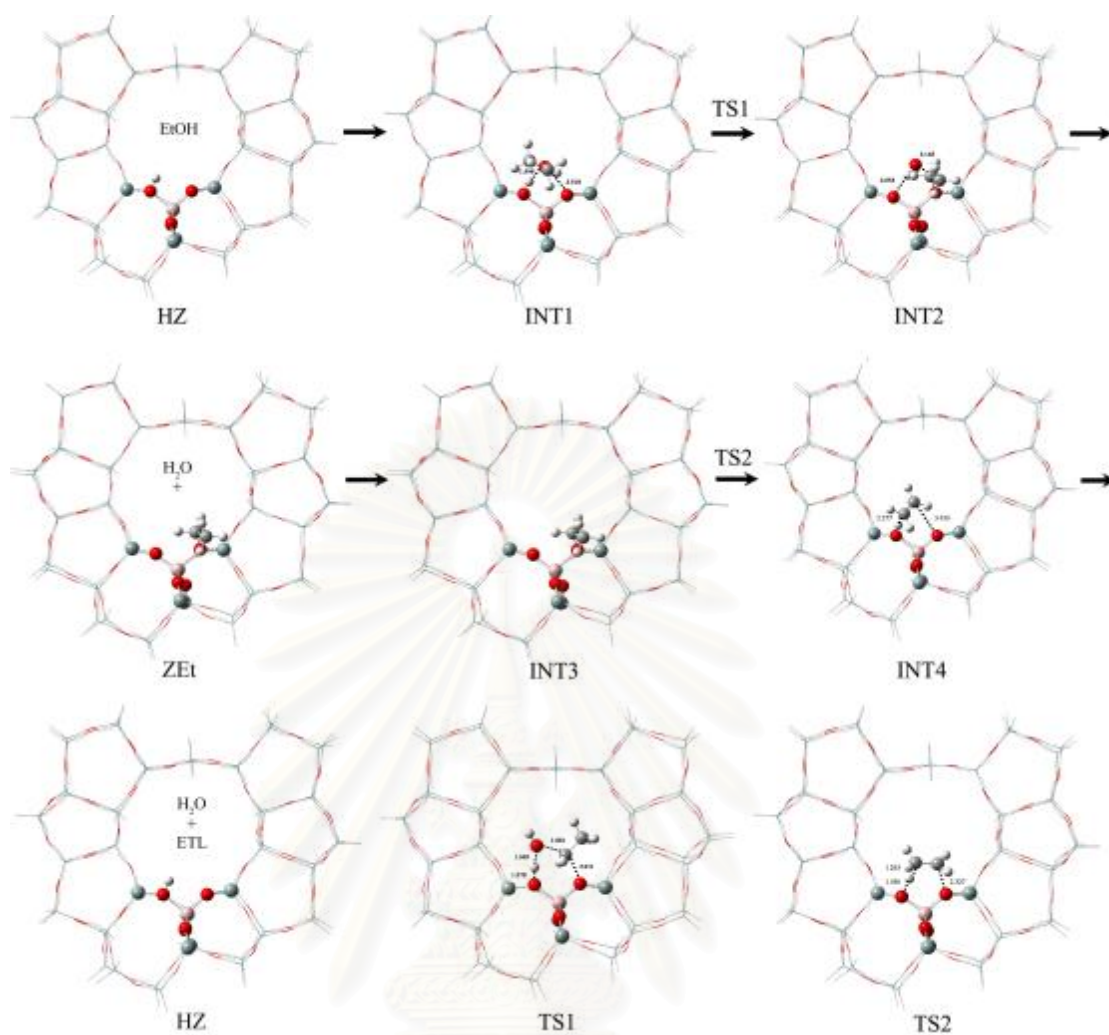


Figure 4.15 Stepwise mechanism of EtOH conversion to ETL on 56/5T cluster model of H-ZSM-5.

สถาบันวิทยบริการ
จุฬาลงกรณ์มหาวิทยาลัย

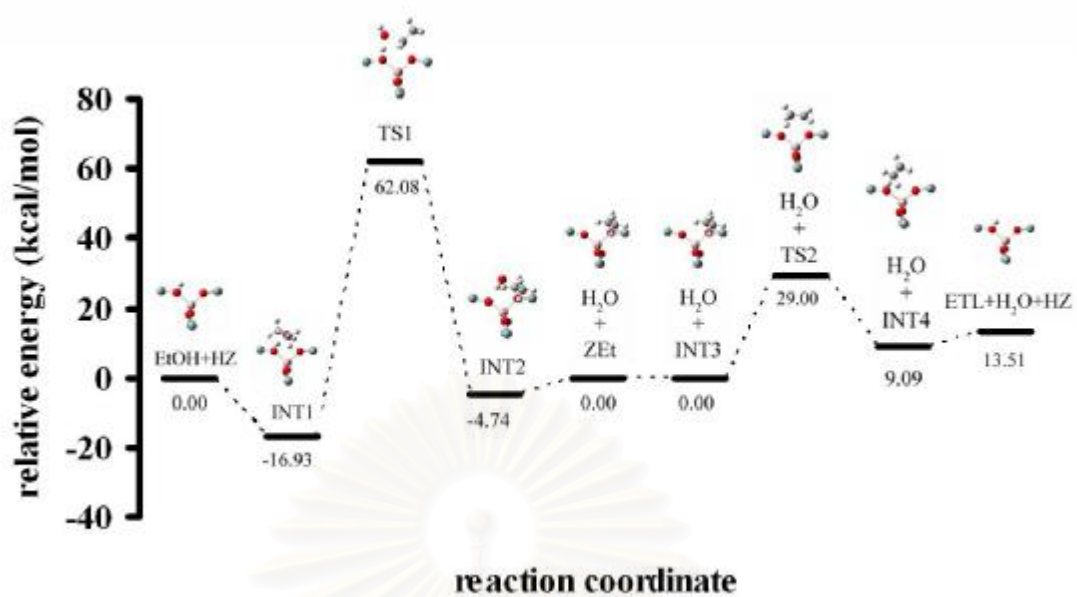


Figure 4.16 Relative energy profile for EtOH conversion to ETL on H-ZSM-5 (modeled as 56/5T cluster) via stepwise mechanism.

Table 4.15 Geometrical data based on the ONIOM(B3LYP/6-31G(d):AM1) calculations of intermediate and transition state in EtOH conversion to ETL via stepwise mechanism in gas phase

Parameter/Conformer	INT1	TS1	INT2	INT3	TS2	INT4
Bond distance (Å)						
O1-H1	1.030	1.672	2.053	-	-	-
O2-C1	3.518	2.095	1.492	1.490	2.327	3.456
O3-H1	2.157	1.011	0.974	-	-	-
O3-C1	1.443	2.120	3.165	-	-	-
C2-H2	-	-	-	1.092	1.265	2.277
O1-H2	-	-	-	3.736	1.430	0.992
C1-C2	-	-	-	1.516	1.392	1.338
Bond Angle (Degree)						
Si1-O1-Al	139.20	138.31	156.75	160.99	145.64	138.78
Si2-O2-Al	140.53	138.26	125.93	124.86	134.57	144.36
O1-Al-O2	99.07	107.69	101.38	102.62	99.20	101.15

Table 4.16 Energies and thermodynamic quantities of the stepwise mechanism of the EtOH conversion to ETL in H-ZSM-5-catalyzed system

Reaction ^a	$\Delta^\ddagger E$ ^{b,c}	$\Delta^\ddagger G$ ^{b,c}	k_{298} ^d	ΔE ^c	ΔG_{298}^o ^c	ΔH_{298}^o ^c	K_{298}
HZ + EtOH $\overset{\curvearrowright}{\rightleftharpoons}$ INT1	-	-	-	-16.93	-7.32	-18.60	2.33×10^5
INT1 $\overset{\curvearrowright}{\rightleftharpoons}$ TS1 $\overset{\curvearrowright}{\rightleftharpoons}$ INT2	79.01	85.59	1.12×10^{-50}	12.19	13.12	13.43	2.40×10^{-10}
INT2' $\overset{\curvearrowright}{\rightleftharpoons}$ ZMe + H ₂ O	-	-	-	4.74	-2.24	7.13	4.42×10^1
ZMe $\overset{\curvearrowright}{\rightleftharpoons}$ INT3	-	-	-	0.00	0.00	0.00	1.00×10^0
INT3 $\overset{\curvearrowright}{\rightleftharpoons}$ TS2 $\overset{\curvearrowright}{\rightleftharpoons}$ INT4	29.00	33.99	7.47×10^{-13}	9.10	9.99	12.93	4.75×10^{-8}
INT4 $\overset{\curvearrowright}{\rightleftharpoons}$ HZ + ETL	-	-	-	4.42	-3.33	5.21	2.75×10^2

^a Based on the 56/5T cluster model of H-ZSM-5, computed at the ONIOM(B3LYP/6-31G(d):AM1) level.

^b Activation state.

^c In kcal/mol.

^d In s⁻¹.

สถาบันวิทยบริการ
จุฬาลงกรณ์มหาวิทยาลัย

4.3.2.2 Concerted reaction mechanism.

Reaction steps of the concerted mechanism of EtOH conversion on the 56/5T cluster model of H-ZSM-5 are shown in Fig. 4.15. The ONIOM(B3LYP/6-31G(d):AM1) optimized structures of the 56/5T-cluster-modeled H-ZSM-5 zeolite (symbolized as HZ and ZH for their acid protons positioned on oxygen atoms at the left and right of aluminum atom, respectively), free EtOH reactant, their adsorbed-state intermediate reactant (INT1), transition state (TS) and adsorbed-state intermediate product (INT2) are also given in Fig. 4.15.

The activation energy and free energy of activation, reaction thermodynamic quantities of the concerted mechanism of EtOH conversion to ETL on H-ZSM-5 are given in Table 4.16. It shows that adsorption of an EtOH molecule on H-ZSM-5 is exothermic (-16.93 kcal/mol) and spontaneous ($\Delta G_{298}^{\circ} = -7.32$ kcal/mol) reactions. Due to the transition state of concerted mechanism, the activation energy and free energy of activation are somewhat high, 88.12 and 97.09 kcal/mol, respectively and this free energy of activation results very small rate constant, $k_{298} = 4.14 \times 10^{-59} \text{ s}^{-1}$. The equilibrium constant of conversion reaction over the activation step, computed using the thermodynamic equation $K_{298} = \exp(-\Delta G_{298}^{\circ}/RT)$ is 9.37×10^{-15} . The intermediate product, INT2 is the adsorption state of ETL and a water molecule on Brønsted acid site of H-ZSM-5 zeolite in which the ETL will be released during desorption process. Relative energy profile of concerted mechanism of EtOH conversion on 56/5T cluster model of H-ZSM-5 is shown in Fig. 4.16.

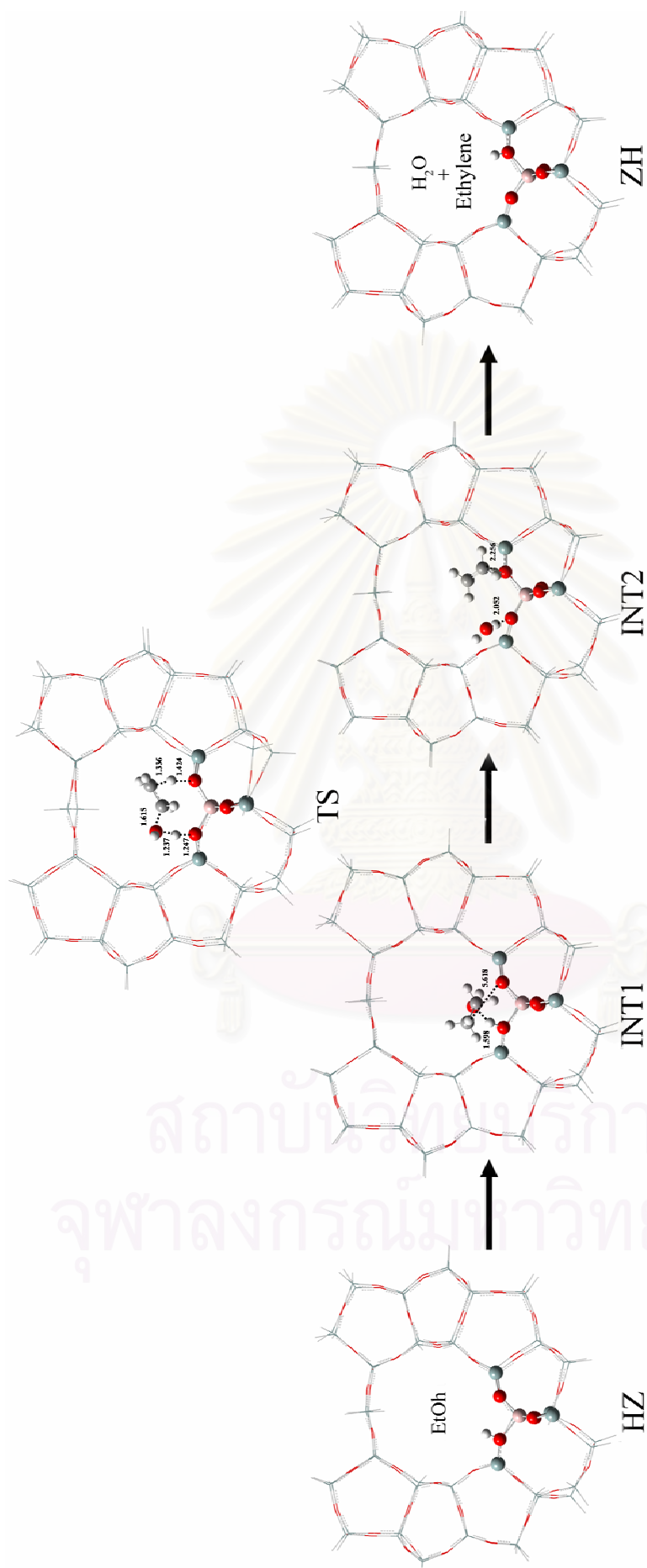


Figure 4.17 Concerted mechanism of EtOH conversion to ETL on 56/5T cluster model of H-ZSM-5.

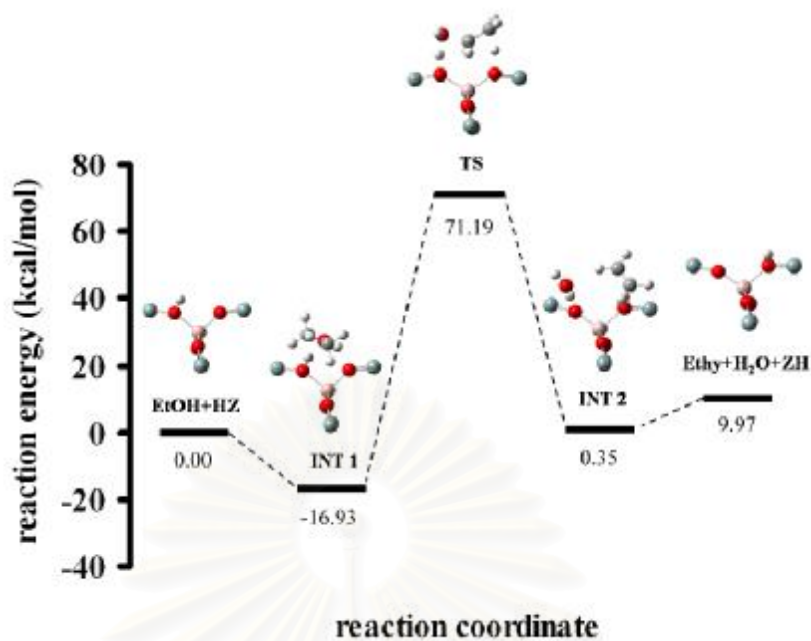


Figure 4.18 Relative energy profile for EtOH conversion to ETL on H-ZSM-5 (modeled as 56/5T cluster) via concerted mechanism.

Table 4.17 Geometrical data based on the ONIOM(B3LYP/6-31G(d):AM1) calculations of intermediate and transition state in EtOH conversion to ETL via concerted mechanism in gas phase

Parameter/Conformer	INT1	TS	INT2
Bond distance (Å)			
O1-H1	1.030	1.247	2.052
O2-H2	5.618	1.424	0.994
O3-H1	1.598	1.237	0.974
O3-C1	1.443	1.615	3.242
C1-C2	1.517	1.440	1.339
C2-H2	1.095	1.336	2.256
Bond Angle (Degree)			
Si1-O1-Al	139.20	136.56	153.09
Si2-O2-Al	140.53	133.12	131.13
O1-Al-O2	99.07	118.22	105.11

Table 4.18 Energies and thermodynamic quantities of the concerted mechanism of EtOH conversion to ETL in H-ZSM-5-catalyzed system

Reaction ^a	$\Delta^\ddagger E$ ^{b,c}	$\Delta^\ddagger G$ ^{b,c}	k_{298} ^d	ΔE ^c	ΔG_{298}° ^c	ΔH_{298}° ^c	K_{298}
HZ+EtOH $\overset{\curvearrowright}{\rightarrow}$ INT1	-	-	-	-16.93	-7.32	-18.60	2.33×10^5
INT1 $\overset{\curvearrowright}{\rightarrow}$ TSS $\overset{\curvearrowright}{\rightarrow}$ INT2	88.12	97.09	4.14×10^{-59}	17.28	19.14	21.90	9.37×10^{-15}
INT2 $\overset{\curvearrowright}{\rightarrow}$ ETL + H ₂ O + ZH	-	-	-	9.62	-5.36	13.44	8.49×10^3

^a Based on the 56/5T cluster model of H-ZSM-5, computed at the ONIOM(B3LYP/6-31G(d):AM1) level.

^b Activation state.

^c In kcal/mol.

^d In s⁻¹.



สถาบันวิทยบริการ
จุฬาลงกรณ์มหาวิทยาลัย

4.4 Arrhenius plot for diethyl ether and ethylene formation

The ONIOM(B3LYP/6-31G(d):AM1) optimized structures of EtOH, intermediates INT1 and transition states TS, in concerted mechanism of EtOH conversion to DEE and concerted mechanism of EtOH conversion to ETL using H-ZSM-5 catalyst and vary temperature were obtained. The dependence of natural logarithm of rate constants, $\ln k$, was shown in the Arrhenius plot in Fig. 4.17.

Table 4.19 Rate constants between intermediate INT1 and the transition state TS for different temperature in DEE and ETL formation via concerted mechanism

T ^a	k ^{b,d}	k ^{c,d}
298.15	2.83×10^{-37}	4.14×10^{-59}
373.15	1.24×10^{-24}	1.34×10^{-46}
473.15	2.69×10^{-18}	2.02×10^{-38}
573.15	1.62×10^{-13}	2.31×10^{-27}
673.15	1.68×10^{-10}	5.70×10^{-27}

^a In K.

^b Based on EtOH conversion to DEE in H-ZSM-5 via concerted mechanism.

^c Based on EtOH conversion to ETL in H-ZSM-5 via concerted mechanism.

^d In s⁻¹.

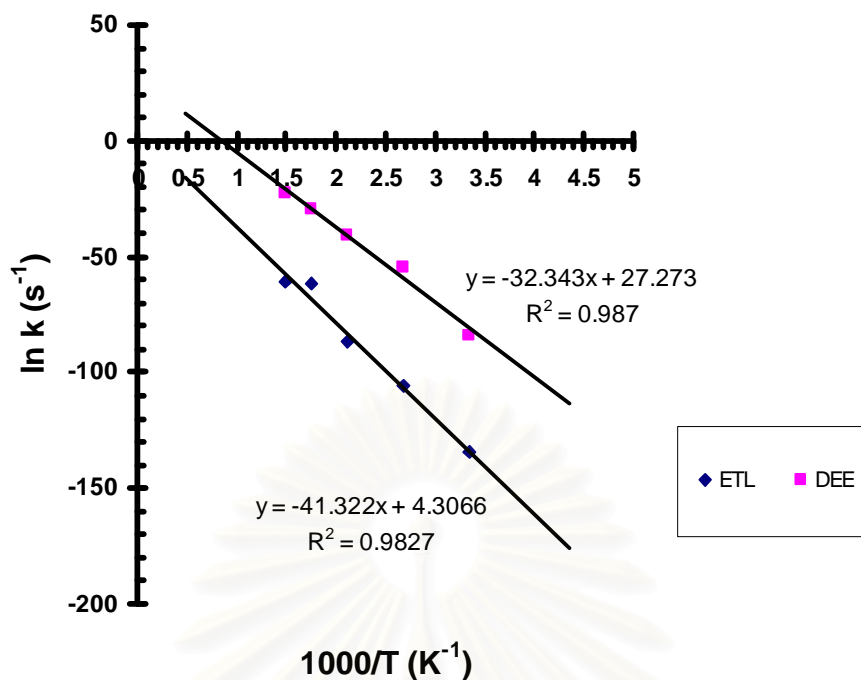


Figure 4.19 Arrhenius plot: temperature (T) dependence of the natural logarithm of the rate constants, $\ln k$, in the conversion of EtOH to DEE and ETL via concerted mechanism using H-ZSM-5 catalyst.

Table 4.19 shows the rate constants of DEE formation via concerted mechanism and ETL formation via concerted mechanism, they increase very rapidly to very large values at high temperatures. From the linear fit of the curves, see in Fig. 4.19, the Arrhenius plots, Arrhenius activation energies were obtained. From the eq. (26) in chapter II and the Arrhenius plots in Fig. 4.19, the activation energies (ΔE^\ddagger) of the DEE formation via concerted mechanism is 64.23 kcal/mol and 82.06 kcal/mol in the ETL formation via concerted mechanism they are more than the activation energy at room temperature of DEE formation via concerted mechanism by 5.37 kcal/mol and smaller than the activation energy at room temperature of ETL formation via concerted mechanism by 6.06 kcal/mol, respectively.

4.5 Discussion

In acid-catalyzed system, the synthesis reaction for ETL is more favorable by 6.46 kcal/mol and 5.78 kcal/mol than the synthesis reaction for DEE and the synthesis reaction for DME, respectively, shown in Table 4.20.

The synthesis reactions for DME, DEE and ETL in acid-catalyzed system are more favorable by 64.54 kcal/mol, 68.11 kcal/mol and 74.57 kcal/mol than the stepwise reactions and more favorable by 53.17 kcal/mol, 47.96 kcal/mol and 83.68 kcal/mol than the concerted reactions of the synthesis reactions for DME, DEE and ETL in H-ZSM-5-catalyzed system, respectively, shown in Table 4.20.

In H-ZSM-5-catalyzed system, the synthesis reaction for DME via stepwise reaction is more favorable by 4.25 kcal/mol than the synthesis reactions for DEE and ETL via stepwise reaction. The synthesis reaction for DME via concerted reaction is more favorable by 24.73 kcal/mol than the synthesis reaction for ETL via concerted reaction, but less favorable by 4.53 kcal/mol than the synthesis reaction for DEE via concerted reaction, shown in Table 4.20.

In H-ZSM-5-catalyzed system, the synthesis reaction for ETL via stepwise reaction is more favorable by 50.01 kcal/mol than the synthesis reaction for DEE via stepwise reaction, shown in Table 4.20. But in the synthesis reaction for DEE via concerted reaction is more favorable by 29.26 kcal/mol than the synthesis reaction for ETL via concerted reaction.

Some equilibrium constants of the synthesis reaction for DME, DEE and ETL were shown in Table 4.20, $K(\text{INT1} \rightleftharpoons \text{TSS} \rightleftharpoons \text{INT2})$ is the equilibrium constant of the conversion of INT1 to INT2 in the reactions and $K(\text{INT3} \rightleftharpoons \text{TSS} \rightleftharpoons \text{INT4})$ is the equilibrium constant of the conversion of INT3 to INT4 in the reactions, according to the results. Rate constants that calculated from the transition-state theory was shown in Table 4.20.

Table 4.20 Rate constants k (s^{-1}), equilibrium constants K and activation energies ΔE^\ddagger (kcal/mol) of the synthesis reactions for DME, DEE and ETL in acid-catalyzed system and H-ZSM-5-catalyzed system

Catalyst / K / E_a / k	DME	DEE	ETL
Hydronium ion catalyst			
ΔE^\ddagger (TS)	10.22	10.90	4.44
k	5.46×10^4	3.51×10^4	5.12×10^5
K (INT1 \ddot{S} TS \ddot{S} INT2)	1.13×10^7	1.28×10^9	8.52×10^{-2}
H-ZSM-5 zeolite catalyst			
Step wise mechanism			
ΔE^\ddagger_1 (TS1)	74.76	79.01	79.01
k_1	2.54×10^{-46}	1.12×10^{-50}	1.12×10^{-50}
K (INT1 \ddot{S} TS \ddot{S} INT2)	6.21×10^{-10}	2.40×10^{-10}	2.40×10^{-10}
ΔE^\ddagger_2 (TS2)	56.92	57.07	29.00
k_2	9.89×10^{-35}	6.94×10^{-36}	7.47×10^{-13}
K (INT3 \ddot{S} TS \ddot{S} INT4)	1.47×10^8	2.96×10^8	4.75×10^{-8}
Concerted mechanism			
ΔE^\ddagger (TS)	63.39	58.86	88.12
k	1.45×10^{-40}	2.83×10^{-37}	4.14×10^{-59}
K (INT1 \ddot{S} TS \ddot{S} INT2)	8.10×10^{-4}	3.22×10^{-3}	9.37×10^{-15}

The comparison of computational modeling mechanisms of the conversion of MeOH to DME in H-ZSM-5-catalyzed system with experimental data can be obtained. According to the experimental data [28], that obtained the methoxy surface when the MeOH reactant reacted on the surface of H-ZSM-5 zeolite catalyst and then another MeOH reacts with methoxy surface to produce the DME product, see in Fig. 4.20, 4.21. In this work, the methoxy surface can be obtained in the stepwise mechanism of the conversion of MeOH to DME, that suggests the ethoxy surface of the DEE and ETL formation in the stepwise mechanism.

According to the results, the comparison of computational modeling mechanisms of the conversion of EtOH to DEE and ETL in H-ZSM-5-catalyzed system with experimental data can be obtained. In the experimental data [29], in most cases of zeolites below 400 °C, low reaction temperature favored the exclusive formation of DEE by intermolecular dehydration between two EtOH molecules, although the conversion of EtOH was low. The conversion of EtOH as well as the selectivity of ETL increased with the increase in the reaction temperature, while the selectivity of DEE was decreased. ETL was formed by intermolecular dehydration, see in Fig. 4.22. This work shows that the conversion of EtOH to DEE is more favorable than the conversion of EtOH to ETL in the concerted mechanism of their reactions, that follow the experimental data of the conversion of EtOH to DEE and ETL at low temperature of reaction. At high temperature, the experimental data showed the increase of ETL. This work shows that the conversion of EtOH to ETL is more favorable than the conversion of EtOH to DEE in the stepwise mechanism of their reactions, that follow the experimental data of the conversion of EtOH to DEE and ETL at high temperature reaction.

From the result and discussion, the stepwise and concerted mechanisms of the DME, DEE and ETL formation using H-ZSM-5 zeolite catalyst that obtained in this work should be possible path-ways of these reactions.

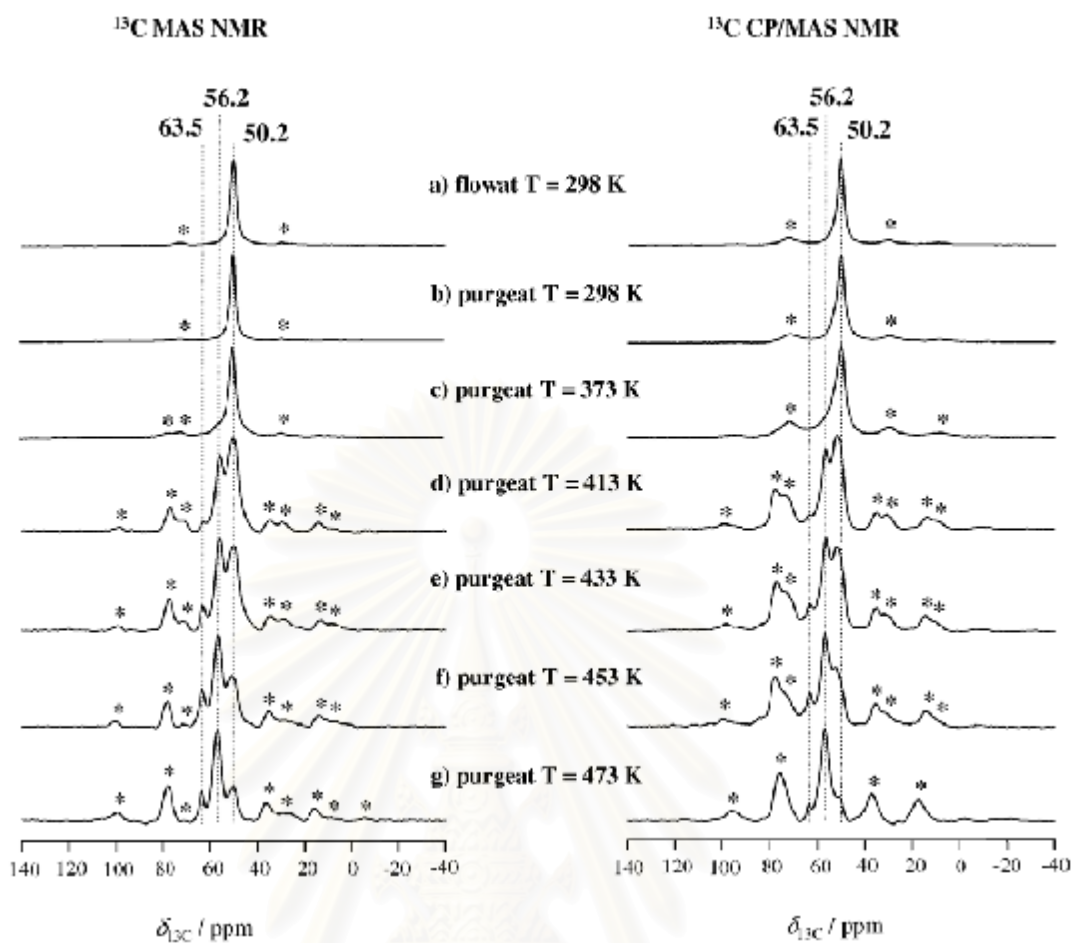


Figure 4.20 In situ ^{13}C MAS NMR spectra of zeolite H-Y recorded during the formation of methoxy groups (56.2 ppm), methanol (50.2) and dimethyl ether (63.5) at different temperatures [28].



Figure 4.21 The reaction of ^{13}C -enriched surface methoxy groups with $^{12}\text{CH}_3\text{OH}$ leading to $^{13}\text{CH}_3\text{O}^{12}\text{CH}_3$ [28].

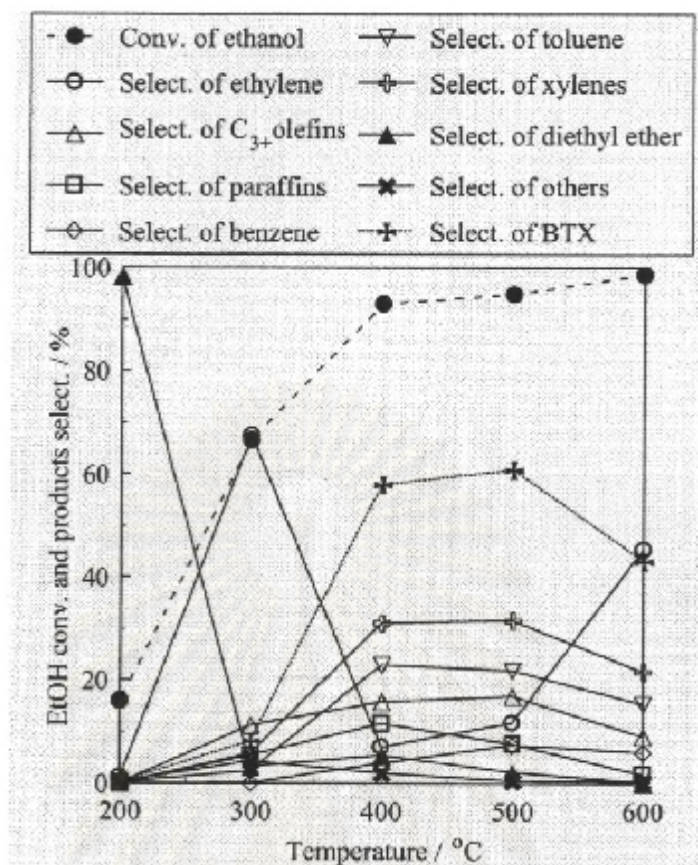


Figure 4.22 Effect of reaction temperature on conversion of ethanol and selectivity of each product over H-ZSM-5 zeolite catalyst [29].

CHAPTER V

CONCLUSIONS AND SUGGESTIONS

5.1 Acid-catalyzed system.

All reactants (MeOH and EtOH), intermediates (INT1 and INT2), transition state (TS) and products (DME, DEE and ETL), their molecular structures and energies were computed using the B3LYP/6-31G(d). From the results, it can be concluded as follows:

1. The reaction of MeOH conversion to DME and EtOH conversion to DEE consist of five reaction steps. The first step reaction, the first MeOH molecule is protonated by hydronium ion to prepare the protonated. The second step reaction, the MeOH_2^+ reacts with the second MeOH molecule to produce INT1. The third step reaction is the transition state TS. The fourth step reaction affords the DME.H^+ . The last step is the releasing process for freeing a molecule of hydronium ion and DME.

2. The EtOH conversion to ETL consists of four reaction steps. The first step reaction, the first EtOH molecule is protonated by hydronium ion to prepare the EtOH_2^+ . The second step reaction, the EtOH_2^+ reacts with the second EtOH molecule to produce INT1. The third step reaction is the transition state TS. The last step reaction affords the EtOH_2^+ and ETL.

3. The comparison of the activation energies, rate constants and equilibrium constants in the third step (INT1 \rightarrow TS \rightarrow INT2) of the reaction of MeOH conversion to DME, EtOH conversion to DEE and EtOH conversion to ETL are reported. The order of the activation energies, rate constants and equilibrium constants is in decreasing order: the activation energies of formation of DEE > DME > ETL, rate constants of formation of ETL > DME > DEE, and equilibrium constants of formation of DEE > DME > ETL, respectively.

5.2 H-ZSM-5-catalyzed system.

All the intermediates (INT1, INT2, INT3, INT4) and free species, their molecular structures and energies were computed using the B3LYP/6-31G(d). The H-ZSM-5 and its adsorption complexes, a 56/5T cluster model of H-ZSM-5 was employed in corporation with the two-layer ONIOM(B3LYP/6-31G(d):AM1) approach. The concerted and stepwise mechanisms for the conversion of MeOH to DME and EtOH to DEE and ETL were found and their relative energies were compared. The reaction energies and thermodynamic properties of all reaction steps of both of the concerted and stepwise mechanisms of the MeOH and EtOH conversion are reported. From the results, it can be concluded as follows:

1. The stepwise mechanism of the conversion of MeOH and EtOH to DME and DEE, respectively, consists of six reaction steps and its the second and fifth steps are activation reaction barriers. The first step is an adsorption of the first MeOH molecule or EtOH molecule on H-ZSM-5. The second step is the transition state TS1 (rate determining step). The third step is a dehydration process of INT2 to afford MeZ or EtZ. The fourth step is an adsorption of a MeOH molecule or an EtOH molecule on the methoxylated ZSM-5 or ethoxylated ZSM-5, respectively, as INT3 species. The fifth step is transition state TS2. The last step is a desorption process of the product DME or DEE.

2. The stepwise mechanism of the conversion of EtOH to ETL consists of six reaction steps and its the second and fifth steps are activation reaction barriers. The first step is an adsorption of a EtOH molecule on H-ZSM-5. The second step is transition state TS1 (rate determining step). The third step is a dehydration process of INT2 to afford ZEt species. The fourth step, the ethoxylated ZSM-5 as INT3 species protonate its proton to prepare INT4. The last reaction step is a desorption process of the product ETL.

3. The concerted mechanism of the conversion of MeOH to DME and EtOH to DEE consists of three reaction steps and its the second step is activation barriers. The first step is an adsorption of two MeOH or two EtOH molecules on H-ZSM-5. The second step is transition state TS. The third step, INT2 is an adsorption state of DME or DEE and water molecules on H-ZSM-5. The last step is a desorption process of the product DME or DEE.

4. The concerted mechanism of the conversion of EtOH to ETL consists of three reaction steps and its the second step is activation barriers. The first step is an adsorption of an EtOH molecule on H-ZSM-5. The second step is transition state TS. The third step, INT2 is an adsorption state of ETL and water molecule on H-ZSM-5. The last step is a desorption process of the product ETL.

5. The comparison of the activation energies, rate constants and equilibrium in the second step (INT1 \checkmark TS1 \checkmark INT2) and the fifth step (INT3 \checkmark TS2 \checkmark INT4) of the reactions of MeOH conversion to dimethyl ether, EtOH conversion to DEE and EtOH conversion to ETL in stepwise mechanisms are reported. The order of the activation energies, rate constants and equilibrium constants is in decreasing order: the activation energies in the second step of formation of DEE \sim ETL $>$ DME and the fifth step of formation of DEE $>$ DME $>$ ETL, rate constants in the second step of formation of DME $>$ DEE \sim ETL and the fifth step of formation of ETL $>$ DME $>$ DEE, and equilibrium constants in the second step of formation of DME $>$ DEE \sim ETL and the fifth step of formation of DEE $>$ DME $>$ ETL, respectively.

6. The comparison of the activation energies, rate constants and equilibrium constants in the third step reaction (INT1 \checkmark TS \checkmark INT2) of the reaction of MeOH conversion to dimethyl ether, EtOH conversion to DEE and EtOH conversion to ETL in concerted mechanisms are reported. The order of the activation energies, rate constants and equilibrium constants is in decreasing order: the activation of ETL $>$ DME $>$ DEE, rate constants of formation of DEE $>$ DME $>$ ETL, and equilibrium constants of formation of DEE $>$ DME $>$ ETL, respectively.

7. Although, in the acid-catalyzed system of MeOH conversion to DME and EtOH conversion to DEE and ETL shows that are more favorable to synthesize their products than in the H-ZSM-5-catalyzed system. But the properties, as shape-size selectivity, of H-ZSM-5 catalyst in H-ZSM-5-catalyzed system are more favorable to synthesize the gasoline and another products that more expensive than ethers and ETL, because of the DME, DEE and ETL were intermediate products in H-ZSM-5 catalytic reaction that DME, DEE and ETL then convert to the gasoline and another products in MTG and BTG process, at least.

5.3 Suggestions for further work

1. The conversion of methanol to dimethyl ether, ethanol to DEE and ethanol to ethylene on H-ZSM-5 assume that the first reaction step of MTG or BTG process. Next step, dimethyl ether, DEE and ethylene products are converted to gasoline and another hydrocarbons that should be studied for further work.

2. The ONIOM3 method for three-layer such as ONIOM(B3LYP/6-31G(d):HF/3-21G:AM1) or ONIOM(B3LYP/6-31G(d):HF/STO-3G:AM1) should be employed for getting more reliable results.



สถาบันวิทยบริการ
จุฬาลงกรณ์มหาวิทยาลัย

REFERENCES

- [1] Hölderich, W.; Hesse, M. and Näumann, F. Zeolites: Catalysts for organic synthesis. Angew. Chem. Int. Ed. Engl. 27 (1988): 226.
- [2] Corma, A. Inorganic solid acids and their use in acid-catalyzed hydrocarbon reaction. Chem. Rev. 95 (1995): 559.
- [3] Ghobarkar, H.; Schäf, O. and Guth, U. Zeolites-from kitchen to space. Prog. Solid St. Chem. 27 (1999): 29.
- [4] Sen, S. E.; Smith, S. M. and Sullivan, K. A. Organic transformations using zeolites and zeotype materials. Tetrahedron 55 (1999): 12657.
- [5] Valyon, J.; Onyestyák, G. and Rees, L. V. C. Study of the dynamics of NH₃ adsorption in ZSM-5 zeolites and the acidity of the sorption sites using the frequency-response technique. J. Phys. Chem. B 102 (1998): 8994.
- [6] Farneth, W. E. and Gorte, R. J. Methods for characterizing zeolite acidity. Chem. Rev. 95 (1995): 615.
- [7] Yin, F.; Blumenfeld A. L.; Gruver, V. and Fripiat, J. J. NH₃ as a probe molecule for NMR and IR study of zeolite catalyst acidity. J. Phys. Chem. B 101 (1997): 1824.
- [8] Paukshtis, E. A.; Malysheva, L. V. and Stepanov, V. G. Interaction of aromatics with Brønsted sites in zeolites: Demarcation line between regions of stable existence of H-complexes and ion pairs for various types of bases. React. Kinet. Catal. Lett. 65 (1998): 75.
- [9] Barthos, R.; Lónyi, F.; Onyestyák, G. and Valyon, J. An IR, FR, and TPD study on the acidity of H-ZSM-5, sulfated zirconia, and sulfated zirconia-titania using ammonia as the probe molecule. J. Phys. Chem. B 104 (2000): 7311.
- [10] Lónyi, F. and Valyon, J. A TPD and IR study of the surface species formed from ammonia on zeolite H-ZSM-5, H-mordenite and H-beta. Thermochim. Acta 373 (2001): 53.
- [11] Lónyi, F. and Valyon, J. On the interpretation of the NH₃-TPD patterns of H-ZSM-5 and H-mordenite. Microporous Mesoporous Mater. 47 (2001): 293.

- [12] Bore'ave, A.; Auroux, A. and Guimon, C. Nature and strength of acid sites in HY zeolites: a multitechnical approach. Micropor. Mater. 11 (1997): 275.
- [13] Kao, H.-M. and Grey, C. P. Probing the Brønsted and Lewis acidity of zeolite HY: A $^1\text{H}/^{27}\text{Al}$ and $^{15}\text{N}/^{27}\text{Al}$ TRAPDOR NMR study of monomethylamine adsorbed on HY. J. Phys. Chem. 100 (1996): 5105.
- [14] Jacobs, W. P. J. H.; de Haan, J. W.; van de Ven, L. J. M. and van Santen, R. A. Interaction of ammonia with Brønsted acid sites in different cages of zeolite Y as studied by proton MAS NMR. J. Phys. Chem. 97 (1993): 10394.
- [15] Kapustin, G. I. and Brueva, T. R. A simple method for determination of heats of ammonia adsorption on catalysts from thermodesorption data. Thermochim. Acta 379 (2001): 71.
- [16] Katada, N.; Igi, H.; Kim, J.-H. and Niwa, M. Determination of the acidic properties of zeolite by theoretical analysis of temperature-programmed desorption of ammonia based on adsorption equilibrium. J. Phys. Chem. B 101 (1997): 5969.
- [17] Brueva, T. R.; Mishin, I. V. and Kapustin, G. I. Distribution of acid-site strengths in hydrogen zeolites and relationship between acidity and catalytic activity. Thermochim. Acta 379 (2001): 15.
- [18] Parrillo, D. J. and Gorte, R. J. Characterization of acidity in H-ZSM-5, H-ZSM-12, H-Mordenite, and H-Y using microcalorimetry. J. Phys. Chem. 97 (1993): 8786.
- [19] Lee, C.; Parrillo, D. J.; Gorte, R. J. and Farneth, W. E. Relationship between differential heats of adsorption and Brønsted acid strengths of acidic zeolites: H-ZSM-5 and H-Mordenite. J. Am. Chem. Soc. 118 (1996): 3262.
- [20] Zecchina, A.; Geobaldo, F.; Spoto, G.; Bordiga, S.; Ricchiardi, G.; Buzzoni, R. and Petrini, G. FTIR investigation of the formation of neutral and ionic hydrogen-bonded complexes by interaction of H-ZSM-5 and H-Mordenite with CH_3CN and H_2O : Comparison with the H-NAFION superacidic system. J. Phys. Chem. 100 (1996): 16584.

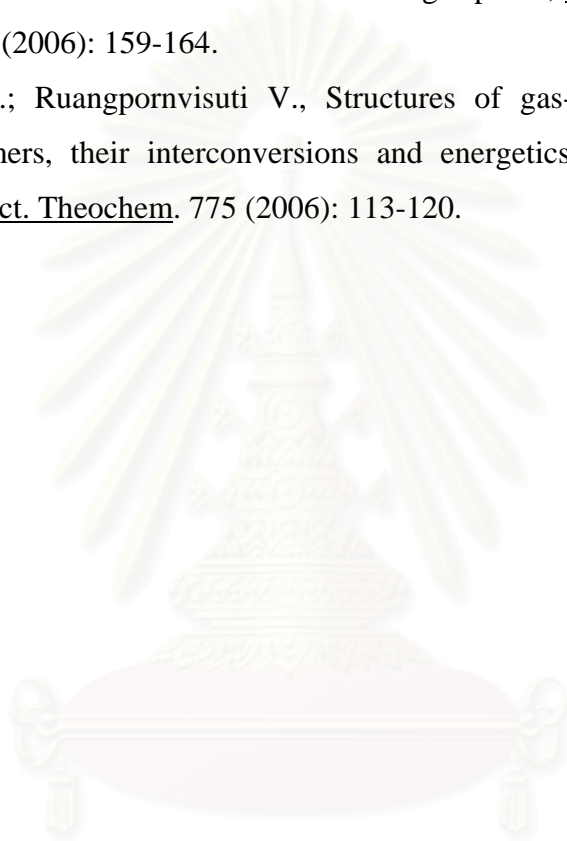
- [21] Pazé, C.; Bordiga, S.; Lamberti, C.; Salvalaggio, M.; Zecchina, A. and Bellussi, G. Acidic properties of H- β zeolite as probed by bases with proton affinity in the 118-204 kcal mol⁻¹ range: A FTIR investigation. J. Phys. Chem. B 101 (1997): 4740.
- [22] Morokuma, K. ONIOM and its applications to material chemistry and catalyze. Bull. Korean Chem. Soc. 24 (2003): 797-801.
- [23] Breck, D. W. Zeolite molecular sieves. Union Carbide Corporation: Tarrytown New York (1984): pp. 312, 373, 529-588.
- [24] Varisli, D.; Dogu, T. and Dogu, G. Ethylene and diethyl-ether production by dehydration reaction of ethanol over different heteropolyacid catalysts. Chemical Engineering Science 62 (2007): 5349 – 5352.
- [25] Bjørgen, M.; Svelle, S.; Joensen, F.; Nerlov, J.; Kolboe, S.; Bonino, F.; Palumbo, L.; Bordiga, S. and Olsbye, U. Conversion of methanol to hydrocarbons over zeolite H-ZSM-5: On the origin of the olefinic species. Journal of Catalysis 249 (2007):195–207.
- [26] Dogu, T. and Varisli, D. Alcohols as Alternatives to Petroleum for environmentally clean fuels and petrochemicals. Turk. J. Chem. 31 (2007): 551–567.
- [27] Arenamarta, S. and Trakarnpruk, V. Ethanol conversion to ethylene using metal-mordenite catalysts. Int. J. Appl. Sci. Eng. 4 (2006): 21-32.
- [28] Wang, W.; Jiang, Y.; and Hunger, M.; Mechanistic investigations of the methanol-to-olefin (MTO) process on acidic zeolite catalysts by in situ solid-state NMR spectroscopy. Cat. Today. 113 (2006): 102–114.
- [29] Inaba, M.; Murata, K.; Saito, M. and Takahara, I. Production of chemical compound from bio-ethanol by zeolite catalysts. IEEE. (2005): 866-872.
- [30] Jiang, S.; Hwang, J.; Jin, T.; Cai, T.; Cho, W.; Baek, Y. and Park, S. Dehydration of methanol to dimethyl ether over ZSM-5 zeolite. Bull. Korean Chem. Soc. 25 (2004): 185-189.
- [31] Fu, Y.; Bertran, J.; Hong, T.; Chen, J.; Auroux, A. and Shena, J. Surface acidity and the dehydration of methanol to dimethyl ether. Thermocimica Acta 434 (2004): 22-26.

- [32] Wetwatana, A. Production of ethylene from ethanol on modified ZSM-5 zeolites. Master's thesis, Petrochemistry and Polymer Science Faculty of Science Chulalongkorn University. Bangkok. 2002.
- [33] Phillips, B. C. and Datta, R. Production of ethylene from hydrous ethanol on H-ZSM-5 under mild conditions. Ind. Eng. Chem. Res. 36 (1997): 4466-4475.
- [34] Carlson, L. K.; Isbester, P. K.; and Munson, E. J. Study of the conversion of methanol to dimethyl ether on zeolite HZSM-5 using in situ flow MAS NMR. Sol. Stat. Nuc. Mag. Res. 16 (2000): 93-102.
- [35] Dulya, K. and Ruangpornvisuti, V. Theoretical study of hydrophosphonylation of aldehydes catalyzed by acid in water. Master's thesis, Petrochemistry and Polymer Science Faculty of Science Chulalongkorn University. Bangkok. 2006.
- [36] Rattanasumrit, A.; Ruangpornvisuti V., Theoretical study of conversion reactions of ketone to hydroxyalkylene in cluster models of zeolite H-ZSM-5, J. Mol. Catal. Chem. A. 239 (2005) 67-75.
- [37] Zheng, X. and Blowers, P. An ab initio study of ethane conversion reactions on zeolites using the complete basis set composite energy method. J. Mol. Catal. A: Chem. 229 (2005): 77-85.
- [38] Govind, N. H.; Andzelm, J. B.; Reindel, K. and Fitzgerald, G. Zeolite-catalyzed hydrocarbon formation from methanol: density functional simulations. Int. J. Mol. Sci. 3 (2002): 423-434.
- [39] Vollmer, M. J. and Truong, N. T. Mechanisms of hydrogen exchange of methane with H-Zeolite Y: An ab Initio embedded cluster study. J. Phys. Chem. B 104 (2000): 6308-6312.
- [40] Shah, R.; Gale, J. D. and Payne, M. C. In situ study of reactive intermediates of methanol in zeolites from first principles calculations. J. Phys. Chem. B 101 (1997): 4787-4797.
- [41] Jensen, F. Introduction to computational chemistry. Chichester: John Wiley & Sons, 1999.

- [42] Lewars, E. Computational chemistry: Introduction to the theory and applications of molecular & quantum mechanics. Peterborough Ontario: Trent University Press, 2003.
- [43] Koch, W. and Holtjausen, C.M.A. Chemist's guide to density functional theory. Chichester: John Wiley & Sons, 2000.
- [44] Becke D., Density-functional exchange-energy approximation with correct asymptotic behavior, Phys. Rev. A 38 (1988): 3098-3100.
- [45] Lee C.; Yang W.; Parr R.G., Phys. Rev. B 37 (1988): 385.
- [46] Rattanasumrit, A.; Ruangpornvisuti V., Theoretical study of conversion reactions of ketone to hydroxyalkylene in cluster models of zeolite H-ZSM-5, J. Mol. Catal. A-Chem. 239 (2005): 67-75.
- [47] Maseras F.; Morokuma K., IMOMM: A new ab initio + molecular mechanics geometry optimization scheme of equilibrium structures and transition states, J. Comput. Chem. 16 (1995): 1170-1179.
- [48] Dewar M. J. S.; Reynolds C. H., An improved set of MNDO Parameters for sulfur, J. Comp. Chem. 7 (1986): 140-143.
- [49] Humbel S.; Sieber S.; Morokuma K., The IMOMO method: integration of different levels of molecular orbital approximations for geometry optimization of large systems. Test for n-butane conformation and SN₂ reaction: RCl + Cl-, J. Chem. Phys. 105 (1996): 1959-1967.
- [50] T Vreven.; Morokuma K.; On the application of the IMOMO (integrated molecular orbital + molecular orbital) method, J. Comput. Chem. 21 (2000): 1419-1432.
- [51] Remko M.; Walsh O.A.; Richards W.G., Theoretical study of molecular structure, tautomerism, and geometrical isomerism of moxonidine: two layered ONIOM calculations, J. Phys. Chem. A 105 (2001): 6926-6931.
- [52] Remko M., The gas-phase acidities of substituted hydroxamic and silahydroxamic acids: A comparative ab initio study, J. Phys. Chem. A 106 (2002): 5005-5010.
- [53] Peng C.; Ayala P. Y.; Schlegel H. B.; Frisch M. J., Using redundant internal coordinates to optimize geometries and transition states, J. Comp. Chem. 17 (1996): 49.

- [54] Frisch M. J.; Trucks G. W.; Schlegel H. B., Scuseria G. E., Robb M. A., Cheeseman J. R., Montgomery J. A., Jr., Vreven T., Kudin K. N., Burant J. C., Millam J. M., Iyengar S. S., Tomasi J., Barone V., Mennucci B. i, Cossi M., Scalmani G., Rega N., Petersson G. A., Nakatsuji H., Hada M., Ehara M., Toyota K., Fukuda R., Hasegawa J., Ishida M., Nakajima T., Honda Y., Kitao O., Nakai H., Klene M., Li X., J. Knox E., Hratchian H. P., Cross J. B., Bakken V., Adamo C., Jaramillo J., Gomperts R., Stratmann R. E., Yazyev O., Austin J., Cammi R., Pomelli C., Ochterski J. W., Ayala P. Y., Morokuma K., Voth A., Salvador P., Dannenberg J. J., Zakrzewski V. G., Dapprich., Daniels A. D., Strain M. C., Farkas O., Malick D. K., Rabuck A. D., Raghavachari K., Foresman J. B., Ortiz J. V., Cui Q., Baboul A. G., Clifford S., Cioslowski J., Stefanov B. B., Liu G., Liashenko A., Piskorz P., Komaromi I., Martin R. L., Fox D. J., Keith T., Al-Laham M. A., Peng C. Y., Nanayakkara A., Challacombe M., Gill P. M. W., Johnson B., Chen W., Wong M. W., Gonzalez C., and Pople J. A., Gaussian 03. Revision C.02. Wallingford : CT. Gaussian, 2004.
- [55] Schaftenaar G., MOLDEN 3.7.: Nijmegen Toernooiveld Nijmegen Netherlands: CAOS/CAMM Center, 1991.
- [56] Flükiger P.; Lüthi H.P.; Portmann S.; Weber J. R., MOLEKEL 4.3, Switzerland: Swiss Center for Scientific Computing Manno, 2000.
- [57] Ochterski J. W., In Gaussian. Pittsburgh: PA Gaussian, 2000.
- [58] Thipyapong K.; Arano Y.; Ruangpornvisuti V., Conformational investigation of benzylhydroxamamide, its oxotechnetium (V) complexes and determination of their reaction energies, J. Mol. Struct. Theochem. 676 (2004): 65-71.
- [59] Ruangpornvisuti V.; Wannoo B.; DFT investigation of conformational geometries and interconversion equilibria of phenylthiosemicarbazone and its complexation with zinc, J. Mol. Model. 10 (2004): 418-426.
- [60] Wannoo B.; Ruangpornvisuti V., Tautomeric and rotameric transformations of 4-methyl-3,6-pyridazinedione isomers, Chem. Phys. Lett. 415 (2005): 176-182.

- [61] Rungnim C.; Ruangpornvisuti V., A density functional study of propylene glycol conversion to propanal and propanone of various acid-catalyzed reaction models: A water-addition effect, J. Comput. Chem. 26 (2005): 1592-1599.
- [62] Wannoo B.; Ruangpornvisuti V., DFT investigation of structures of nitrosamine isomers and their transformations in gas phase, J. Mol. Struct. Theochem. 766 (2006): 159-164.
- [63] Wannoo B.; Ruangpornvisuti V., Structures of gas-phase nitrosamine-dimer isomers, their interconversions and energetics: a DFT study. J. Mol. Struct. Theochem. 775 (2006): 113-120.



สถาบันวิทยบริการ
จุฬาลงกรณ์มหาวิทยาลัย



APPENDIX

สถาบันวิทยบริการ
จุฬาลงกรณ์มหาวิทยาลัย

**Table A1** Geometrical parameters for H₂O

Bond Length	Value (Angstroms)	Angle	Value (Degrees)
R(1,2)	0.9620	A(2,1,3)	105.0609
R(1,3)	0.9620		

**Table A2** Geometrical parameters for H₃O⁺

Bond Length	Value (Angstroms)	Angle	Value (Degrees)
R(1,2)	0.9799	A(2,1,3)	113.5380
R(1,3)	0.9799	A(2,1,4)	113.5380
R(1,4)	0.9799	A(3,1,4)	113.5379

**Table A3** Geometrical parameters for MeOH₂⁺

Bond Length	Value (Angstroms)	Angle	Value (Degrees)	Dihedral	Value (Degrees)
R(1,2)	1.5236	A(2,1,3)	115.4651	A(5,2,1,3)	55.6246
R(1,3)	0.9754	A(2,1,4)	115.4652	A(6,2,1,3)	-65.6080
R(1,4)	0.9754	A(3,1,4)	110.6231	A(1,2,1,3)	173.1591
R(2,5)	1.0857	A(5,2,1)	104.3754	A(5,2,1,4)	-173.1596
R(2,6)	1.0866	A(6,2,1)	108.0701	A(6,2,1,4)	65.6061
R(2,7)	1.0857	A(7,2,1)	104.3753	A(1,2,1,4)	-65.6251
		A(5,2,6)	113.6092		
		A(6,2,7)	113.6093		
		A(5,2,7)	111.8481		

**Table A4** Geometrical parameters for MeOH

Bond Length	Value (Angstroms)	Angle	Value (Degrees)	Dihedral	Value (Degrees)
R(1,2)	1.4234	A(2,1,3)	108.8752	A(4,2,1,3)	61.4371
R(1,3)	0.9612	A(4,2,1)	112.1210	A(5,2,1,3)	-61.5063
R(2,4)	1.0969	A(5,2,1)	112.1200	A(6,2,1,3)	179.5658
R(2,5)	1.0969	A(6,2,1)	106.7097		
R(2,6)	1.0902	A(4,2,5)	108.9605		
		A(5,2,6)	108.3901		
		A(4,2,6)	108.3891		

**Table A5** Geometrical parameters for EtOH₂⁺

Bond Length	Value (Angstroms)	Angle	Value (Degrees)	Dihedral	Value (Degrees)
R(1,2)	0.9823	A(2,1,3)	113.1216	A(2,1,3,7)	-61.9674
R(1,3)	1.5673	A(2,1,6)	108.5399	A(6,1,3,7)	61.9674
R(1,6)	0.9823	A(3,1,6)	113.1216	A(1,3,7,8)	180.0000
R(3,4)	1.0896	A(1,3,7)	111.3291	A(1,3,7,9)	-62.6098
R(3,5)	1.0896	A(4,3,1)	101.0114	A(1,3,7,10)	62.6098
R(3,7)	1.5018	A(4,3,5)	110.4601		
R(7,8)	1.0977	A(4,3,7)	115.5353		
R(7,9)	1.0946	A(5,3,1)	101.0114		
R(7,10)	1.0946	A(3,7,8)	106.8829		
		A(3,7,9)	112.5610		
		A(3,7,10)	112.5610		
		A(8,7,9)	107.1638		
		A(8,7,10)	107.1638		
		A(9,7,10)	110.1586		

**Table A6** Geometrical parameters for EtOH

Bond Length	Value (Angstroms)	Angle	Value (Degrees)	Dihedral	Value (Degrees)
R(1,2)	0.9692	A(2,1,3)	107.8206	A(2,1,3,6)	180.0000
R(1,3)	1.4251	A(1,3,4)	110.9994	A(7,6,3,1)	180.0000
R(2,4)	1.1027	A(1,3,5)	110.9994	A(8,6,3,1)	-59.7551
R(2,5)	1.1027	A(1,3,6)	107.7697	A(9,6,3,1)	59.7551
R(2,6)	1.5194	A(4,3,5)	107.2066		
R(6,7)	1.0958	A(4,3,6)	109.9381		
R(6,8)	1.0950	A(5,3,6)	109.9381		
R(6,9)	1.0950	A(3,6,7)	110.6642		
		A(3,6,8)	110.3645		
		A(3,6,9)	110.3645		
		A(7,6,8)	108.6042		
		A(7,6,9)	108.6042		
		A(8,6,9)	108.1695		

**Table A7** Geometrical parameters for DME.H⁺

Bond Length	Value (Angstroms)	Angle	Value (Degrees)	Dihedral	Value (Degrees)
R(2,3)	1.0888	A(3,2,4)	112.8367	A(3,2,1,6)	-51.1826
R(2,4)	1.0908	A(3,2,5)	111.3043	A(4,2,1,6)	70.1891
R(2,5)	1.0882	A(4,2,5)	112.5565	A(5,2,1,6)	-168.9464
R(2,1)	1.4964	A(3,2,1)	105.4902	A(2,1,7,8)	-61.1164
R(1,6)	0.9798	A(4,2,1)	108.9021	A(2,1,7,9)	59.7563
		A(5,2,1)	105.1780	A(2,1,7,10)	-178.8842
		A(2,1,6)	111.4491		
		A(2,1,7)	117.4795		

**Table A8** Geometrical parameters for DME

Bond Length	Value (Angstroms)	Angle	Value (Degrees)	Dihedral	Value (Degrees)
R(2,3)	1.0933	A(3,2,4)	108.8772	A(3,2,1,6)	180.0000
R(2,4)	1.1029	A(3,2,5)	108.8772	A(4,2,1,6)	-60.7026
R(2,5)	1.1029	A(4,2,5)	108.1115	A(5,2,1,6)	60.7026
R(2,1)	1.4098	A(3,2,1)	107.2563	A(2,1,6,7)	60.7026
R(1,6)	1.4098	A(4,2,1)	111.8241	A(2,1,6,8)	180.0000
		A(5,2,1)	111.8241	A(2,1,6,9)	-60.7026
		A(2,1,6)	112.3209		

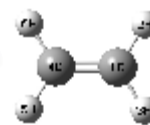
**Table A9** Geometrical parameters for DEE.H⁺

Bond Length	Value (Angstroms)	Angle	Value (Degrees)	Dihedral	Value (Degrees)
R(2,3)	1.0933	A(2,6,1)	108.1267	A(2,6,1,16)	174.8421
R(2,4)	1.0956	A(6,1,9)	119.0046	A(2,6,1,9)	61.2230
R(2,5)	1.0961	A(6,1,16)	109.3969	A(6,1,9,12)	-61.9674
R(2,6)	1.5085	A(9,1,16)	110.4448		
R(6,7)	1.0929	A(1,9,12)	109.5696		
R(6,8)	1.0884				
R(6,1)	1.5206				
R(1,16)	0.9794				
R(1,9)	1.5276				

สถาบันวิทยบริการ
จุฬาลงกรณ์มหาวิทยาลัย

**Table A10** Geometrical parameters for DEE

Bond Length	Value (Angstroms)	Angle	Value (Degrees)	Dihedral	Value (Degrees)
R(5,6)	1.0958	A(5,2,1)	108.4743	A(5,2,1,9)	180.0000
R(5,7)	1.0949	A(2,1,9)	113.2227	A(2,1,9,12)	180.0000
R(5,8)	1.0949	A(1,9,12)	108.4743		
R(5,2)	1.5199				
R(2,3)	1.1042				
R(2,4)	1.1042				
R(2,1)	1.4168				
R(1,9)	1.4168				

**Table A11** Geometrical parameters for ETL

Bond Length	Value (Angstroms)	Angle	Value (Degrees)	Dihedral	Value (Degrees)
R(1,2)	1.0875	A(2,1,3)	116.2724	A(2,1,4,5)	180.0000
R(1,3)	1.0875	A(2,1,4)	121.8637	A(2,1,4,6)	0.0000
R(1,4)	1.3308			A(3,1,4,5)	0.0000
				A(3,1,4,6)	180.0000

สถาบันวิทยบริการ
จุฬาลงกรณ์มหาวิทยาลัย

Table A12

Energies and thermodynamic quantities of the concerted mechanism of ethanol conversion to diethyl ether in the H-ZSM-5-catalyzed system

Reaction ^a	$\Delta^{\ddagger}E$ ^{b,c}	$\Delta^{\ddagger}G$ ^{b,c}	$k_{373.15}$ ^d
HZ+2EtOH $\overset{\curvearrowright}{\text{S}}$ INT1	-	-	-
INT1 $\overset{\curvearrowright}{\text{S}}$ TS $\overset{\curvearrowright}{\text{S}}$ INT2	59.41	62.82	1.24×10^{-24}
INT2 $\overset{\curvearrowright}{\text{S}}$ DEE + H ₂ O + ZH	-	-	-

^a Based on the 56/5T cluster model of H-ZSM-5, computed at the ONIOM(B3LYP/6-31G(d):AM1) level.

^b Activation state.

^c In kcal/mol.

^d In s⁻¹.

Table A13

Energies and thermodynamic quantities of the concerted mechanism of ethanol conversion to diethyl ether in the H-ZSM-5-catalyzed system

Reaction ^a	$\Delta^{\ddagger}E$ ^{b,c}	$\Delta^{\ddagger}G$ ^{b,c}	$k_{473.15}$ ^d
HZ+2EtOH $\overset{\curvearrowright}{\text{S}}$ INT1	-	-	-
INT1 $\overset{\curvearrowright}{\text{S}}$ TS $\overset{\curvearrowright}{\text{S}}$ INT2	62.13	66.17	2.69×10^{-18}
INT2 $\overset{\curvearrowright}{\text{S}}$ DEE + H ₂ O + ZH	-	-	-

^a Based on the 56/5T cluster model of H-ZSM-5, computed at the ONIOM(B3LYP/6-31G(d):AM1) level.

^b Activation state.

^c In kcal/mol.

^d In s⁻¹.

Table A14

Energies and thermodynamic quantities of the concerted mechanism of ethanol conversion to diethyl ether in the H-ZSM-5-catalyzed system

Reaction ^a	$\Delta^\ddagger E$ ^{b,c}	$\Delta^\ddagger G$ ^{b,c}	$k_{573.15}$ ^d
HZ+2EtOH \ddot{S} INT1	-	-	-
INT1 \ddot{S} TS \ddot{S} INT2	61.41	67.83	1.62×10^{-13}
INT2 \ddot{S} DEE + H ₂ O + ZH	-	-	-

^a Based on the 56/5T cluster model of H-ZSM-5, computed at the ONIOM(B3LYP/6-31G(d):AM1) level.

^b Activation state.

^c In kcal/mol.

^d In s⁻¹.

Table A15

Energies and thermodynamic quantities of the concerted mechanism of ethanol conversion to diethyl ether in the H-ZSM-5-catalyzed system

Reaction ^a	$\Delta^\ddagger E$ ^{b,c}	$\Delta^\ddagger G$ ^{b,c}	$k_{673.15}$ ^d
HZ+2EtOH \ddot{S} INT1	-	-	-
INT1 \ddot{S} TS \ddot{S} INT2	63.82	70.59	1.68×10^{-10}
INT2 \ddot{S} DEE + H ₂ O + ZH	-	-	-

^a Based on the 56/5T cluster model of H-ZSM-5, computed at the ONIOM(B3LYP/6-31G(d):AM1) level.

^b Activation state.

^c In kcal/mol.

^d In s⁻¹.

Table A16

Energies and thermodynamic quantities of the concerted mechanism of ethanol conversion to ethylene in the H-ZSM-5-catalyzed system

Reaction ^a	$\Delta^\ddagger E$ ^{b,c}	$\Delta^\ddagger G$ ^{b,c}	$k_{373.15}$ ^d
HZ+EtOH $\overset{\curvearrowright}{\text{S}}$ INT1	-	-	-
INT1 $\overset{\curvearrowright}{\text{S}}$ TS $\overset{\curvearrowright}{\text{S}}$ INT2	93.81	100.32	1.34×10^{-46}
INT2 $\overset{\curvearrowright}{\text{S}}$ Ethy + H ₂ O + ZH	-	-	-

^a Based on the 56/5T cluster model of H-ZSM-5, computed at the ONIOM(B3LYP/6-31G(d):AM1) level.

^b Activation state.

^c In kcal/mol.

^d In s⁻¹.

Table A17

Energies and thermodynamic quantities of the concerted mechanism of ethanol conversion to ethylene in the H-ZSM-5-catalyzed system

Reaction ^a	$\Delta^\ddagger E$ ^{b,c}	$\Delta^\ddagger G$ ^{b,c}	$k_{473.15}$ ^d
HZ+EtOH $\overset{\curvearrowright}{\text{S}}$ INT1	-	-	-
INT1 $\overset{\curvearrowright}{\text{S}}$ TS $\overset{\curvearrowright}{\text{S}}$ INT2	101.46	109.73	2.02×10^{-38}
INT2 $\overset{\curvearrowright}{\text{S}}$ Ethy + H ₂ O + ZH	-	-	-

^a Based on the 56/5T cluster model of H-ZSM-5, computed at the ONIOM(B3LYP/6-31G(d):AM1) level.

^b Activation state.

^c In kcal/mol.

^d In s⁻¹.

Table A18

Energies and thermodynamic quantities of the concerted mechanism of ethanol conversion to ethylene in the H-ZSM-5-catalyzed system

Reaction ^a	$\Delta^\ddagger E$ ^{b,c}	$\Delta^\ddagger G$ ^{b,c}	$k_{573.15}$ ^d
HZ+EtOH $\overset{\curvearrowright}{\text{S}}$ INT1	-	-	-
INT1 $\overset{\curvearrowright}{\text{S}}$ TS $\overset{\curvearrowright}{\text{S}}$ INT2	93.20	104.14	2.31×10^{-27}
INT2 $\overset{\curvearrowright}{\text{S}}$ Ethy + H ₂ O + ZH	-	-	-

^a Based on the 56/5T cluster model of H-ZSM-5, computed at the ONIOM(B3LYP/6-31G(d):AM1) level.

^b Activation state.

^c In kcal/mol.

^d In s⁻¹.

Table A19

Energies and thermodynamic quantities of the concerted mechanism of ethanol conversion to ethylene in the H-ZSM-5-catalyzed system

Reaction ^a	$\Delta^\ddagger E$ ^{b,c}	$\Delta^\ddagger G$ ^{b,c}	$k_{673.15}$ ^d
HZ+EtOH $\overset{\curvearrowright}{\text{S}}$ INT1	-	-	-
INT1 $\overset{\curvearrowright}{\text{S}}$ TS $\overset{\curvearrowright}{\text{S}}$ INT2	103.87	121.32	5.70×10^{-27}
INT2 $\overset{\curvearrowright}{\text{S}}$ Ethy + H ₂ O + ZH	-	-	-

^a Based on the 56/5T cluster model of H-ZSM-5, computed at the ONIOM(B3LYP/6-31G(d):AM1) level.

^b Activation state.

^c In kcal/mol.

^d In s⁻¹.

CURRICULUM VITAE

NAME, NICKNAME : Mr. Chedthapicharn Saenharn, Kongbeng

BIRTH DATE : March 26th, 1982

BIRTH PLACE : Khonkaen Province, Thailand

EDUCATION : YEAR INSTITUTION DEGREE/DIPLOMA

2000 Khonkaen High School

Wittayayon

2004 Khonkaen Univ. B.S. (Physic)

2007 Chulalongkorn Univ. M.S.

(Petrochemistry and Polymer Science)

ADDRESS : 2/3, Ammart Rd., Naimuang,
Muang, Khonkaen,
40000, Thailand. Tel. 089-6207006

E-MAIL : beng_manu@hotmail.com

สถาบันวิทยบริการ
จุฬาลงกรณ์มหาวิทยาลัย